Single Crystal Growth of Lithium Tetra Borate and its Characterization as a Multi-functional Material for Personal Dosimetry

By

GIRI DHARI PATRA

PHYS01201204017

Bhabha Atomic Research Centre, Mumbai

A thesis submitted to the

Board of Studies in Physical Sciences

In partial fulfillment of requirements

for the Degree of

DOCTOR OF PHILOSOPHY

of

HOMI BHABHA NATIONAL INSTITUTE

January, 2017

Homi Bhabha National Institute

Recommendations of the Viva Voce Committee

As members of the Viva Voce Committee, we certify that we have read the dissertation prepared by **Giri Dhari Patra** entitled **"Single Crystal Growth of Lithium Tetra Borate and its Characterization as a Multi-functional Material for Personal Dosimetry"** and recommend that it may be accepted as fulfilling the thesis requirement for the award of Degree of Doctor of Philosophy.

Chairman - Prof. S.K. Gupta **Date:** 5/7/17

Guide / Convener - Prof. S.C. Gadkari **Date:** 05/07/17

Examiner – Prof. A. Thamizhavel **Date:** 5/7/2017

Member 1- Dr. S. Ganesamoorthy **Date:** 5/7/17.

Member 2- Dr. M.P. Chougaonkar **Date:** 5/7/2017

The Technology Adviser - Dr. M.S. Kulkarni **Date:** 5/7/2017

Final approval and acceptance of this thesis is contingent upon the candidate's submission of the final copies of the thesis to HBNI.

I hereby certify that I have read this thesis prepared under my direction and recommend that it may be accepted as fulfilling the thesis requirement.

Date: 05.07.2017

Place: Mumbai

05/07/17

Prof. S. C. Gadkari

Guide

STATEMENT BY AUTHOR

This dissertation has been submitted in partial fulfillment of requirements for an advanced degree at Homi Bhabha National Institute (HBNI) and is deposited in the Library to be made available to borrowers under rules of the HBNI.

Brief quotations from this dissertation are allowable without special permission, provided that accurate acknowledgement of source is made. Requests for permission for extended quotation from or reproduction of this manuscript in whole or in part may be granted by the Competent Authority of HBNI when in his or her judgment the proposed use of the material is in the interests of scholarship. In all other instances, however, permission must be obtained from the author.

Giri dhari Patra

Giri Dhari Patra

DECLARATION

I, hereby declare that the investigation presented in the thesis has been carried out by me. The work is original and has not been submitted earlier as a whole or in part for a degree / diploma at this or any other Institution / University.

Giri dhari Patra

Giri Dhari Patra

List of Publications arising from the thesis

Journal

1. "Photo-luminescence properties of Cu and Ag doped $Li_2B_4O_7$ single crystals at low temperatures", **G.D. Patra**, Mohit Tyagi, D.G. Desai, Babita Tiwari, Shashwati Sen, S.C. Gadkari, *J. Lumin.*, **2012**, *132 (5),* 1101-1105.

2. "Thermally stimulated luminescence process in copper and silver co-doped lithium tetraborate single crystals and its implication to dosimetry", **G.D. Patra**, S.G. Singh, B. Tiwari, S. Sen, D.G. Desai, S.C. Gadkari, *J. Lumin.,* **2013**, *137,* 28-31.

3. "Silver doped lithium tetraborate ($Li_2B_4O_7$) single crystals as efficient dosimeter material with sub-micro-Gy sensitivity", **G.D. Patra**, S.G. Singh, A.K. Singh, M. Tyagi, D.G. Desai, B. Tiwari, S. Sen and S.C. Gadkari, *J. Lumin.,* **2015**, *157, 3*33-337.

4. "Optically stimulated luminescence in Ag doped $Li_2B_4O_7$ crystal and its application in neutron detection and dosimetry", **G.D. Patra**, S.G. Singh, B. Tiwari, A.K. Singh, D.G. Desai, M. Tyagi, S. Sen and S.C. Gadkari, *Radiat. Meas.,* **2016,** 88, 14-19.

Conferences

1. "Low Dose Measurement of 150 ns Pulsed X-Ray Source with Silver Doped $Li_2B_4O_7$ Single Crystals", **G.D. Patra**, S.G. Singh, B. Tiwari, M. Tyagi, R. M. Agarwal, A. Sharma, S. Sen and S.C. Gadkari, *61st DAE-BRNS Symposium on Nuclear Physi*cs, **2016**, Kolkata.

2. "Growth and Characterization of Silver Doped $Li_2B_4O_7$ Single Crystals for Environmental Dose Measurement", **G.D. Patra,** S.G. Singh, B. Tiwari , D.G. Desai, A.K. Singh, M. Tyagi, S. Sen, and S.C. Gadkari, *XX National Seminar on Crystal Growth and Applications,* **2016**, Mumbai.

3. "Doped Lithium Tetraborate Single Crystals for Different Dosimetric applications", B. Tiwari, **G.D. Patra,** S.G. Singh, M. Sonawane, D.G.

Desai, A.K. Singh, M. Tyagi, S. Sen, and S.C. Gadkari, *XX National Seminar on Crystal Growth and Applications*, **2016**, Mumbai.

4. "Development of Thermal Neutron Detector based on Lithium Tetraborate (LTB) Single Crystal", **G.D. Patra**, A.K. Singh, B. Tiwari, S.G. Singh, D.G. Desai, M. Tyagi, S. Sen, S.C. Gadkari and S.K. Gupta, *BARC NEWSLETTER, Issue No. - 344*, Mar - Apr **2015**.

5. "LTB:Ag- A good TL and OSL material for neutron dosimetry", B. Tiwari, S.G. Singh, **G.D. Patra**, A.K. Singh, D.G. Desai, M. Tyagi, Shashwati Sen and S.C. Gadkari, *20th National symposium on Radiation Physics*, **2015**, Mangalore.

6. "Real-time detection of thermal neutrons using $Li_2B_4O_7$:Ag single crystal", **G.D. Patra**, S.G. Singh, S. Sen, D.G. Desai, S.S. Desai, S.C. Gadkari and S.K. Gupta, *Proceedings of the conference on 75-years of nuclear fission: present status and future perspectives-abstract book*, **2014.**

7. "Growth and Characterization of Silver Doped $Li_2B_4O_7$ Single Crystals for Dosimetry Applications", **G.D. Patra**, A.K. Singh, S.G. Singh, M. Tyagi, D.G. Desai, B. Tiwari, S. Sen and S.C. Gadkari, 59th *DAE SSPS*, **2014**, VIT, Vellore.

8. "Development of single crystal based detectors for thermal neutrons", **G.D. Patra,** S.G. Singh, M. Tyagi, A.K. Singh, S. Sen and S.C. Gadkari, *Young materials Researchers Meet*, **20**14, Mumbai.

9. "Growth Of Silver Doped $Li_2B_4O_7$ Single Crystals For Dosimetric Application", **G.D. Patra**, S.G. Singh, A.K. Singh, D.G. Desai, B. Tiwari, S. Sen and S.C. Gadkari, *AIP Conf. Proc.*, **2013**, *1512(1)*, 862-863, http://dx.doi.org/10.1063/1.4791311.

10. "Silver doped Lithium tetraborate single crystals for Optically stimulated luminescence (OSL) based personal dosimetry", **G.D. Patra**, S.G. Singh, D.G. Desai, Shaswati Sen, S.C. Gadkari and S.K. Gupta, *Synergy in physics and Industry*, **2013**, Mumbai.

11. "Comparison of optical properties of pure and doped lithium teraborate single crystals and glasses",, **G.D. Patra**, A.K. Singh, S.G. Singh, M. Tyagi, S. Sen, B. Tiwari and S.C. Gadkari, *AIP Conf. Proc.* **2012**, *1447(1)*, 1335-1336, doi: 10.1063/1.4710507.

12. “Elevated temperature optically stimulated luminescence studies on Cu and Ag doped $Li_2B_4O_7$ single crystals”, N.S. Rawat, D.R. Mishra, M.S. Kulkarni, **G.D. Patra**, S.C. Gadkari, S.K. Gupta, *Proceedings of the thirtieth IARP conference on radiological protection and safety in nuclear reactors and radiation installations*, **2012.**

13. "Growth and optical characterization of Cu and Ag co-doped LTB single crystals with different Ag concentrations", **G.D. Patra**, B. Tiwari, D.G. Desai, Shashwati Sen and S.C. Gadkari, *XVI National Seminar on Crystal Growth*, **2012**, Tiruchendur, TN.

14. "Growth of copper and silver co-doped lithium tetraborate single crystals for dosimetric application", **G.D. Patra**, Babita Tiwari, A.K. Singh, S.G. Singh, M. Tyagi, D.G. Desai, N.S. Rawat, M.S. Kulkarni and S.C. Gadkari, *XV National Seminar on Crystal Growth*, **2011**, Tirunelveli, TN.

Giri dhari Patra

Giri Dhari Patra

DEDICATIONS

This thesis is dedicated to my Family

ACKNOWLEDGEMENTS

I would like to express my heartfelt and indebted gratitude to my guide **Prof. S.C. Gadkari** for his invaluable guidance, expert suggestions and continuous encouragement provided by him throughout my work, without which the timely completion of this work was not possible. The inspiration given by him guided me to present my best in all the circumstances**.** I would never be able to forget his affectionate and friendly behavior towards me.

I would like to express my gratitude to Chairman **Prof. S.K. Gupta** and members **Dr. S. Ganesamoorthy, Dr. M.P. Chougaonkar** and **Dr. M.S. Kulkarni** of my doctoral committee for sharing their knowledge and experience with me and guiding me through the research.

I also express thanks to **Prof. Saibal Basu, Dr. Archana Shrama, Dr. Rajesh Kumar, Dr. S.S. Desai and Dr. N.S. Rawat** who helped me during this research work. We had various discussions from which I learn many new things.

I am extremely grateful to **Dr. Shashwati Sen** for sharing her expertise and taking time from her regular duties with constant support for the research work.

I am extremely grateful to **Dr. S.G. Singh** for valuable advices and consistent encouragement and support in each and every step of the research work.

I am extremely grateful to **Sh. D.G. Desai, Dr. Mohit Tyagi, Dr. Babita Tiwari, Shri A.K. Singh** for their support and helping me in carrying out different experiments.

I would like to thanks **Dr. M.G. Ghosh** and **Dr. Shreyas Pitale** for their help, support and encouragement while carrying out the research work.

I would like to extend my sincere thanks **Ms. S.V. Shinde, Mr. K. Chennakesavulu, Mr. S. Chavhan, Smt M. Sonawane, Mr. P.N. Keluskar, Mr. K.V.P. Apparao, Mr. N.**

Velmanickam, Mr. A.N. Patil, Mr. J. Loganatahan, Smt. Chhaya More and Smt. S. S. Kamble for their valuable help and support during this research work.

At last, but not the least I would like to convey my deep heartiest gratitude to **my parents**, my wife **Mrs. Sima Patra** and my son **Master Joydeep Patra** for giving me perpetual inspiration, affection and encouragement, which has been my privileged to receive from them during the entire period of my research work and course of study. I would also like to thanks all **my friends** for their backing and encouragement during the research work.

Giri dhari Patra

(Giri Dhari Patra)

CONTENTS

SYNOPSIS

Radiation is a part of nature that exists in the background and cannot be avoided. With the advent of technologically advanced and complex systems like nuclear reactors, accelerators and radiations based medical and imaging equipment/devices, radiation has become an integral part of modern society [1]. It is therefore necessary to understand the nature of radiation and estimate its impact on environment and people. Various types of radiations that exit in nature or produced artificially can be classified as charged (electrons, heavy charged particles) and uncharged radiation (electromagnetic radiation and neutrons). The nature and energy (which can vary from a few meV to TeV based on its origin) of these particles govern their interactions with a material. The radiation may interact with materials either with deposition of energy partially or fully in the medium or may leave without any interaction at all. These interactions of radiation with matter (living and non-living) often damages or generate defects in the medium. For example, the interaction of the radiation with the living tissues such as in personal exposed to radiation fields may lead to severe damage either partial or permanent that may lead to different kinds of illness depending upon the type of radiation and the specific organ [2]. The deposition of energy in the material is called dose and is defined in terms of energy deposited per unit mass of the medium and the materials/equipment used to measure it are called dosimeters [3]. As the impact of radiation associated with facilities such as nuclear reactors, accelerators, medical diagnostic/treatment etc. can be serious, the monitoring of personnel involved in these facilities becomes a strenuous and stringent requirement. There is also specific demand for an accurate assessment of dose in environment and space related experiments.

Among various dosimetry techniques, the thermoluminescence dosimetry (TLD) based on thermally stimulated luminescence (TSL) is one of the most widely used technique that has been a mainstay of health physics professionals for over 50 years because of its operational simplicity and cost effectiveness [4]. TLDs have been extremely valuable in monitoring the safety of radiation workers, performing environmental dose control, archaeological, geological dating and medical dosimetry [5]. Thermally stimulated luminescence (TSL) is emission of UV-Vis photons (other than black body radiation) from the materials when subjected to heating after exposure to ionizing radiation. The phenomenon of TSL is mostly observed in insulators/semiconductors having meta-stable trap levels in their forbidden band gap due to the presence of impurities and defects. When exposed to ionizing radiation at room temperature, electron-hole pairs are generated which freely move through conduction and valance bands respectively and subsequently get trapped at various meta-stable trap levels. Heating of the material leads to release of one type of charge carriers (e.g. electrons or holes) to respective de-localized bands and their subsequent recombination with trapped charges of opposite polarity give rise to emission of photons via its luminescence center, known as TSL. The plot of TSL intensity as function of temperature gives a TSL glow curve and the integrated area under this curve is directly proportional to the absorbed dose.

Approximately over two thirds of the known natural minerals are known to exhibit TSL. For dosimetric applications, a phosphor should have the attributes like simple glow curve, main glow peak at about 200°C, high sensitivity, good linearity with respect to dose exposure, stable trap centers and good chemical stability. Some of the important TSL materials that have been developed over the years and use for different dosimetric applications are LiF:Mg,Ti (TLD 100, 600 and 700), LiF:Mg,Cu,P, CaF_2:Dy (TLD-200), CaF_2:Tm (TLD-300), CaF_2:Mn (TLD-400), $CaSO_4$:Dy (TLD-900), $Li_2B_4O_7$:Mn (TLD-800) etc. In the last two decades several new dosimeters like Al_2O_3:C, BeO, Feldspar etc have been invented that could be read using an optical stimulation rather than thermal. These are called optically stimulated luminescence (OSL) materials that have certain advantages compared to the TSL [6]. Though there are several TSL and OSL phosphor materials but not all of are suitable for radiation dosimetry. For the personal dosimetry, it is required that dosimeter should have an effective atomic number (Z_{eff}) close to that of the biological tissue (tissue equivalence). In addition, for an OSL phosphor the photo-ionization cross-section for stimulation wavelength should be large enough to enable one to extract the luminescence signal in minimum time i.e. the feasibility of fast readout and hence large throughput. Since, only very few materials are found to possess most of the above features, the quest for the highly sensitive and eligible phosphors continues. There have been continuous efforts to develop better TLD using new materials with better quality compared to existing ones. To improve the quality of TLD of the existing materials, different routes of synthesise of materials and different dopants are tried. Single crystal dosimeters have some advantages such as colorless, transparent and resistant to humidity, compared to other forms. The single crystals have the advantage that they can be used almost indefinitely, since the detector can be annealed to reset its sensitivity [7].

In the present work dosimetric properties of single crystals of Cu, Ag and Cu-Ag doped $Li_2B_4O_7$ (lithium tetra borate, LTB) have been investigated. The LTB is important due to its tissue equivalence with Z_{eff} ~ 7.3, which is relatively close to that of human tissue (Z_{eff} ≈7.4). It has a low photon energy dependence and high dose linearity over a wide dynamic range. Lithium tetraborate (LTB), is a crystal that contains lithium and boron isotopes, each with high probabilities of interaction with thermal neutrons via nuclear reactions. Single crystals of LTB:Cu, LTB:Ag and LTB:Cu,Ag are grown using the Czochralski technique and extensively investigated by photoluminescence, TSL, OSL techniques and also for thermal neutron detection. Details of luminescence characteristic at low temperatures (-196°C) have been investigated to understand the nature of the luminescence centers. The role of Ag as a sensitizer in LTB: Cu,Ag single crystal has been studied in detail using different techniques including optical absorption (OA), photoluminescence (PL) and TSL and the enhancement of sensitivity in LTB:Cu,Ag has been compared with LTB:Cu. The reason of apparent inferior TSL response of Ag doped LTB single crystal employing conventional readout set-up has been considered and it was overcome by using a proper readout system. This system covers its emission band and gives a significant improvement in the dosimetric characteristic and its performance compared to LTB:Cu and LTB:Cu,Ag. The optimum concentration of Ag doping has been achieved that enabled it to detect radiation in sub-micro Gray region. The ability of LTB:Ag to respond to thermal neutrons has also been demonstrated. Environmental dose monitoring for a period of 60 days are also carried out. This material being highly tissue equivalent, offers its suitability for various dosimetric applications, including personnel and clinical.

The research work carried out is compiled in the form of thesis and has been grouped under seven chapters as follows:

Chapter 1: Introduction

This chapter begins with a brief description of the radiation and its effects on humankind. The use of dosimeters for the determination of doses employing Thermally (TSL) and Optically Stimulated Luminescence (OSL) processes, has been discussed [8,9]. An overview of popular TSL/OSL phosphor materials (viz. fluorides, borates and oxides) used in the radiation dosimetry is presented [10]. Different challenges in making an ideal dosimeter have been discussed. The advantages of using the single crystals as a dosimeter as compared to pelletized powers are elaborated. A brief description of single crystal and their use is discussed. A brief introduction of the LTB material that is a subject of the present study along with literature survey is also given in this chapter.

Chapter 2: Theory and Experimental Techniques

In this chapter different single crystal growth techniques with the emphasis on the Czochralski technique are described. A description of various methods for TSL/OSL characterization and kinetic analysis of phosphors that are used in the present work are given. Other techniques used for material characterization like powder X-ray Diffraction, Laue diffraction, X-ray excited luminescence, thermo-gravimetric Analysis (TG/DTA) and microscopic investigation of defects like optical absorption, photoluminescence (PL), UV-Vis spectroscopy used during the course of this work are also discussed.

Chapter 3: Single crystals growth and characterization of Cu doped $Li_2B_4O_7$

This chapter starts with the growth of single crystals of pure and Cu doped LTB by the Czochralski technique. The problems in the growth of single crystals are addressed and optimum growth parameters are elaborated. The crystals are characterized for optical absorption, PL, TSL and OSL properties. The optical absorption of the grown single crystal samples confirms the presence of Cu^+ with an absorption band at 242 nm. Further, reports on the PL characterization of Cu^+ luminescence centers are given. To understand the position of Cu^+ center in the host lattice, PL is also measured in the temperature range from -196ºC to 27ºC. An explanation regarding the excitation band having a doublet structure at 240 nm and 262 nm observed for the emission at 370 nm that corresponds to $^1A_{1g} \rightarrow ^1Eg$ and $^1A_{1g} \rightarrow ^1T_{2g}$ crystal field components of the $3d^{10} \rightarrow 3d^9 4s$ transition of Cu^+ is given in this chapter [11]. The relative intensity of these components and their temperature dependence to measure the off-center displacement of the Cu^+ ground state in the crystal lattice site is a major outcome of the various studies given in this chapter [12]. The TSL glow curve consists of two well defined and well separated glow peaks at 95°C and 220°C.

The first peak at 95°C, not suitable for the TLD application, has not been considered for further studies, while the second peak at about 220°C shows a linear dose response in the region from 0.1 Gy to 150 Gy [13]. The TSL kinetics and process in Cu doped LTB has been studied and presented in this chapter.

Chapter 4: Single crystals growth and characterization of Cu+Ag doped $Li_2B_4O_7$

In this chapter the growth of single crystals of LTB co-doped with Cu-Ag using the Czochralski technique has been described and the luminescence properties (Transmission, PL and TSL) are investigated. In transmission spectra, there are two absorption bands centered at 205 nm and 242 nm corresponding to Ag^+ and Cu^+ respectively. The PL spectra revealed the presence of intrinsic luminescence centers of Cu and Ag in LTB and indicate an energy transfer from Ag^+ centers to Cu^+ centers. The Ag^+ centers play a sensitizer role as the emission at 270 nm from Ag^+ lies in the excitation (265 nm) of Cu^+. The TSL glow curve shows two peaks at 160ºC and 230ºC. From TSL studies it is found that, despite an energy transfer from Ag^+ to Cu^+ centers, emission from both the centers participate in the TSL. A possible scheme for the TSL processes in the co-doped LTB crystal has been proposed based on PL and TSL studies. The crystals show a dose linearity response in the range from 1 mGy to 10 Gy. The minimum detection dose (MDD) has been improved from 10 mGy in LTB:Cu to 1 mGy in the LTB:Cu,Ag crystal. The investigations on the TSL study suggest that the LTB:Cu,Ag crystal would be a better and efficient material for dosimeters (TSL as well as OSL) compared to singly doped LTB:Cu crystals in a photo-readout system having a maximum response in the 200 nm to 600 nm range [14].

Chapter 5: Single crystals growth and characterization of Ag doped $Li_2B_4O_7$

In this chapter a detail study on the growth of silver doped LTB single crystals and TSL properties has been described. Single crystals with varying Ag are grown and characterized for optical absorption, PL and TSL properties. The optimum Ag concentration in the LTB single crystal was found to be about 500 ppm for the best TSL properties. The apparent inferior property of Ag as an activator reported earlier by other researchers is addressed and a TSL readout set-up has been designed that uses a solar blind photo-multiplier tube (PMT) to match the emission from Ag which is in the UV region (peak at 270 nm) [15]. This TSL set-up significantly improved the performance by lowering the dark counts and enhancing the signal due to a better matching between the emission from Ag ions and the PMT response. In addition, the use of the solar blind PMT also minimized the thermal noise generated from heating of sample in the TSL set-up. The dose linearity is found to be in the range from 10 μGy to 100 Gy. Radiation doses lower than 5μGy have been measured using this set-up with small LTB:Ag crystal samples (100 mg) and minimum detection dose (MDD) is estimated to be 500 nGy from extrapolation of dose linearity curve. The stability of TSL glow peak (160°C) of LTB:Ag at room temperature in two conditions viz. (i) samples kept in dark and (ii) kept in light after the irradiation is investigated. The study shows that the fading is fast when the irradiated samples were exposed to day light. The ability of LTB:Ag to measure environmental dose is also checked and found that a very low doses (5 μGy) could easily be measured.

Chapter 6: OSL characterization of Ag doped $Li_2B_4O_7$ single crystal and thermal neutron detection

In this chapter the OSL properties of the LTB:Ag single crystal have been investigated and reported for the first time and it is compared with LTB:Cu crystal samples. This material shows a good OSL intensity when stimulated with light at 460 nm. The OSL characteristics of LTB:Ag are comparable with LTB:Cu and have larger photo-ionization cross-sections which leads to faster decay and enables fast readout of irradiated samples as desirable for a good OSL phosphor. The OSL intensity of LTB:Ag has a linear response in the measured range of doses (0.1 to 500 Gy). The OSL properties are compared with commercially available Al_2O_3:C powder.

The ability to respond to thermal neutrons is also tested and described in this chapter. The LTB:Ag samples irradiated by thermal neutrons show similar TSL characteristic as for gamma irradiation. The TSL for low to high neutron fluences has been measured and it exhibited a linear response. In-situ detection of thermal neutrons is also demonstrated with a modified setup. Using this set-up, a neutron flux of 1000 n/s/cm^2 has been measured. The OSL sensitivity for neutrons irradiated samples has been studied and the results are reported for the first time. The study suggests that the LTB:Ag may be a useful material to develop devices based on OSL for mixed-field dosimetry and imaging applications in neutrons radiography.

Chapter 7: Conclusions and Future scope of work

The novel findings of the investigations carried out for differently doped LTB single crystals have been listed out in this chapter. Out of the different investigated activators, Ag doped LTB is found to be suitable for dosimetric applications for of all types of radiations using both TSL and OSL techniques. The chapter concludes with some of the aspects that are yet to be answered and explored, setting the tune for the future scope of work.

References:

1. G.F. Knoll, *Radiation Detection and Measurements*, **2000**, John Wiley & Sons, Inc.
2. D.M. Christensen, C.J. Iddins, S.L. Sugarman, *Emerg. Med. Clin. North. Am.,* **2014**, ***32 (1)***, 245.
3. E.H. Donnelly, J.B. Nemhauser, J.M. Smith, *South. Med. J.*, 2010, *103 (6)*, 541.
4. Y.S. Horowitz, (ed.), "*Thermoluminescence and Thermoluminescent Dosimetry*", **1983**, CRC Press, Boca Raton.
5. T. Kron, L. DeWerd, Mobit, *Phys. Med. Biol.*, **1999**, *44*, L15.
6. S.W.S. McKeever, M. Moscovitch, *Radiat. Prot. Dosim.,* **2003,** *104,* 263.
7. E.G. Yukihara, S.W.S. Mckeever, *"Optically Stimulated Luminescence-fundamentals and applications",* ISBN: 978-0-470-69725-2.
8. A.B. Goldberg, D.S. McClure, C. Pedrini, *Chem. Phys. Lett.,* **1982**, *87*, 508.
9. S.W.S. McKeever, "*Thermoluminescence of Solids*", **1985**, Cambridge University Press, Cambridge.
10. L. Bøtter-Jensen, S.W.S. McKeever, and A.G. Wintle, "*Optically Stimulated Luminescence Dosimetry*", **2003**, Elsevier, Amsterdam.
11. S.W.S. Mckeever, M. Moscovitch, Peter David Townsend, "*Thermoluminescence dosimetry materials: properties and uses*", **1995**, Nuclear Technology Publishing.
12. G.D. Patra, Mohit Tyagi, D.G. Desai, Babita Tiwari, Shashwati Sen, S.C. Gadkari, *J. Lumin.,* **2012**, *132,* 1101.
13. Babita Tiwari, N.S. Rawat, D.G. Desai, S.G. Singh, M. Tyagi, P. Ratna, S.C. Gadkari, M.S. Kulkarni, *J. Lumin.,* **2010**, *130,* 2076.
14. G.D. Patra**,** S.G. Singh, B. Tiwari, S. Sen, D.G. Desai, S.C. Gadkari, *J. Lumin.,* **2013**, *137,* 28.
15. G.D. Patra, S.G. Singh, A.K. Singh, M. Tyagi, D.G. Desai, B. Tiwari, S. Sen and S.C. Gadkari, *J. Lumin.*, 2015, ***157***, 333.

LIST OF FIGURES

LIST OF TABLES

CHAPTER 1

INTRODUCTION

1.1 Motivation and Background

Radiation is the energy emitted from a source and transported through medium or space and is an integral part of universe. The radiation can be broadly put in four categories; (i) electromagnetic, (ii) particle, (iii) acoustic and (iv) gravitational radiation. They play a very important role in our daily life and have found various applications in medicine, communication, industry and science [1]. Some of these radiations are categorized as ionizing radiation. Based on their energy and nature of interaction with a medium, the electromagnetic and particle radiation falls into the category of ionizing radiation. The ionizing radiations are further divided into; (i) directly and (ii) indirectly ionizing that has a very profound effect on any kind of organic life and is therefore a matter of study for the welfare of human kind. Generally there are two sources of ionizing radiation; (i) cosmic and earth crust and (ii) manmade. With the advancement of technology, new systems like nuclear reactors, accelerators, imaging equipment for medical applications and nuclear medicines, radiation have become a part of civilization. These systems utilize the radiation for the welfare of society but at the same time become the source of radiation that may be harmful too [2]. Therefore it becomes necessary to monitor and control these radiations to maximize the benefits at minimum cost in terms of side effects.

Ionizing radiations interact with materials by depositing their energy partially or fully in the medium along its path. The interaction of radiation with the matter depends on the energy and the type of radiation and is specific for a particular type. The energy deposited by the radiation in the medium is of great concern and is required to be measure accurately in various activities and applications [3]. Furthermore, as the impact of radiation associated with radiation facilities is high, monitoring of personnel involved in these facilities becomes a strenuous and stringent requirement.

The deposition of energy by radiation in the medium is called dose and is defined in terms of energy deposited per unit mass of the medium. The materials/equipments used to measure the radiation dose are called dosimeters [4]. Apart from personal dose measurement, there are also specific demands for accurate dose assessment for environmental and in space related experiments [5]. Depending upon the interaction of various ionizing radiations with matter, different kinds of detection techniques and dosimeters have been developed and used over the period of time for the assessment and accurate dose measurements. In general, a dosimeter is a kind of devices that quantify or analyze, either directly or indirectly exposure, kerma, absorbed dose, equivalent dose or other associated quantities of the ionizing radiation. A dosimeter along with its reader is referred to as a dosimetry system. The various kinds of dosimetric system available are described briefly:

1. Ionization Chamber Dosimetry: These types of dosimeters measure the charge from the number of ion-pairs generated by the radiation when it interacts with a gas medium of the chamber. It is one of the simplest systems to measure radiation dose over a wide range of energies and is widely used in the nuclear power industry, research labs, radiography, radiobiology, and environmental monitoring. The well known examples of ionization chamber based dosimeters are cylindrical (thimble type) ionization chamber, parallel-plate (plane-parallel) ionization chamber, brachytherapy chamber, extrapolation chambers, segmented chamber etc [6].
2. Film Dosimetry: This dosimetry uses silver film emulsion sensitive to radiation to measure the dose. It is generally used as personal dose monitor. This device was first

developed by Ernest O. Wollan whilst working on project Manhattan. The main disadvantage of these types of dosimeters is their energy dependency [7].

3. Semiconductor Dosimetry: Silicon diode (p-n junction diode) and metal–oxide–semiconductor field-effect transistor (MOSFET) are used as semiconductor dosimeters. The charges (minority carriers) produced by the radiation within the medium (depletion region) are collected by the electric field due to the intrinsic potential and generate a current in the reverse direction in the diode which is proportional to the dose. They are mostly used for in-vivo dosimetry for patient with online readout. These dosimeters gradually loss their sensitivity with use and need to be calibrated for reuse [8].
4. Luminescence Dosimetry: In this type of dosimetric systems special kind of luminescent materials, called dosimeters are used. The specific properties of these materials are that interaction with the radiation produces electron hole pairs and few of these electron and holes get trapped at defects sites called trap centers. Later on, this stored information can be retrieved by a system called reader. Based on the reader technique there are two types of dosimeters; (i) Thermally stimulated luminescence (TSL) dosimeters; are materials that emit light when heated after exposure to ionizing radiation and (ii) Optically stimulated luminescence (OSL) dosimeters; are materials that upon excitation with a light source, emit light of shorter wavelength than the excitation source after exposure to ionizing radiation [9].

Owing to the inherent operational simplicity and cost effectiveness, luminescence dosimetry based on TSL of various phosphors has emerged as the most viable option [10]. The TSL in particular has demonstrated its exceptional adaptability in terms of its successful application in diverse fields of ionizing radiation viz. personnel, environmental, medical and space which arises from its versatile nature and its ability to retrieve dose information in active as well as passive modes [11]. Thermoluminescence dosimeter (TLD) has been a stronghold of health physics professionals for over 50 years [12]. However the OSL based dosimetry is a relatively new technique but is highly promising and is evolving at an unprecedented rate.

The OSL is the light emitted during stimulation of crystalline insulators or semiconductors that were previously excited, typically by exposure to ionizing radiations. The excitation puts the crystal in a meta-stable state, characterized by electrons and holes separately trapped at defects in the crystal lattice. During the OSL process, light stimulates the release of these electrons and holes from these trapping centers, resulting in electron/hole recombination and excitation of luminescence centers in the crystal. The OSL consists of photons emitted when these excited luminescence centers decay to the ground state [13].

At present, of all the types, the dosimeters based on the luminescence materials are most popular and widely used in personal, medical, industrial and environmental dosimeters. Though the branch of radiation dosimetry is quite old but is still evolving either by infusing new technologies in reader systems making the reading faster, more efficient and accurate or by improving the properties of existing materials and discovering new materials [14]. The main thrust of the research has always been to develop the perfect dose reading system and ideal dosimeter material. The desired properties of an ideal dosimeter material and reading system are listed as follows:

i) Desired material properties: Linearity of signal with dose over a wide range, dose rate independence, flat energy response, small directional dependence, readout convenience, tissue equivalence (for personal and medical dosimetry).

ii) Desired reader properties: High signal to noise ratio, high accuracy and precision, convenience of use, high throughput, physical size, simple system, low cost.

Obviously, no single dosimeter can satisfy all the desired characteristics and hence the research on dosimeters continues.

1.2 Literature Survey and Material Selection

Approximately, over two thirds of the known minerals exhibit TSL or OSL properties [15]. In October 28, 1663, Robert Boyle presented the first official report on the discovery of TSL to the royal Society of London, narrating TSL as a 'glimmering light' that was noticed during heating of diamond in dark [16]. The term 'Thermoluminescence' was first used by Eilhardt Wiedemann while examining variety of luminescence occurrence in 1889 [17]. Wiedemann and Schmidth were the first to detect TSL of materials irradiated with cathode rays and they were also the first to probe TSL activators such as manganese, iron and rare earth elements [18]. They were also the first to record TSL of fluorite and CaF_2:Mn [18]. But the actual uplift to the TSL field started by the initiating work of Farrington Daniels and his group on lithium fluoride (LiF) [19]. Simultaneously, the quantitative theory of kinetics of TSL was given by Randall and Wilkins in 1945 and Garlick and Gibson in 1948 [20, 21]. It started with the simple model and helps to analysis different TSL parameters like trap depth, frequency factor, concentration of traps etc. LiF was employed to evaluate the radiation dose after an atomic bomb test in USA. The presence of Mg and Ti in LiF gave the desirable TSL property and its realization emerged from the work of Cameron and colleagues [22] which leads to the patenting of TLD-100 by the Harshaw Chemical Company in 1963 [23]. Later on in 1986, LiF:Mg,Cu,P known as GR-200 was registered as an extremely sensitive material with sensitivity as high as 50 times that of TLD-100 [24]. In 1957, two other materials BeO and CaF_2:Mn were discovered [25, 26]. The CaF_2:Mn was found to have magnificent sensitivity with simple glow curve structure and is still in use. Rare earth doped phosphors such as CaF_2:Dy,

CaF_2:Tm having efficient emission centers, are more sensitive as comparison to the LiF:Mg,Ti phosphor [27, 28]. Further improvements of sensitivity was achieved in $CaSO_4$:Dy with a lower fading rate as compared to others [29]. This was followed by even more sensitive materials such as Al_2O_3:C [30]. In the last four decades, several TSL materials were developed as dosimeters by harnessing their various properties to determine the dose more accurately and effectively. Some of the important materials and their specific dosimetric properties are listed in Table 1.1.

Table 1.1. General Characteristics of Some Commercially Available TLDs.

TLD type	**Effective atomic no.(Z_{eff})**	**Main TL peak (°C)**	**Emission max. (nm)**	**Sensitivity relative to TLD-100**	**Fading (at 25°C) in dark**	**Dose range**
LiF:Mg,Ti (TLD-100, 600, 700) [31]	8.14	200	400	1	5%/year	20 µGy-10 Gy
LiF:Mg,Cu,P (GR-200A) [32]	8.14	210	400	25	5%/year	0.2 µGy-10 Gy
CaF_2:Dy (TLD-200) [27]	16.3	215	480-570	15	8%/2 months	10 µGy-10 Gy
CaF_2:Tm (TLD-300) [33]	16.3	150 240	400-520	-	20%/38 days	1 µGy-10 Gy
CaF_2:Mn (TLD-400) [34]	16.3	260	500	5	16%/2 weeks	10 µGy-10 Gy
$CaSO_4$:Dy (TLD-900) [35]	15.3	220	480-570	30	1%/2 months	2 µGy-10 Gy
$CaSO_4$:Tm [36]	15.3	220	452	30	2%/2 months	2 µGy-10 Gy
BeO (Thermal ox 995) [37, 38]	7.13	190	200-400	0.20	8%/2 months	0.1 mGy-0.5 Gy
$Li_2B_4O_7$-Mn (TLD-800) [39]	7.3	220	605	0.20	4%/ month	0.1 mGy-3 Gy

$Li_2B_4O_7$:Cu [40]	7.3	205	368	2	10%/2 months	10 μGy-10^3 Gy
α-Al_2O_3:C [41]	10.2	190	420	60	5%/year	0.1 μGy-10 Gy
Mg_2Si0_4:Tb [42]	11	200	380-400	40	very slight	10 μGy-1 Gy
MgB_4O_7:Dy/ Tm [43]	8.4	190	490	10	4%/ month	5 μGy-50 Gy

Though, the use of TLD is very popular due to its simple operation and economic, but in last two decades a new type of dosimeter came out that can be read out by optical stimulation instead of thermal stimulation known as OSL dosimeters. The OSL is a versatile technique with some inherent advantages like fast readout, option of multiple readouts, optical resetting of trapped charges and freedom from thermal quenching. Sulfides (MgS, CaS, SrS) were one of the earliest material systems to be investigated as a prospective OSL phosphor for dosimetric applications [44, 45]. BeO is another OSL material that possesses near tissue equivalence, wide separation between emission and excitation wavelengths and low cost. However, its toxicity has discouraged its large scale application [46]. Quartz doped with Cu^+ has been reported to be a strong candidate for OSL based radiation dosimetry [47]. In the recent past, phosphors like MgO:Tb^{3+}, YAG:Ce^{3+},Tb^{3+},C, SiO_2:Cu, BaFBr:Eu too have been reported to possess a high OSL sensitivity [48, 49, 50, 51]. A group at the Oklahoma State University revealed that Al_2O_3:C can be used as a very sensitive OSL phosphor for radiation dosimetry that later became the first commercially available OSL based dosimeter [52]. Some of the OSL phosphor materials developed over the decades and their dosimetric properties are summarized in Table 1.2.

Table 1.2. Summary of OSL materials, relevant properties.

OSL material	**Application or potential application**	**Optimum stimulation wavelength**	**Emission bands and lifetimes**	Z_{eff}
Al_2O_3:C [53]	Personal, environmental, medical and space dosimetry	525 nm (green)	335 nm (<7 ns), 420 nm (35 ms)	11.3
BeO [54]	Personal dosimetry	435 nm (blue)	335 nm (TSL), 380 nm (OSL)	7.2
MgO:Tb [55]	Personal dosimetry	500–570 nm (green)	350–700 nm (Tb^{3+}lines)	10.8
BaFX:Eu^{2+}(X = Br, Cl, I) [56]	X-ray imaging	495 nm, 590 nm	490 nm (750 ns)	~ 50
Cu^+- doped fused quartz [47]	Optical fiber dosimetry	790 nm (red)	540 nm	11.8
Quartz [57]	Luminescence dating, retrospective dosimetry	Blue	365 nm (~30–40 μs)	11.8
Feldspar [58]	Luminescence dating, retrospective dosimetry	IR	Visible (Schott BG-39)	11.5 (albite) 13.7(K-feldspar)
MgS:Ce,Sm SrS:Ce, SmCaS:Ce,Sm [59, 60, 61]	Optical fiber dosimetry, integrated sensor	IR	490 nm (36 ns, 165 ns)	14.6 (MgS) 34.6 (SrS) 18.5 (CaS)
KCl:Eu and KBr:Eu [62, 63]	X-ray imaging, optical fiber dosimetry	560 nm (KCl) 620 nm (KBr)	420 nm (~1 μs)	18.1 (KCl) 31.5 (KBr)

So far, various TSL and OSL materials for radiation dosimetry have been described. A crucial parameter of a good TSL or OSL material is its tissue equivalence that is its ability to mimic the response of a human tissue. In the light of this, **lithium tetraborate ($Li_2B_4O_7$)** abbreviated as **LTB**, commonly known as lithium borate is one of the preferred phosphors in ionizing radiation dosimetry in particular for personal and clinical applications. It has several favourable properties that make it a promising material for dosimetric applications. Equivalence of LTB's Z_{eff} (7.3) for photoelectric absorption to human tissues (Z_{eff}=7.4) effectively rules out the need of energy calibration of the dosimeter [64]. Dosimetric properties of LTB like, a small variation in photon energy response, very low detection limit (~25 microGray) and simple annealing procedure makes it suitable for radiation dosimetry applications. Further, a large band gap (~8eV) of LTB provides a large transparent window that allows several elements as dopant and co-dopants. This particular phenomenon offers a large possibility for defect engineering to tailor the properties of the material to enhance its suitability to particular application [65]. In addition to these favorable properties, constituent elements as ^{10}B and ^{6}Li of LTB show a high thermal neutron capture cross section that offers possibility for the use in neutron and mixed field dosimetry applications.

For the first time TSL properties of lithium tetraborate with Mn as activator was presented by Schulman *et al.* at the 1st International Conference on Luminescence Dosimetry, Stanford, 1965 [66]. This material was characterized by a low sensitivity and a TSL emission in the range of 590 nm (red light) which is unfavorable for the photomultipliers tube used in most TSL readout equipment [39]. The TSL emission spectrum was refined by Takenaga, after introducing Cu-activated LTB powder (by the sintering method) with emission peak at ~370 nm and a good TSL efficiency [40, 67]. The sensitivity was improved 10 times compared to LTB:Mn. Later Prokic developed LTB:Cu sintered pellets with a TSL sensitivity similar to that of TLD-100 [68]. The copper activated LTB phosphors were investigated by many researchers and found the sensitivity higher or equivalent to TLD-100 material (LTB:Mg,Ti) [69,70].

The undoped and Cu-doped of lithium tetraborate single crystals were developed by the Czochralski technique in Ukraine for photoluminescence applications [71]. These transparent and colorless samples (6×6×1 mm^3) exhibited high mechanical sturdiness and had negligible light sensitivity as compared to other types of lithium tetraborate photoluminescence materials. Following these, several studies were carried out to improve the TSL properties of borates either by changing the preparation technique, or by the use of different modifiers and/or activators. These studies involved preparation of phosphor materials in all the three forms, namely, single crystals [72], polycrystalline powders [73] and glasses [74]. With regard to modifiers, several alkali/alkaline metals were used as modifiers to fortify the relative stability of borate glass. With regard to activators, a variety of dopants and co-dopants either transition metals [75, 76] or rare earths [77] have been added to the host by various researchers in order to enhance the luminescence. This enhancement is attributed to the formation of electron traps and/or hole trap centers. Recently it was reported that co-dopants such as In, Ag and Ag+P help in further enhancing the TSL sensitivity of the LTB:Cu phosphor [78, 79]. Ag doped LTB were studied in polycrystalline powder as well as single crystal and it is found that the emission of the material lies in the UV range (270-300 nm) and its sensitivity is slightly improved than the Mn doped LTB and much lower than the Cu doped LTB. The lower sensitivity is due to a mismatch of its emission from the wavelength sensitivity of most of the photo multiplier tubes used in a TSL reader. Luminescence studies on LTB doped with different dopants (Ce, In, Ni, Cu and Ti ions) have been described by many researchers in polycrystalline and glassy samples [80]. Still, the main disadvantages normally pointed out for the current LTB based TSL dosimeters are a substantial light-induced fading and a lowering of dosimetric properties under high humidity atmosphere. The OSL possibility of Mn doped LTB was first proposed by M. Danilkin followed by T. Aydin in Cu doped LTB [81, 82]. There is also report of OSL in Cu and Ag co-doped LTB [83]. The improvement of TSL properties over the year in LTB is given in Table 1.3.

Table 1.3. Comparison of doped $Li_2B_4O_7$ based TSL phosphors prepared using different methods.

Phosphor	**Main TSL peak (°C) Heating rate (°C /s)**	**TSL emission peak (nm)**	**Relative sensitivity to TLD-100**	**Dose range**	**Remarks**
$Li_2B_4O_7$:Mn (0.1 wt %) [39]	200 (1°C /s)	600	0.4	0.1 mGy–10^3 Gy	Emission at 600 nm is far from the good response region of most photo multipliers tube. Material is affected by humidity.
$Li_2B_4O_7$:Mn, Si (0.1, 0.25 wt %) [84]	200 (1°C /s)	600	0.4	0.1 mGy–10^3 Gy	Adding silica (0.25% by weight) improves moisture resistance
$Li_2B_4O_7$: Ag (0.1 wt %) [85]	100 170 (1°C /s)	260 365	-	-	Marginal improvement in the sensitivity and is comparable to that of $Li_2B_4O_7$:Mn
$Li_2B_4O_7$: Cu,Ag (0.02, 0.02 wt %) [86]	-	260 360	1.2	-	Three times higher than $Li_2B_40_7$:Mn
$Li_2B_4O_7$: Cu [40, 67, 87]	205 (7°C /s)	360	3	3×10^{-4}–10^3 Gy	Phosphors prepared by stoichiometric matrix composition exhibit greater moisture resistance
$Li_2B_4O_7$:Cu (0.1 mol %). [68]	-	370	4	3×10^{-4}–10^3 Gy	Marginal increase in sensitivity
$Li_2B_4O_7$:Cu single crystals grown by the Czochralski method [88]	240 (5°C /s)	366	Sensitivity higher than the powder	2×10^{-4}–20 Gy	Minimum detectable dose (MDD) is 10 mGy
$Li_2B_4O_7$:Cu,Ag,Mg (0.02 wt % each) prepared by the sintering technique [89]	Main TSL Peak at 219	421 380 350	-	10^{-4} – 3×10^3 Gy	Ag can enhance the intensity of TSL peak at 219°C and reduce that of TSL peak at 130°C
$Li_2B_4O_7$:Cu,Ag,P powder [78]	165 220 (1°C /s)	365 450	-	10^{-4} – 3×10^3 Gy	Ag and P increases the efficiency of the LTB:Cu
$Li_2B_4O_7$:Cu ,Ag	160	250	-	-	The material were

[83]	230 (1°C /s)	370			found OSL sensitive with MDD of 10 mGy
$Li_2B_4O_7$:Cu [81]	243 (4°C /s)	370	-	10^{-5}-10 Gy (TSL) 1- 60 Gy (OSL)	Possibility of personal dosimetry monitor by OSL.

It is reported that LTB as single crystals has advantageous as dosimeter material compared with polycrystalline materials. Single crystals have higher TSL intensity, good thermal stability and low hygroscopicity compared to other forms [90]. Another advantage of single crystal as compared to other forms is being colorless and transparent which makes it more suitable for luminescence dosimetry application. In addition, they can be used almost indefinitely, since the detector can be annealed to reset its sensitivity [91]. Due to all of the advantages, single crystal detectors give very stable performance and not affected by humidity.

LTB melts congruently at 917°C and single crystals are generally grown by Czochralski technique [92]. The LTB crystallize into a tetragonal lattice (space group $I4_1cd$) with lattice constants $a = b = 9.475$ Å and $c = 10.283$ Å. It possess eight formula units with 104 atom per unit cell and a repeating $(B_4O_9)^{6-}$ basic anionic structural constituent, which contains two planner trigonal BO_3 and two tetrahedral BO_4 motifs [93]. Every oxygen atom covalently binds to two boron atoms and every lithium atom has five neighboring oxygen atoms.

The LTB forms an anion sublattice of $(B_4O_9)^{6-}$ as shown in Fig.1.1, constructed by the boron-oxygen 3-D lattice network associated in a spiral axis of 4I symmetry. Within the sub-lattice, they are weakly attached to lithium atoms and oriented in the [001] direction or c axis and charge compensates the crystal. The lithium atom contributes an electron to the B-O anion subcomponent, thus polarizing the crystal. The band gap of LTB is found to be in the range of 8.9 eV to 10.1 eV in four different crystal orientations as determined by different experimental techniques like photoemission spectroscopy and inverse photoemission spectroscopy [94]. It has a density of 2.44 g/cm^3 and is a strong insulator having resistivity of the order of $10^{10}\Omega$-cm in room temperature.

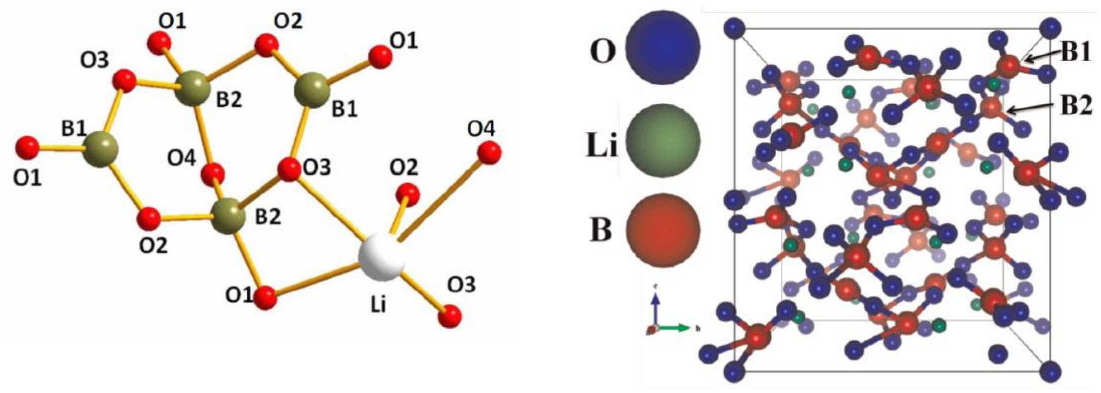

Figure 1.1: *Basic B_4O_9 structural unit of $Li_2B_4O_7$ (left); orientation of B_4O_9 structural units and Li^+ ions in the crystal lattice (right).*

1.3 Scope and Aim of the Thesis

Research on various phosphor materials is an on-going activity to improve the various dosimetric properties of the material for different applications, along with finding new suitable materials. The LTB shows favorable properties for dosimetric applications and Cu is one of the suitable activator for potential use which can be read out by TSL as well as OSL technique. It is also observed that single crystals give the most desired result as far as dosimetric properties are concerned as compared to the polycrystalline material. This thesis deals with single crystals of LTB with two types of activators; Cu and Ag as (a) LTB:Cu, (b) LTB:Cu, Ag and (c) LTB:Ag; for their application in dosimetry.

As the different dopants/activators gives their characteristic dosimetric properties in the materials, the main aim of the thesis is to investigate the dosimetric properties for each of the dopant like Cu or Ag and the effect of co-dopant like Cu+Ag in LTB and further find out the way in which the materials can gives maximum sensitivity for dosimetry application. The defect structure of the LTB:Cu has been reported using various characterization techniques, the details of defect nature i.e. the position of Cu^+ in the LTB lattice is very important in respect of luminescence efficiency. For this purpose, LTB:Cu was investigated in the low temperature regime by photoluminescence (PL) technique. Further it was found that the use of co-dopant like Ag or P with Cu can increases the overall sensitivity of the material. The effect of co-doping in LTB and luminescence process involved was investigated in details using optical absorption (OA), PL and TSL techniques. This work was aimed to improve the sensitivity of the co-doped crystal. The TSL properties of silver doped LTB has been reported but its sensitivity was found to be low as compared to LTB:Cu. As per literature, silver emit in the UV region which is not suitable for most of the TSL reader and this may be the reason of not showing good sensitivity in LTB:Ag. A modified TSL reader with employing a UV sensitive photomultiplier tube was used to investigate the possibility of better efficiency and sensitivity in LTB:Ag. As LTB contains ^6Li and ^{10}B, which has high capture cross section for thermal neutrons, thermal neutrons dosimetry and mixed field dosimetry applications was explored. Neutron dosimetry was also tried to explore by using TSL and OSL techniques. Further the OSL sensitivity of Cu and Ag doped LTB has been investigated for neutron and gamma dosimetry. A setup for online detection of neutrons using the dosimetric technique was designed and measurements were carried out at a beamline of a nuclear reactor.

CHAPTER 2

THEORY AND EXPERIMENTAL TECHNIQUES

2.1 Single Crystals Growth: Theory and Techniques

A material can be transformed into single crystal by slow and continuous solidification of its melt, solution or vapor phase or gradual re-crystallization from a solid phase. Crystal growth is a first order phase transformation that requires the change of phase where atoms or molecules lose their random character gradually in uniform manner and achieve a long-range order in the form of crystalline solid [95]. It is a two-step process that involves nucleation in the first step and growth in the second step through mass transport followed by addition in the lattice of the building units at the active site of crystal surface. In case of nucleation or growth, transformation from solution phase to solid phase takes place because of change in free energy which is favorable under specific conditions (Gibbs 1876, 1878) [96, 97]. Either of the two steps may control the overall growth process depending on the character of the crystal surface, temperature of the system and the degree of supersaturation or supercooling of solution phase. Theoretical understanding of crystal growth process started with the development of thermodynamics and nucleation theories in the late 19th century (Gibbs, Arrhenius, Van't Hoff) and the advent in understanding the role of transport phenomena in the 20th century [98].

2.1.1 *The Thermodynamics of Crystal Growth from Melt*

When the free energy of the solid and liquid phases is equal, the thermodynamic equilibrium between these phases takes place. The free energy of a system is associated to the internal energy and the entropy of the system, is given by the Gibbs equation

$$G = H - TS \tag{2.1}$$

Where H is the enthalpy, S is the entropy and T is the temperature. The creation of a crystal is the process of controlled change of phase from liquid to solid phase. Lowering the free energy provides the driving force for crystallization of the system throughout the phase transformation. The free energy change for such a transition is given by

$\Delta G = \Delta H - T\Delta S$; where $\Delta G = G_L - G_S, \Delta H = H_L - H_S, and\ \Delta S = S_L - S_S$, G_L and G_S refers to Gibbs free energy of liquid and solid states.

At equilibrium; $\Delta G = 0$; $\Delta H = T_e.\Delta S$, where T_e is the equilibrium temperature.

$$\Delta G = \Delta H.\Delta T/T_e, \text{ where } \Delta T = T_e - T \tag{2.2}$$

ΔG becomes negative when $T_e < T$ and it is related to the latent heat of transition. The free energy change of a system can also be regarded as the product of the entropy change ΔS and super cooling ΔT, and written as $\Delta G = \Delta S.\Delta T$. Super-cooling is the state of solution when the liquid is cooled below the melting temperature. This state in a system imparts the driving force for nucleation and further crystallization in case of single crystal growth from melts. A controlled supercooling is a must for the growth of a single crystal from the melt.

Supercooling of the melt is followed by the nucleation that is a process of agglomeration of atoms or molecules to form the first nuclei on which further crystal growth take place. Nucleation may take place spontaneously or it may be induced artificially and is referred as homogeneous or heterogeneous nucleation, respectively. Both these nucleation are called primary nucleation and take place in systems that do not hold crystalline matter. Nucleation can often be induced by external processes like agitation, friction, mechanical shock, electromagnetic fields, extreme pressure, ultraviolet radiation, X-rays, γ -rays, sonic and ultrasonic radiation etc [99]. Numbers of nuclei are often formed spontaneously due to localized condition/fluctuations within the supercooled melt which is called as "embryos". The change in free energy associated with the formation of embryos decides the probability that it will grow to produce a stable nucleus or get destroyed. The free energy of the system decreases by an amount ΔG_v for each unit volume of the solid formation and increases by an amount equal to the surface energy σ**,** for each unit area creation of the solid-liquid interface. So, the change in Gibbs free energy ΔG , resulted during the formation of a spherical embryo of a radius r is given by

$$\Delta G = 4\pi r^2 \sigma - 4/3\, \pi r^3 \Delta G_v \qquad (2.3)$$

Figure 2.1 is a graphical representation of this equation and it shows the contribution of surface energy and volume energy towards the free energy change of the system. The contribution of surface energy increases as a function of r^2 whereas the volume energy decreases with r^3. With the increment in size, the change in net free energy increases, achieve a maximum value and decline for the further growth in the size of the nucleus. The size of the nucleus for which the free energy changes attains maximum value is known as the "critical nucleus". This is the smallest sized embryo that can grow further with reduction in the free energy of the system. However, if the size of the created nucleus is lower than the critical dimension, no further growth is feasible and it will dissolve/merged into the system. The critical i.e. minimum stable sized of nucleus is prevailed by the maximization of equation 2.3 for r, which further gives

$$r^* = -\frac{2\sigma}{\Delta G_v} \qquad (2.4)$$

The rate of nucleation (the number of nuclei created per unit volume per unit time) can be manifested by Arrhenius reaction velocity [100],

$$J = Aexp\left(\frac{-\Delta G^*}{KT}\right) \qquad (2.5)$$

Where, A is a pre-exponential factor, K is Boltzmann's constant, T is the absolute temperature and ΔG^* is calculated by replacing r in equation 2.3 with the critical radius given in equation 2.4.

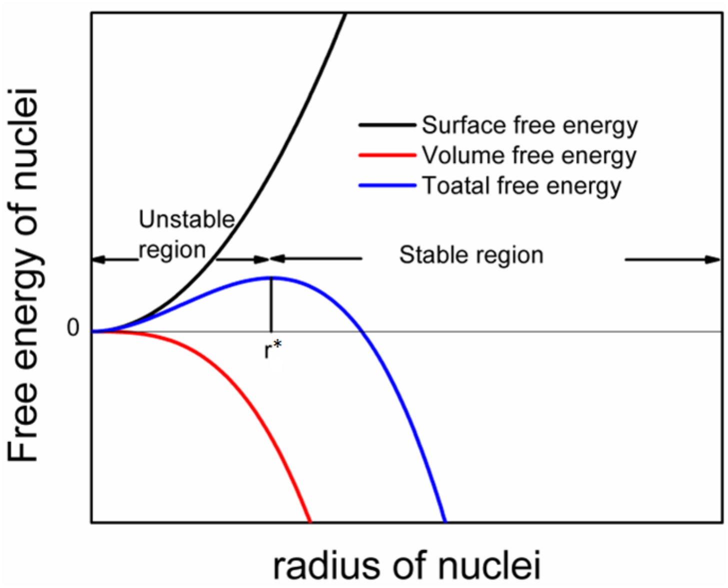

Figure 2.1: *Free-energy curve for the surface free-energy, volume free-energy and total free-energy as a function of radius of nuclei.*

The final step in the growth of single crystal is the growth of a select nucleus. In a supercooled melt, more than one nuclei of the radius greater than the critical radius may be formed. These nuclei may have different crystallographic orientation that is not conducive for the single crystal growth. To have a single crystal one has to kill all but one nucleus. This is done with the help of a proper temperature profile, specially designed crucibles and slow cooling rate (Homogeneous nucleation: generally occurs in the Bridgman growth technique) or by initiating growth by introducing a seed crystal (Heterogeneous nucleation: in the Czochralski growth technique). Nearly all the single crystal growth techniques are based on these steps, though the methods to achieve these stages are different in different techniques.

2.1.2 Techniques for Single Crystals Growth from Melt

Among the total global production of single crystal, 80% of the total numbers of crystals are grown by melt growth techniques despite the fact that it is used only for selected congruently melting materials compared with roughly 5% from vapour, 5% from low temperature solution, 5% from high temperature solution, and 3% from the solid and only 2% by hydrothermal methods [101]. The Verneuil melt growth technique, one of the oldest techniques used for the industrial production of sapphire crystal, is called the father of industrial crystal production [102, 103]. All the other melt growth techniques draw their fundamentals (to control nucleation and then increase the diameter etc) from the Verneuile method like Bridgman method, Czochralski method, Kyropoulos technique, Zone melting technique etc. The choice of a crystal growth technique to grow single crystals of a particular material is not trivial. The suitability of a specific technique for a given crystal is controlled by material properties like melting temperature, melt viscosity, melting behavior, thermal expansion, thermal conductivities and chemical stabilities of melt/solid, requirement of size and quality, vapor pressure of components at melting temperatures etc. The materials studied in this thesis are grown using the Czochralski melt growth technique. In the following section this technique is described in details.

2.1.3 Czochralski Technique (CZ)

The process is named after Jan Czochralski, a polish chemist who discovered the method in 1916 while investigating the crystallization rates of metals [104]. With time, many variations of these techniques like liquid encapsulated CZ method, high pressure CZ method, top seeded solution growth (TSSG) were evolved to grow many complex semiconductors and inter-metallic compounds [101, 105]. The main advantage of this technique lies in the conveniences with which parameters can be controlled during the growth like temperature gradients, growth orientation, the ambient, the forced convection by rotation, applied magnetic field and many others to match the requirement of grown single crystal of particular material. Further benefit of this method is to observe the process of seeding and growth that allows making corrective measures in real time. These points make the CZ as the most versatile and preferred technique for the crystal growth of semiconductors and oxide materials at industrial scale.

In CZ technique, a growth station holds the crucible and heat losses (by conduction and radiation) are minimizes by employing suitable ceramic tubes, felts, and wools. The starting charge, which could be pre-synthesized phase in powder form, or a stoichiometric mixture of constituents or polycrystalline chunk is taken and melted in a crucible by heating it in a suitable furnace (resistive heating, radio frequency (RF) heating, Arc heating, etc). To initiate the crystal growth a seed crystal/wire/capillary is slowly lowered and brought in contact with the melt at the center of the crucible. The melt temperature is tuned to create thermal equilibrium between the rotating seed and the melt. The seed is subsequently withdrawn (pulled) in a controlled way confirming that pull rate (at a typical rate 0.2-5 mm/h) is smaller or equal to the rate of melt crystallization, establishing again a dynamic equilibrium between the two phases with rotation (at a typical rate of 5-25 rpm). Under normal conditions (if there is no stoichiometric deviation due to decomposition and dissimilar evaporation of melt components), the power required to maintain the melt temperature is nearly constant during the growth. The shape of the crystal can be determined by controlling the diameter of the growing crystal through the manipulation of the melt temperature and pull rate depending on properties of the material under consideration. After the completion of the crystal growth with desired length and diameter, the process is terminated by suitably adjusting pull rate and temperature at the solid-melt interface. Then the grown crystal is retained close to the melt surface and cooled down to room temperatures at a slow cooling rate suitable for the material.

Theoretically, every material which melts congruently and does not undertake any phase transition throughout cooling, can be grown by this technique but there are some practical restrain that put some limits on the materials which can be grown by this technique [101]. These limits are: suitable crucible material (nonreactive, withstand high temperatures, easy in cleaning, easy in fabrication, e.g. platinum, iridium, graphite, quartz etc), a low vapor pressure of melt, high thermal conductivity of the material (to conduct away the heat released from crystallization at the solid-melt interface) etc.

Crystal growth system: The experimental set up for crystal growth using CZ technique is termed “CZ crystal puller”. The CZ crystal puller is equipped with an RF heating coil, a weighing device and control circuit for power and weight. A photograph and schematic of an automatic diameter controlled (ADC) crystal puller system Model: Oxypuller, Cyberstar, France used in the present work is given in the Fig.2.2. This system employed 50 kW and 20-100 kHz induction supply, a weighing head of 6 kg capacity with an accuracy of 10 mg and total crystal translation of 600 mm with positioning accuracy of 0.01 mm. The system controls the diameter of the single crystal through a closed-loop feedback system. The ADC software generates the reference growth rate (solidified mass/h) based on the predefined geometry of the single crystal to be grown. The difference between the reference growth rate and actual growth rate (as measured by the weighing device) of the system produces an error signal and feed through a proportional–integral–

derivative (PID) control to regulate the power so that error signal comes close to zero [106].

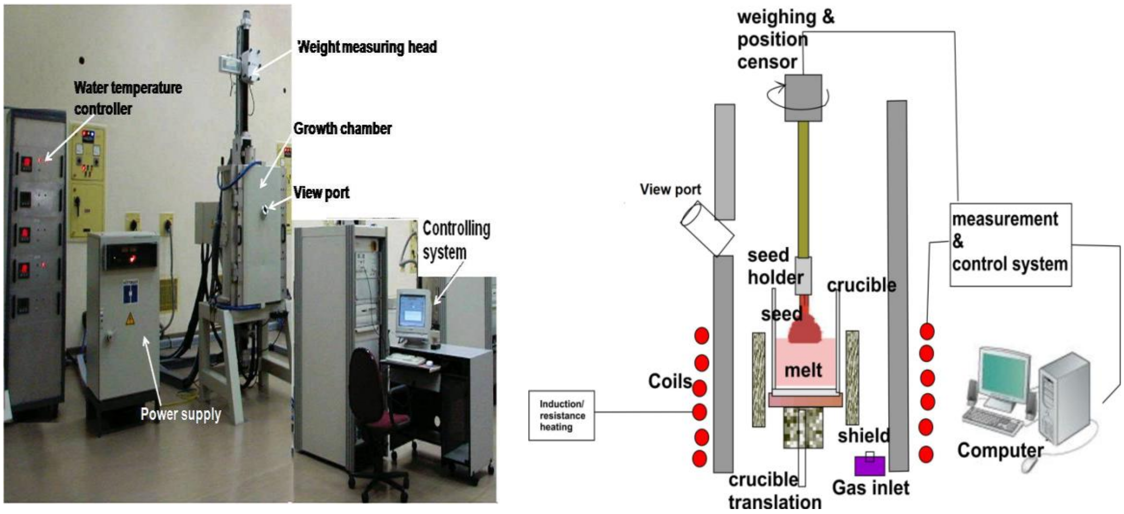

Figure 2.2: *Photograph of the Crystal puller system [Cyberstar make Oxypuller] along with schematic of CZ puller.*

For crystal growth of $Li_2B_4O_7$, a flat bottom platinum (Pt) crucible of 50 mm diameter, 50 mm length and 2 mm wall thickness was used for containing and melting of the starting charge. For thermal shield of the crucible, it was surrounded by ceramic cylinders and fibrous zirconia wool. In different growth experiments the temperature gradient in the growth zone could be adjusted in the range of 20^{o}C/cm to 80^{o}C/cm by changing the arrangements of thermal shields and also by suitable adjustment of the crucible position with respect to the induction coil [107]. The input control parameters for personal computer (PC) are pull rate, rotation rate, densities of solid crystal/melt, diameters/lengths of the crystal seed, shoulder, cylindrical, tail portions and translation length for crystal detachment. Accurate system control also requires inputs on proportion and integration term as governed by thermal inertia of the hot zone and temperature oscillation occurring in the melt which in turn depend on the material properties.

2.2 Thermally Stimulated Luminescence (TSL): Theory and Experiments

TSL is emission of UV-Vis photons (not black body emission from matter) on heating of an insulator or semiconductors that has interacted with ionizing radiation. The phenomenon of TSL is mostly observed in insulators/semiconductors having meta-stable trap levels in their forbidden band gap due to presence of impurities and defects. The TSL process can be understood in terms of the band structure model of insulators [108]. A pure insulator has an almost filled valence band separated from an almost empty conduction band by a forbidden gap of few eV. However, the electrons from valence band can be excited to conduction band by supplying sufficient energy (energy greater than the band gap energy E_g) to it. The excitation of electron into conduction band leaves a vacancy in valence band that is called “hole” and together they are called electron-hole pair. A schematic diagram of the band structure of an insulator and electronic transition is shown in Fig.2.3.

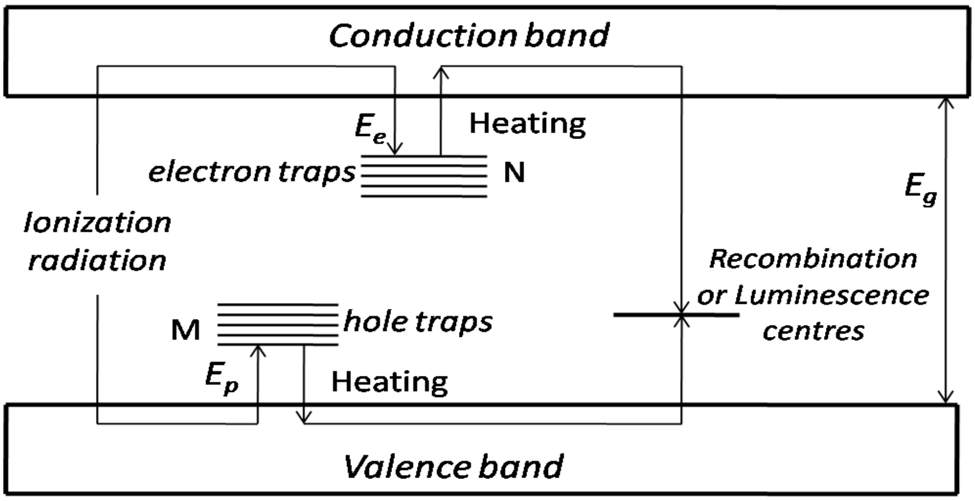

Figure 2.3: *Energy-level presentation of the thermally stimulated luminescence process, N= the total concentration of electron traps with energy E_e, M=the total concentration of hole traps with energy E_p.*

In a relatively perfect crystal, the electron-hole pairs move freely through conduction and valence band and get recombined after certain time. However, imperfections in the crystal, associated with impurities and/or lattice defects may generate new localized or metastable energy levels in the forbidden band gap. The positions of these energy levels depend on the nature of the imperfections/defects and the host lattice. Some of these centers act as recombination centers while some may trap an electron or a hole and so are called electron or hole trap centers, respectively. When such materials (insulators with defects centers) are exposed to ionizing radiation, the electrons and holes are generated and moves freely through conduction and valence band until either they get trapped at a trap level or recombined at a recombination center. In this way the trap centers record and store the exposure history of the material. On heating, the trapped charges get excited by thermal energy that leads to release of one type of charge carriers (e.g. electrons or holes) to respective de-localized band and their subsequent recombination with trapped charges of opposite polarity at a recombination center giving rise to emission of light known as TSL.

2.2.1 TSL Theory

2.2.1.1 Randall-Wilkins Model (First-Order Kinetics)

In 1945 Randall-Wilkins [20] suggested simplest one trap one recombination (OTOR) model for TSL, based on the following assumptions: (i) Re-trapping is negligible compared to the probability of recombination (ii) the population density of the electrons in the conduction band (n_c) is negligible compared to the number of trapped electrons (n) (iii) luminescence intensity at any temperature is directly proportional to the rate of de-trapping of charge carriers. Here, if at a particular time 't', 'n' is the concentration of filled traps at a trap depth of '*E*', then during heating, the intensity of TSL with time is proportional to the rate of change of population density of trapped electrons, and can be given as,

$$I(t) \propto -\frac{dn}{dt}\ ; \qquad\qquad \frac{dn}{dt} = -nP \tag{2.6}$$

'*P*' is the escape probability for a single electron/hole per second and is given as

$$P = s\ \exp\left(-\frac{E}{kT}\right) \tag{2.7}$$

Here $'\exp\left(-\frac{E}{kT}\right)'$ is the probability of the de-trapping of the electron from trap depth 'E' at temperature 'T' in single attempt and 's' is the number of attempt per second made by electron/hole to escape called 'frequency factor'.

$$\frac{dn}{dt} = -ns\ \exp\left(-\frac{E}{kT}\right) \tag{2.8}$$

The negative sign indicates that the population density of trapped electrons *n* decreases with time or temperature. Assuming a linear heating rate of β (= dT/dt), and substituting it in equation (2.8) and on subsequent integration, we obtain

$$n = n_0 \exp\left[-\frac{s}{\beta}\int_{T_0}^{T} \exp\left(-\frac{E}{kT}\right) dT\right] \tag{2.9}$$

Where, n_0 is the number density of trapped electrons (m^{-3}) which is dependent on the radiation dose.

The intensity *I(T)* of TSL at the temperature *T* in Randall-Wilkins model is,

$$I = -\frac{dn}{dt} = n_0 s\ exp\left(-\frac{E}{kT}\right) \exp\left[-\frac{s}{\beta}\int_{T_0}^{T} s\ exp\left(-\frac{E}{kT}\right) dT\right] \tag{2.10}$$

Where, *E* is the activation energy (eV), *s* is the frequency factor (s^{-1}), T_0 is the starting temperature, *T(t)* is temperature at any time t, $\beta = dT/dt$ is the heating rate (Ks^{-1}) and *k* is the Boltzman's constant (eV K^{-1}). Intensity builds up as T increases, reaches a maximum value at 'T_m' and then falls with further heating of the sample. At $T = T_m$, $dI/dT = 0$, one can obtains the condition of maxima of TSL peak as

$$\frac{\beta}{kT_m^2} = s\ exp^{-E/kT_m} \tag{2.11}$$

Equation (2.11) indicates that (a) at constant heating rate β, T_m (peak temperature) we observe shift in towards higher temperature as E increases or s decreases, (b) for a given trap (i.e. constant E & s), T_m shift towards higher temperature as β increases.

2.2.1.2 Garlick-Gibson Model

The Randall-Wilkins model (first order) neglects the re-trapping of the electrons released from the traps. This is an idealistic assumption but during heating, there is a possibility that freed electrons or holes may get re-trapped in the traps during TSL process. Garlick and Gibson [21] in 1948 proposed a new model, which takes into account the re-trapping during the TSL measurement. For simplicity they assumed that the escaping electron/hole from the trap has equal probability of either being re-trapped or of recombining with hole/electron in recombination center.

Let us consider, N = concentration of traps, n = electrons in N, m = concentration of recombination center and n = m for charge neutral condition. The probability that an electron escapes from the trap and recombine in a recombination center is given by

$$\frac{m}{(N-n)+m} = \frac{n}{N} \tag{2.12}$$

and TSL intensity i.e. $I(T)$ at the temperature T is

$$I \propto -\frac{dn}{dT} = \frac{n^2}{N} P = \frac{n^2}{N} s \exp\left(-\frac{E}{kT}\right) \tag{2.13}$$

that can be expressed as

$$I = \frac{n_0^2 s \, exp(-\frac{E}{kT})}{N\left[1+\frac{n_0 s}{\beta N}\int_{T_0}^{T} \exp\left(-\frac{E}{kT}\right)\right]^2} \tag{2.14}$$

The TSL intensity in Garlick-Gibson model is proportional to n^2, implying that the order of kinetics is two i.e. second order. A second order glow curve arises because of the increased possibility of re-trapping as compared to the first-order case i.e., the light emission is delayed. TSL emission during the second half of the peak in second order will have more than for a first-order TSL curved. Therefore, the TSL glow curves are symmetric in Garlick-Gibson model compared to Randall-Wilkins model.

2.2.1.3 Model for General Order Kinetics

The situations in which re-trapping and recombination probabilities are not equal (neither first order nor second order) can be explained by general-order kinetics. In such conditions, the order of kinetics is neither one nor two but between one and two or greater than two. May and Partridge [109] in 1964 proposed an empirical relation representing general order TSL kinetics for such conditions

$$I = n^b s^1 \exp\left(-\frac{E}{kT}\right) \tag{2.15}$$

Where s^1 has dimensions of $m^{3(b-1)}s^{-1}$ and b is defined as the general order parameter (usually between 0.5 and 3). However, 's' does not have much physical significance and the dimensions of 's' change with the kinetic order. A more logical form of the general order kinetics is given by rearranging the general order kinetic equation as proposed by Rasheedy [110]

$$I = -\frac{dn}{dT} = \frac{n^2}{N} p = \left(\frac{n^b}{N^{b-1}}\right) s \exp\left(-\frac{E}{kT}\right) \tag{2.16}$$

This reduces to the first and second-order kinetics equations for b =1 and b = 2. The advantage of the Rasheedy's proposal on general-order model of TSL is that the difficulty encountered in the interpretation of 's' in May and Partridge model is removed.

TSL can provide a perfect passive measurement i.e. integrated irradiation doses over extended duration of the order of years. Thus, it finds immense use in the monitoring of doses received by radiation workers on a routine basis; weakly/monthly/yearly. It should however be borne in mind that most of the TSL phosphors are not tissue equivalent (in terms of energy absorption by irradiation) and hence the relevant dose which is medically significant to a radiation worker from protection point of view is not readily obtained. The main basis in the TSL is that light output is directly proportional to the radiation dose absorbed by the phosphor material and hence by a suitable calibration of dosimeter, unknown doses absorbed by the material can be estimated by measuring TSL.

2.2.2 TSL Measurements

Thermally stimulated luminescence (TSL) studies are carried out to probe the electronic trap/defects and luminescence centers of the material. In microscopic point of view, TSL consists of a perturbation of the electronic system of insulating or semiconducting materials, from a state of thermodynamic equilibrium, via the absorption of external energy, i.e. produced by an ionizing radiation, into a metastable state. This is then followed by the relaxation of the system back to its equilibrium condition after thermal stimulation. A plot of the light intensity as a function of temperature is named glow-curve. A glow-curve may contain one or more maxima, called glow-peaks, each corresponding to a specific energy level trap. The TSL may occur over a range of temperature typically varying from -268 to 450ºC. The glow-curve shape and peak temperature depend on many factors like trap depth, frequency factor, kinetic order etc. All these parameters can be calculated by the analysis of glow peaks. The intensity of luminescence is proportional to the original dose of radiation received and traps density in the material.

The system that is used to record the glow curve is generally called TSL reader that consists of a heating element, an optical readout system and one or more electronic networks. To record a TSL glow curve (intensity vs. temperature), small quantities of sample weighing a few mg are taken and given dose as required for the study using a calibrated gamma or beta-source. After irradiation (in dosimetric applications) the glow curves are recorded in the temperature range of 25 – 350ºC employing a linear heating rate of 1-5ºC/s. The schematic of a typical TSL setup is shown in Fig.2.4.

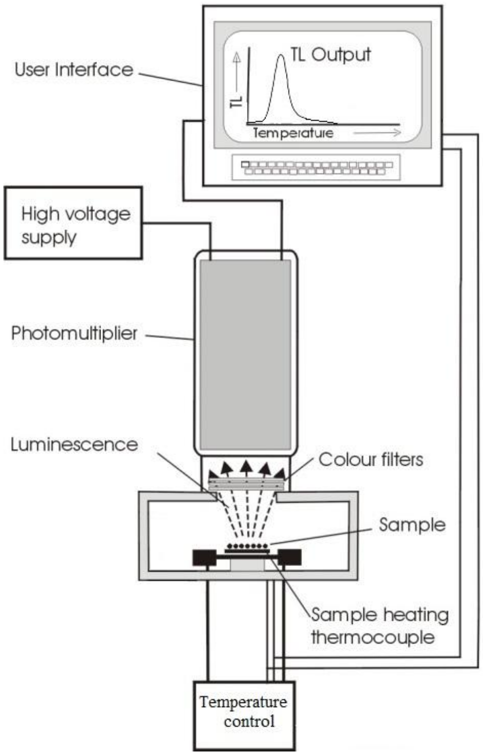

Figure 2.4: *A typical setup for recording thermally stimulated luminescence.*

To record TSL emission spectra, a monochromator (placed between the heater and the reader) is quickly scanned over the 200 to 700 nm range while maintaining the sample isothermal and temperature just below the glow curve peak position. In this study a compact Horiba scientific (H-20UV) monochromator in a low light loss configuration was mounted at an optimized focal distance from the sample. The emitted photons were focused on the monochromator and an output slit corresponding to a window of 10 nm wavelength was selected. To study the spectrally resolved glow curve, the monochromator was fixed at a particular wavelength and corresponding TSL glow curves were recorded.

2.3 Optically Stimulated Luminescence: Theory and Experiments

The first use of OSL in dosimetry was for archeological and geological dating [91]. With time, OSL has found newer applications in the fields of personal, space and medical dosimetry, emerging as a potential technique in dosimetry and related fields. The OSL is a relatively new technique that works on the same basic concepts as TSL except the stimulation energy is supplied by photons in OSL. The plot of the OSL intensity as a function of time gives the information of different parameter of the OSL material. Schematic representation of OSL process is illustrated in Fig.2.5.

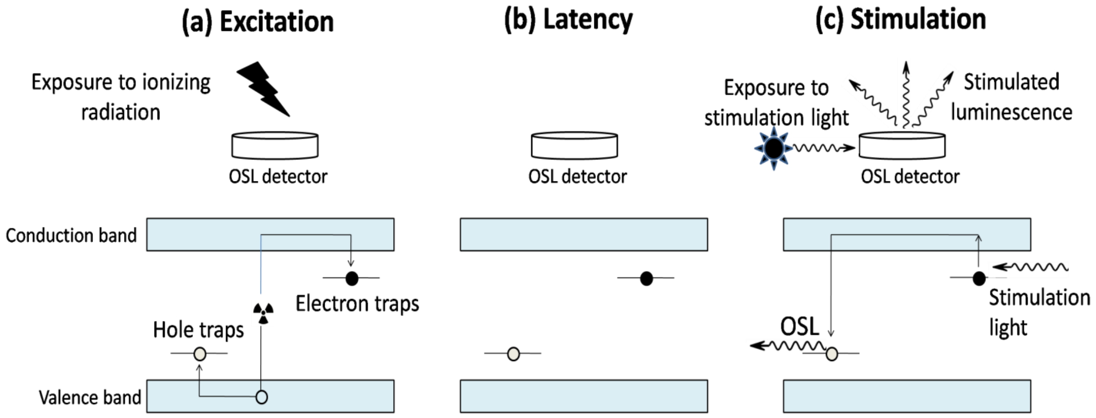

Figure 2.5: *Schematic of OSL process: (a) excitation with creation of free electrons (•) and holes (◦) by ionizing radiation (b) latency period characterized by a metastable concentration of electrons and holes captured at defects in the lattice and (c) stimulation with light, leading to recombination of electron–hole pairs and emission of light (OSL).*

There are three stages associated in the OSL process being: a) **Excitation** in which the OSL phosphor is exposed to ionizing radiation leading to excitations and ionizations and therefore the generation of electron/hole (e/h) pairs across conduction band (CB) and valence band (VB). Subsequently, these e/h pairs has probability of getting trapped at defects in the crystal lattice, the energy levels for which are represented by the short horizontal lines in the band gap, in between the VB and CB (Fig.2.5.a). b) **Latency period** characterized by a metastable concentration of trapped electrons and holes (Fig.2.5.b). If trap depth/potential wells associated with the trapping centers are sufficiently deep, then the thermally induced escape probability of the trapped charges is negligible at room temperature. This stable concentration of trapped electrons and holes is related to the energy absorbed by the crystal during the excitation process, that is, to the absorbed dose of radiation; it represents latent information about the radiation field [91]. c) **Stimulation** by light that is eventually used to read information stored in the OSL detector (Fig.2.5.c). Here a photon of wavelength λ_{stim} (e.g., green light) stimulates the electron to the conduction band. As the electron is free to move in the delocalized conduction band (but within the confines of the crystal/solid), the electron may reach and recombine with the trapped hole that creates a defect in the excited state and get relaxed by radiative transition to the ground state by emitting a photon (OSL light) of wavelength λ_{OSL} (e.g., blue light). Notably, OSL differs from photoluminescence in that the latter involves intra-band transitions rather than ionization of traps [91].

2.3.1 OSL Theory

The transition of charge between energy levels during irradiation and following optical stimulation in phosphor material can be described by a series of non-linear and coupled rate equations. Based on the analysis of OSL signal with absorbed dose, several energy level models have been proposed. Each of these models assumes the transport of electron through the conduction band in order to reach the trapped holes at the radiative recombination site. The simplest model by which OSL can be produced is one trap and one recombination centre (OTOR model) [111]. The charge neutrality for OTOR system can be written as,

$$n_c + n = m_v + m \tag{2.17}$$

Where n_c and n are the concentrations of electrons in the conduction band and the traps, and m_v and m are the concentrations of holes in the valence band and the hole traps respectively. At the end of irradiation if we consider $n_c = m_v = 0$, then we may write that at the start of optical stimulation $n_0 = m_0$. During optical stimulation the charge neutrality condition demands, $n_c + n = m$, from which we may write the rate of change of various concentration as

$$\frac{dn_c}{dt} = -\frac{dn}{dt} + \frac{dm}{dt} \tag{2.18}$$

The terms on the right hand side can be explicitly written as

$$-\frac{dn}{dt} = np + n_c A(N-n) \ and \ \frac{dm}{dt} = n_c A_m m = \frac{n_c}{\tau} \tag{2.19}$$

Where p is the rate of stimulation of electrons, A is the probability of capture of free electrons, A_m is the probability of recombination of free electrons with trapped holes of concentration m and $\tau = 1/A_m m$, the free electron recombination life time. With the assumptions of quasi-equilibrium approximation ($dn_c/dt \ll dn/dt$, dm/dt and $n_c \ll n, m$) and negligible re-trapping $[n_c A(N-n) \ll np, n_c A_m m]$, this leads to

$$I_{OSL} = -\frac{dm}{dt} = \frac{dn}{dt} = np \tag{2.20}$$

The solution of which is

$$I_{OSL} = n_0\, p \exp(-tp) = I_0 \exp\left\{-\frac{t}{\tau}\right\} \tag{2.21}$$

Where n_0 and I_0 are the initial concentration of trapped electron and OSL intensity at time t=0 and τ is the decay constant. This is the first order model which leads to simple exponential decay of OSL intensity with constant optical stimulation. The excitation rate 'p' is given by the product of the excitation intensity, φ and the photo-ionization cross section, σ. i.e. $p = \sigma\varphi$. For multi trap centers with no re-trapping for CW-OSL signal the equation (2.21) can be written as

$$I_{osl} = \sum_{i=1}^{n} n_i p_i \exp(-tp_i) \ , \ p_i = \sigma_i \varphi \tag{2.22}$$

Where, n_i is the initial concentration of charge carriers trapped in i^{th} type trap after irradiation, σ_i is the photoionization cross-section of the trapping center, and φ is the photon fluence rate of stimulation light (photons/cm^2/s)

For significant re-trapping i.e. for general order kinetic, the equation modifies to

$$I_{OSL} = n_0\, p \exp(-tp) = I_0 \exp\,(-\mathrm{t}/\tau)^{\beta}\text{ , with } 0<\beta<1 \tag{2.23}$$

2.3.2 OSL Setup and Measurements

An OSL reader basically consists of two essential elements: a stimulating light source to the OSL phosphor and a detector to detect the luminescence from the phosphor. To select the stimulation wavelength or band that is optimum for a specific OSL material, a stimulation filter is usually placed between the light source and the OSL material with negligible loss of stimulation light. To detect the OSL, a light transducer or detector of high sensitivity and low noise, typically a photomultiplier tube (PMT) is used. Detection filters are placed between the PMT and the OSL material to block the scattered stimulation light and isolate specific OSL emission bands characteristic of the OSL material. The optical elements and detector holder are secured in place in a light-tight enclosure. The major problem in designing an OSL reader is to discriminate the OSL from the stimulation light, which have intensities many orders of magnitude higher than the OSL, while optimizing the collection of OSL by the light detector. Therefore, there is a significant signal-to-noise problem and OSL reader design involves the judicious choice of stimulation light, stimulation filters, light detector and detection filters appropriate for each OSL material. Along with the choice of stimulation wavelength, optimization of the readout process also involves the determination of the best optical modulation and duration of the stimulation intensity. Several approaches for stimulation in OSL readout are as follows. 1) Continuous-Wave OSL (CW-OSL) 2) Pulsed OSL (POSL) 3) Linear

Modulation OSL (LM-OSL). CW-OSL is the most widely used stimulation method in dosimetry and luminescence dating due to its simplicity and satisfactory performance. In this case a light of constant intensity illuminates the sample and emitted photons are detected while illumination is on. The only discrimination, here, between OSL and stimulation light is based on wavelength separation ($\lambda_{OSL} \neq \lambda_{stim}$). Therefore, it is essential that the transmission band of the detection filters does not overlap with the spectrum of the stimulation light, which is determined by the light source and optical filters used in front of it.

During the course of this work, OSL studies were performed at room temperature in the Risø TL/OSL Reader [112] Model DA-20. A schematic of the instrument is shown in Fig.2.6. The samples were irradiated using a β-source (^{90}Sr/^{90}Y, 1.95 GBq) for different doses. The optical stimulation was provided by blue light emitting diodes (λ_{stim}= 458 nm and Δλ= 10 nm) and the emission was detected by a PMT (ET make, Model-ET9235-QB which has an extended UV response with a detection efficiency maximum between 165 nm to 630 nm). A 5 mm thick glass filter (Hoya U-340) was used to prevent the stimulating radiation from reaching PMT. The light intensity at the sample position was measured to be 40 mW/cm^2 for a 350 mA DC through LED cluster. The luminescence intensity was recorded using a photon counting module interfaced to the computer.

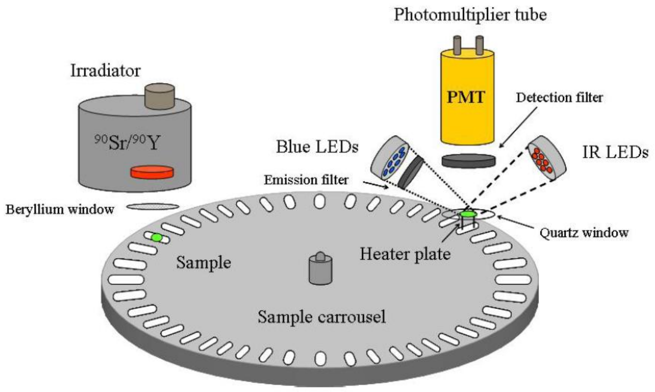

Figure 2.6: *Schematics of the Risø TL/OSL reader (Courtesy Risø National Laboratory, denmark) [113].*

2.4 Photo-Luminescence (PL)

Photo-luminescence (PL) is the emission of UV-Vis-NIR photons from any form of matter after the absorption of UV-Vis-NIR photons. In general, there is a Stokes's shift between absorbed and emitted photon. The wavelength dependent intensity pattern of emitted energy is called emission spectrum, while the distribution of wavelength dependent intensity that causes the emission is known as the excitation spectrum [114]. The PL studies of a material may elucidate the electronic structure and dynamics of excited electronic states, as it is related to the difference between two electronic states, viz. the excited state and the ground state. The difference in the timing between the absorption of the higher energy photon and emission of secondary photon from lower energy is defined by the luminescence decay time or the lifetime of excitation states. The magnitude of the decay time may vary over several orders for different materials and it also depends on whether the transition is allowed or not. In the present work, PL studies were performed over wavelength range from 200 to 800 nm and temperature range of -196 to 27ºC employing Edinburgh fluorescence spectrometer (Model FLP920). The schematic of the system is shown in Fig.2.7. [115].

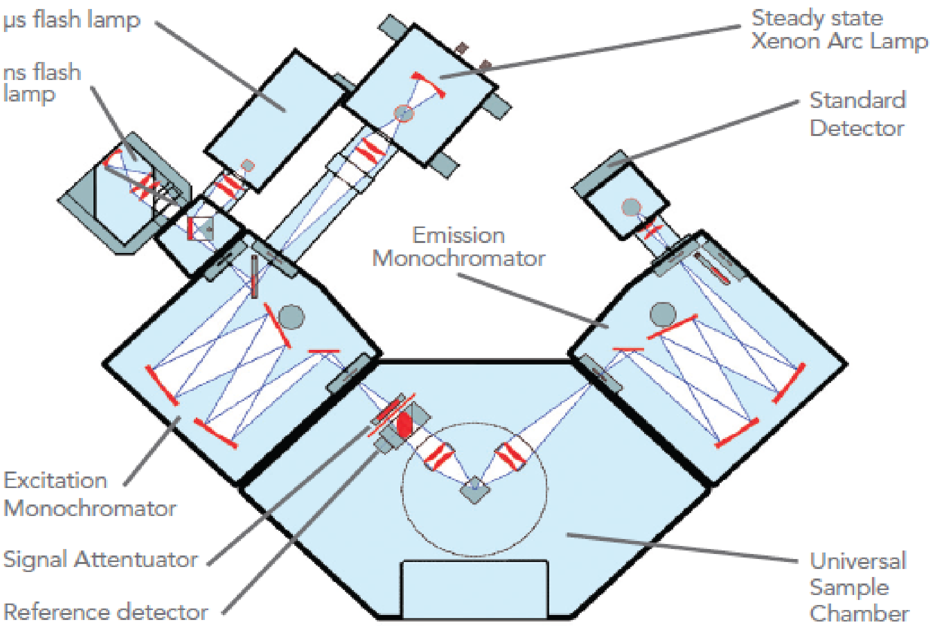

Figure 2.7: *The schematic diagram of fluorescence spectrometer FLP920.*

The spectrometer comprises of an excitation source, excitation monochromator, sample chamber, emission monochromator and detector. As an excitation source, 150 W Xenon flash lamps with 10 μs pulse width were used for recording excitation, emission and decay times. A spectral bandwidth of 1 nm was selected for both excitation and emission monochromators. The lamp produces a broad spectrum of high intensity radiation in UV-Vis-NIR range which is focused onto the entrance slit of the excitation monochromator. A specific excitation wavelength with a bandwidth is selected by the monochromator and passed from an iris (so that the intensity can be controlled) and then focused onto the sample. A portion of luminescence from the sample is collected by a lens system and focused onto the emission monochromator. The emission monochromator selects a wavelength having a bandwidth of this emission and the light is focused into a photomultiplier tube (PMT) for recording. All the emission and excitation spectra were recorded in the reflection geometry by positioning the samples at an angle of 45^o to the excitation beam. Low temperature measurements were carried out by placing the sample in Oxford Cryostat (Model: Optistat DN) and fit to the FLP920. All the recorded luminescence spectra were corrected for spectral sensitivity function of the instrument. The correction file for excitation was produced by recording the spectra under identical conditions after replacing the sample by a standard scatterer.

The lifetime measurement was carried out in this system based on Time Correlated Single Photon Counting (TCSPC) technique [116]. The TCSPC measures single photons – namely, detection at the quantum limit. The technique requires an excitation source with high repetitive pulse output. The schematic of this technique is shown in Fig.2.8. The method makes use of the fact that for low level high repetition rate signals, the light intensity is generally so low that the probability to detect one photon in one signal period is much less than one. As the process of capturing a single photon is reoccurred several thousand or even million times per second, a significantly high number of single photons are processed for the resulting fluorescence lifetime measurement. The TCSPC electronics can be compared to a fast stopwatch with two inputs. The clock is commenced by the START signal pulse and stopped by the STOP signal pulse. The time elapsed for one START – STOP sequence will be represented by an increase of a memory value in a histogram, in which the channels on the x-axis represent the time. With a high repetitive light source, millions of START – STOP sequences can be measured in a short time. The resulting histogram counts versus channels will represent the fluorescence intensity versus time.

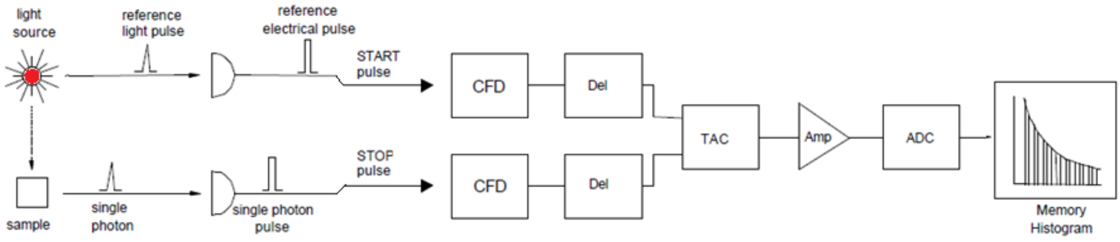

Figure 2.8: *The schematic of TCSPC technique.*

2.5 Optical Transmission

Transmission/absorption spectroscopy is carried out to probe the optical quality of single crystals and find out absorption levels introduced by dopants or impurities and find out the optical band gap. Optical transmission/absorption measurements were carried out on a spectrophotometer, which measures the fraction of incident light transmitted/absorbed through a sample (kept in air or vacuum) [117]. The ratio of the intensity of light passing through a sample (I), to the intensity of light without passes through the sample (I_o) is called the transmittance, and is usually expressed as a percentage (%T). The absorbance, A, is related to the transmittance as

$$A = -\log\left(\frac{T}{100}\right) \tag{2.24}$$

In the present work optical absorption/transmission measurements were carried out in the range from 200 nm to 1100 nm. The schematic diagram of a double beam UV/VIS spectrophotometer (model: Chemito 2500) is shown in Fig.2.9.

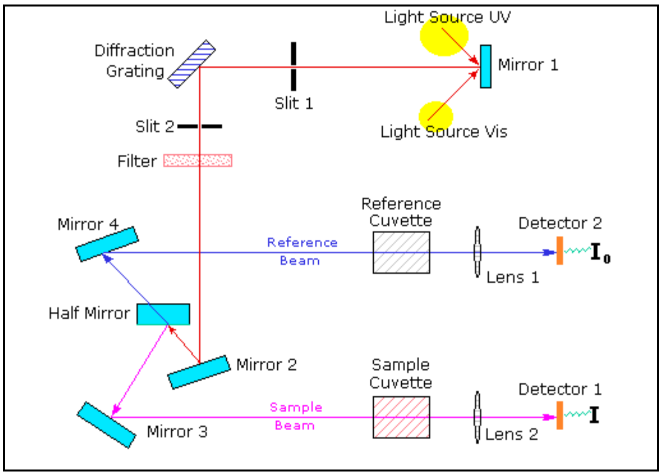

Figure 2.9: *Schematic diagram of a double beam UV-VIS-NIR spectrophotometer.*

In this technique the monochromatic beam of light is split into two identical beams with the help of a beam splitter. These identical beams are then allowed to reach two different detectors and their relative intensities are measured for a baseline correction. Then material is placed in one path of the beam. Transmitted intensity of the light is measured and compared with that of the reference beam, taking into account the base line correction an absolute transmission at that particular wavelength is computed. Here the light is split into two beams before it reaches the sample. One beam is used as the reference and the other beam passes through the sample. Two separate detectors are used for the measurement of light passing through the sample and the reference. Usually two lamps, one deuterium lamp for UV and second tungsten lamp for Vis/NIR, are used to cover UV-Vis-NIR range. Photomultiplier tube is used for UV/Vis (range 190-850 nm) and cooled PbS detector is used for NIR (range 800-2500 nm). Samples were taken in the form of 2-10 mm thick slices prepared from the transverse section of the crystal ingot. The graph of percentage transmission (%T) with respect to wavelength is obtained.

2.6 Powder X-Ray Diffraction (XRD)

The discovery of X-rays in 1895 and X-ray diffraction in 1912 enabled scientists to probe crystalline structure at the atomic level. Powder X-ray diffraction is an analytical technique; primarily used for phase identification and the structure determination of crystalline solid. It is widely used in solid state chemistry and materials science. Other uses of powder XRD are determination of grain size, texture and residual stress of materials or compounds. For such measurements the wavelength of X-rays should be in the range of 0.5 – 2 Å (of the order of distances between atoms or ions in a molecule or crystal). The fundamental of these measurements lie in constructive interference of X-ray beam diffracted from different plane of atoms of crystalline solid as shown schematically in Fig.2.10. The atoms in a crystal are arranged in a regular pattern and give constructive interference between two reflected rays for certain incident angles of the X-ray beam for which Bragg's condition ($2d \sin \Theta = n\lambda$) is satisfied, where d = interplaner spacing, θ = X-ray incident angle, n is a positive integer and λ is the wavelength of incident wave [118]. In powder XRD measurement reflected intensities are measured by moving the detector by 2θ and plotted with respect to the 2θ, giving the powder diffraction pattern. Positions and intensities of the peaks are used for identification of the structure/phase of the material by comparing with available data.

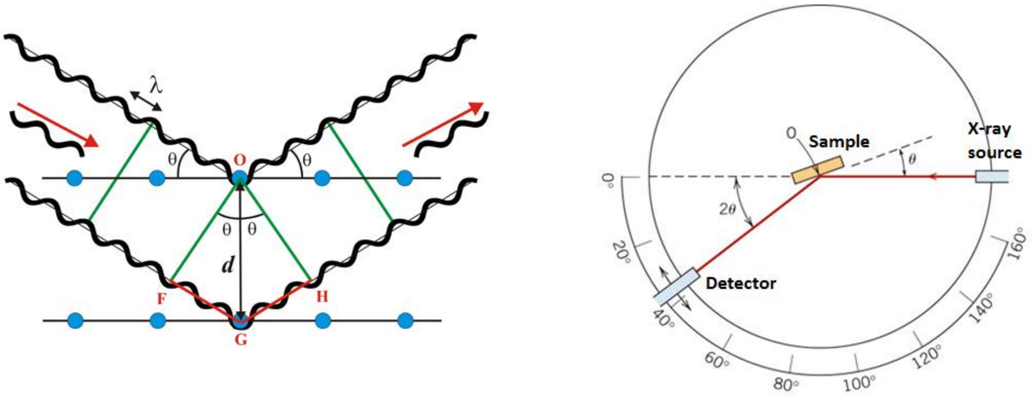

Figure 2.10: *Bragg's law of x-ray diffraction and schematic of X-ray powder diffractometer.*

A typical X-ray powder diffractometer mainly consists of X-ray generator, sample holder and X-ray detector as shown in Fig.2.10 [119]. In the present work, powder XRD patterns were recorded employing Rigaku powder X-Ray diffractometer Model-RINT 2000 consisting of a Cu target X-ray source and a scintillator [NaI(Tl)] detector. The XRD pattern was recorded by employing Cu K_α line (λ = 1.54056 Å) and scanning in the 10°-80° range (2θ) with a typical step size of 0.01°- 0.03° and count time of 1-2 s. Samples for measurements were prepared by crushing the transparent crystal chunks and sieving in to ~10 μm size particles.

2.7 Differential Thermal Analysis (DTA)

The DTA of a material is carried out for determination of phase diagrams (melting/solidification behavior), heat change measurements and decomposition in various atmospheres [120]. DTA gives information of the chemical reaction, phase/structural transformations occurring in samples at different temperatures. Latent energy is either absorbed or released in all the above changes, and this makes the basic principle of DTA experiments. The DTA system (Fig.2.11) consists of two identical crucibles with sample 'S' in one and a reference 'R' (empty crucible) in the second are placed in a furnace in close proximity with a thermocouple located beneath each of them. S and R are made to undergo identical thermal cycles, while recording any temperature difference between sample and reference as a function of time generating DTA plot. This temperature difference indicates endothermic/exothermic reaction or phase change and its magnitude occurring in sample, provides data on the transformations that have occurred, such as glass transitions, crystallization, melting, freezing and sublimation. The DTA of a congruently melting compound would be a single sharp endothermic peak. In case of multi-component system large numbers of peaks are observed and its careful analysis can provide valuable information about its phase diagram.

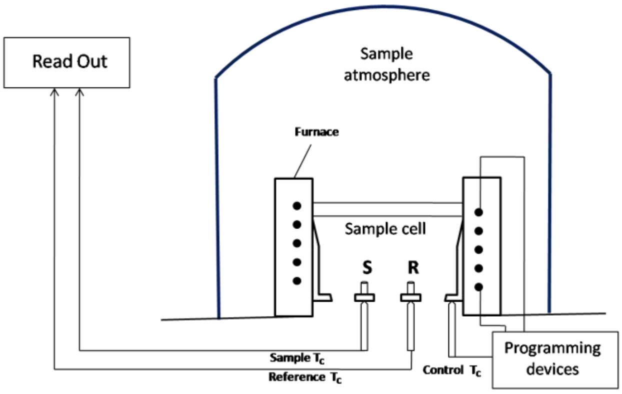

Figure 2.11: *A schematic of differential thermal analysis technique (DTA).*

The DTA measurements for the present work were carried out on SETARAM model TGA-92 in nitrogen atmosphere in the range from 25 to 1600°C. A powdered sample of 30 mg was taken in a 100 µl platinum-rhodium crucible. The temperature was raised uniformly from room temperature to 1600°C with a heating rate of 10ºC/min and dwell time of 300 s at 1600ºC. The system was first calibrated for enthalpy by measuring peak areas on standard samples over specified temperature ranges.

2.8 Laue Back-Reflection

Laue Back-Reflection technique is used to find out the orientation of single crystals [121]. In the back-reflection method, the film is positioned between the x-ray source and the crystal as shown in Fig.2.12.

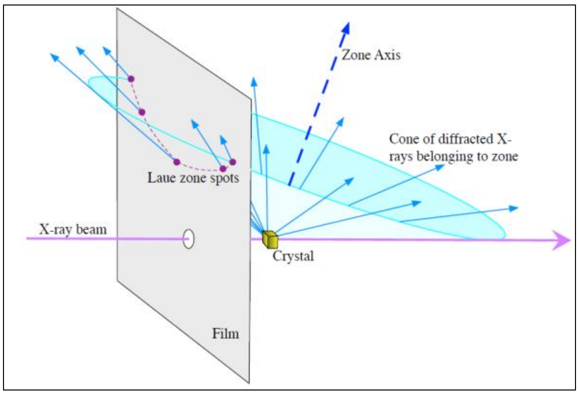

Figure 2.12: *The schematics of Laue back reflection method.*

A white X-ray source is employed to develop the diffraction pattern. As the Bragg angle is fixed for every set of planes in the crystal, each set of planes diffracts a particular wavelength from the white radiation that satisfies the Bragg's law for the values of d and θ associated. Therefore, each point in the diffraction pattern corresponds to a different set of planes. Laue reflections from all planes of the same zone lay on the surface of an imaginary cone whose axis is the zone axis. The film intersects the cone, with the diffraction spots generally lying on a hyperbola, which are seen to lie on curves in the film. Laue Back-Reflection technique for single crystal was recorded with Huber make Laue camera equipped with Cu-target and operated at 40 kV and 30 mA to generate X-ray.

CHAPTER 3

SINGLE CRYSTALS GROWTH AND CHARACTERIZATION OF Cu DOPED $Li_2B_4O_7$

As described in Chapter 1, lithium tetraborate ($Li_2B_4O_7$), LTB is one of the preferred phosphors for personal and clinical thermoluminescent dosimetry (TLD) applications due to its effective atomic number (7.3) which is very close to that of biological tissue (7.4) [122]. Doped LTB polycrystalline materials are used in dosimeters and also available commercially but single crystals may be more advantageous due to some intrinsic property of single crystal [123]. Single crystal does not have any grain boundaries which makes them highly transparent to visible light and very effective for the collection of emitted light from the inner parts of the sample. Also, relatively better resistance to humidity, its stoichiometric composition and easy handling as compared to polycrystalline powder samples make the single crystal form of LTB more suitable for scintillation and TLD applications. From the standpoint of TLD dosimetry, preliminary, Mn doped LTB showed the promising results among other dopants [124]. But due to its near-red emission (~590 nm) which is far from the sensitivity of most photomultiplier tube, the TSL sensitivity of the materials was low. Later on it was found that small doping of Cu makes LTB a thermoluminescent dosimeter with outstanding sensitivities exceeding that of the well-known LiF:Mg,Ti phosphor [125]. Further it is also reported that it can be used as a scintillator suited for the neutron detection [126]. However, doping of copper in the LTB is difficult due to its compact lattice structure. Luminescence studies, with emphasis on photoluminescence, radio-luminescence and TSL of LTB crystals and glasses doped with Cu have been reported by many researchers [71, 74, 124, 127] but most of these studies are confined to room temperature and in a relatively narrow range of excitation energies insufficient to reveal the variety of impurity states which might be involved due to the large band-gap of the material [128].

In this chapter the growth of high quality single crystals of pure and Cu doped LTB by a CZ technique is described. To achieve the high quality crystal, optimization of different growth parameters like pull rate, rotation rate, axial temperature gradient, cooling rate on the crystal growth are discussed. The grown crystals have been characterized for their optical transmission, TSL and OSL properties. Further, to understand the luminescence process thoroughly, temperature dependence photoluminescence characterization of LTB:Cu crystals in the temperature range from -196 to 27ºC has been investigated in details and a possible mechanism has been proposed to explain the temperature dependence of excitation spectra.

3.1 Single Crystal Growth of Pure and Cu Doped LTB

LTB is a congruently melting (at 917ºC) composition in the phase diagram of the Li_2O–B_2O_3 pseudo-binary system [129] as shown in Fig.3.1.

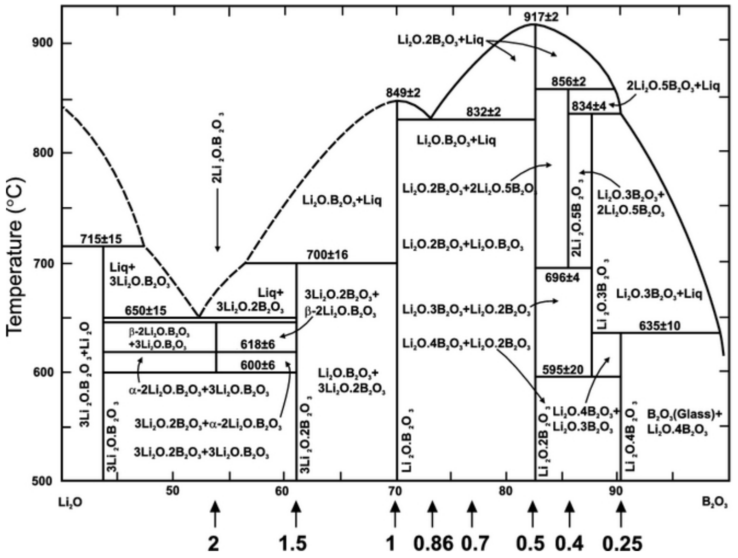

Figure 3.1: *Li_2O-B_2O_3 equilibrium phase diagram (wt %), temperatures in °C. The arrows indicate the Li_2O/B_2O_3 mol ratios of all compositions.*

Single crystals of lithium tetraborate can be grown by various melt growth techniques as discussed in the last chapter, first single crystal growth of LTB was reported by Garrett et al. [130] for use in IR transmission studies. There are several reports on growth of pure and doped LTB crystals up to 4 inch diameter by employing Bridgman as well as CZ melt growth technique [131]. In the present study, the crystals were grown by the Czochralski technique using equipment and process previously described in section 2.1.3 of chapter 2. To establish the optimum growth parameters/conditions for high quality single crystal of Cu doped LTB, proper growth conditions of pure LTB were achieved and subsequently growth parameters for the Cu doped LTB were investigated. Intrinsic property of molten state of LTB, such as, high viscosity, tendency of glass phase formation etc leads to several growth related problems like glass phase transition, core formation, inclusion, bubble trapping etc. All of these barriers are needed to be addressed to grow a single crystal of high structural and optical quality.

To avoid the problem of inclusion from foreign sources, raw materials of very high purity (99.998%) from commercial sources (Aldrich make) were used. High purity (99.99%) platinum crucibles were used to melt and contain the material to avoid contamination. Furthermore, to understand the melting and freezing behaviour of the material, DTA analysis was carried out. The DTA thermo-gram of LTB, as shown in Fig.3.2, shows an exothermic peak at 917°C during heating of the material indicating melting of LTB however during the cooling cycle with cooling rate of 10°Cmin^{-1} shows only a glass phase transition rather than a clear endothermic peak (freezing point). The shape of this curve remained unaltered even for the lowest cooling rate of 1°Cmin^{-1} i.e. LTB has high tendency of glass transformation during cooling from melt to solid phase.

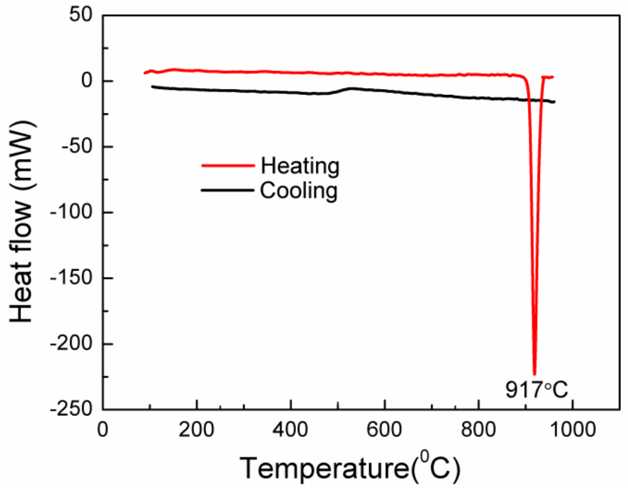

Figure 3.2: *DTA plots obtained over the range RT-950°C during heating and cooling cycles.*

To tackle the tendency of glass transformation, the growth rate which depends on heat removal from the solid-liquid interface were kept very low and to achieve the optimum value, pull rate were varied between 0.1 mmh^{-1} and 2.0 mmh^{-1}. The growth was investigated by varying longitudinal temperature gradients from a low (15°Ccm^{-1}) to high (70°Ccm^{-1}) value. To avoid the void formation, the melt were kept at temperature around 950°C for more than 3 to 4 hour for thermalization which allow to eradicate any gas residual that may get trapped in melt due to high viscosity. As the melt viscosity is very high, crystal rotation rates were varied in the range of 5 to 40 rpm to achieve optimum rotation rate to maintain forced convective flows within the melt to make flat solid-liquid interface. Problem of cracking was resolved by playing with thermal gradient and after growth cooling rate.

In the crystals grown at pull rates higher than 0.5 mm/h, the presence of a defective central core, as also reported by Robertson and Young [132], was invariably noted. However, the application of a pull rate of 0.5 mm/h, a rotation rate of 10 rpm and sharp longitudinal thermal gradient of about 70ºC/cm enabled the growth of clear, transparent, colorless and coreless single crystal. The cooling rates below 40ºC were found to be most suitable in obtaining crack free single crystals. The grown crystals are in size of 20 mm in diameter and of various lengths in the range of 5 mm to 30 mm. The photographs of the few inferior quality crystals grown in early stages and some high optical quality crystals having minimum defects are shown in Fig.3.3.

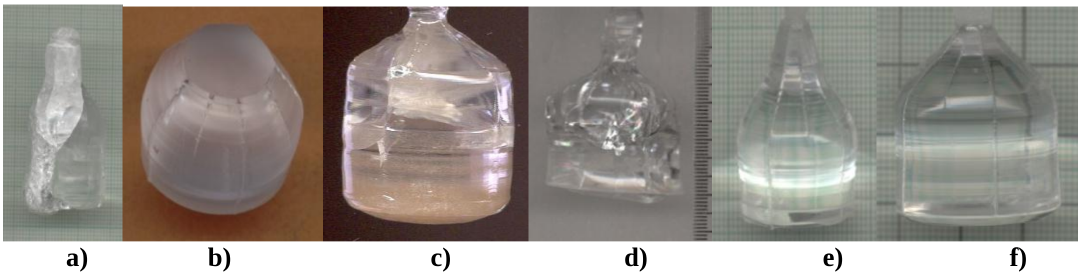

Figure 3.3: *The photographs of* $Li_2B_4O_7$ *crystal ingots obtained using the Czochralski method showing the (a) improper seed b) fogginess c) presence of core d) presence of crack e) and f) absence of any visible defect.*

Few of the grown crystals exhibited facets (flat faces, reflect the underlying symmetry of the crystal structure) on the surface as also reported by several other researchers [133]. These facets were characterized using the Laue’s diffraction. Fig.3.4(a) and Fig.3.4(b) shows a Laue diffraction pattern of as grown crystal and a crystal oriented along c-axis.

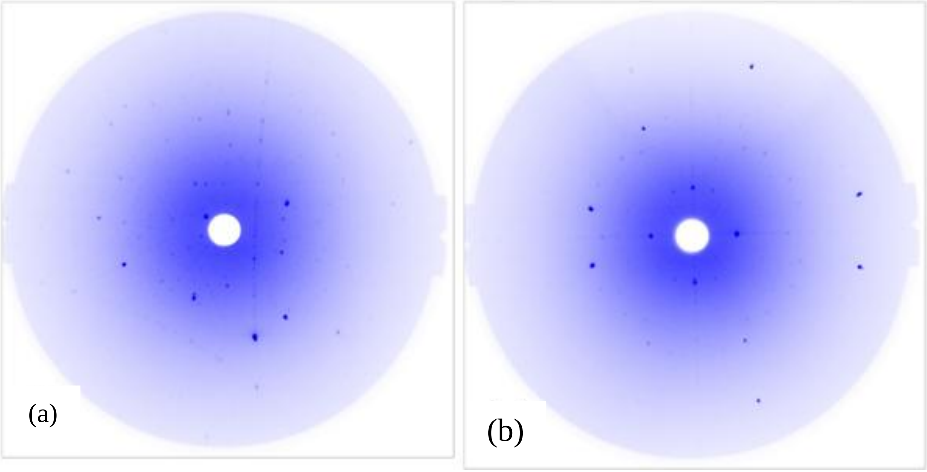

Figure 3.4: *Laue pattern of as grown a) crystal along the growth axis and b) crystal oriented along <001>.*

After achieving the high quality pure LTB single crystals, optimum parameters for crystal growth of Cu doped were investigated. For Cu doping, high purity (99.99%) CuO (0.5 wt % of charge) powders were mixed in the starting charge individually in each growth runs. For the growth, seed crystals were prepared from the pure LTB crystals. The segregation coefficient value *k* (the ratio of an impurity in the solid phase to that in the liquid phase) of Cu in LTB matrix is reported to be less than one [134]. Therefore, the diffusion rate of the impurity atoms (Cu) in solid phase will be less than the diffusion rate of the impurity atoms (Cu) in liquid phase from the solid/liquid interface, imposing further restriction on the growth rate of doped crystal. The different growth parameters were maintained at optimum values similar for pure crystal growth except the pull rate that was varied in 0.2 to 0.5 mm/hr to achieve an optimum pull rate for doped crystals. Application of a pull rate in 0.2 to 0.25 mm/h range yielded good quality Cu doped single crystals, while pull rates higher than 0.25 mm/h introduced inclusion and fogginess across the length of grown crystals. Few of the as grown high quality single crystal of LTB:Cu are shown in Fig.3.5. The phase purity of the grown crystals was confirmed from the powder X-ray diffraction pattern of the grown crystals. For this purpose, the grown crystals were crushed to fine powder in a particle size of less than 50 µm. XRD patterns recorded for a typical powder samples of the LTB:Cu along with pure LTB are shown in Fig.3.6. All the peaks match well with the JCPDS-84-2191 data, implying the formation of a pure phase of LTB. There is no change in the peak positions of LTB:Cu compared to the pure LTB i.e., there is no appreciable change in the lattice parameters due to the 0.5 wt% Cu doping in LTB.

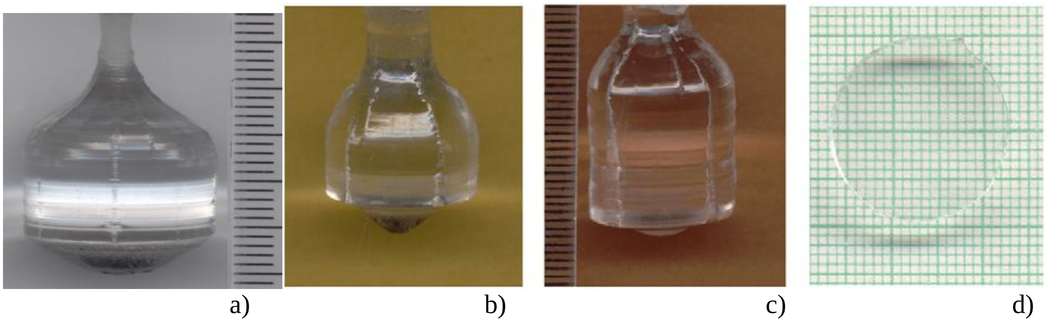

***Figure 3.5:** Single crystals of $Li_2B_4O_7$:Cu obtained using the Czochralski method: (a) (b) (c) as- grown ingots with various dimension and (d) a 3 mm thick polished disc.*

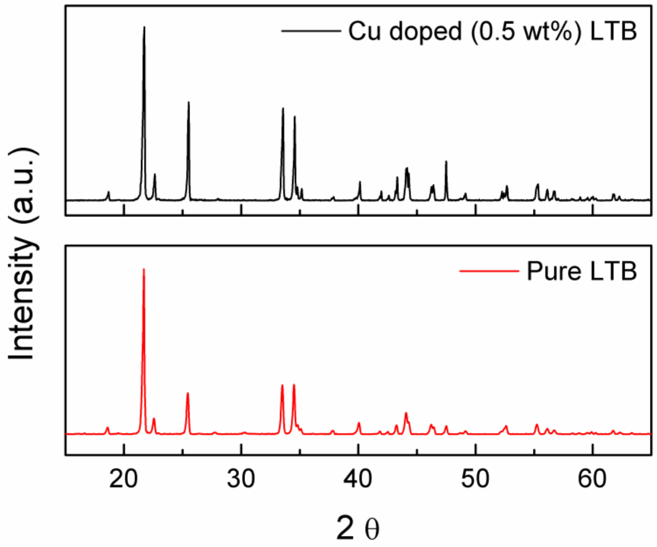

***Figure 3.6:** Powder XRD patterns of $Li_2B_4O_7$:Cu and pure $Li_2B_4O_7$ powder prepared after crushing the single crystal.*

3.2 Optical Characterization

For optical measurements, slices of 2 mm thickness were cut from the grown LTB crystal ingots perpendicular to the growth direction and polished with different grades of alumina powders down to 0.3 μm. The transmission spectra of undoped and Cu-doped LTB crystals are shown in Fig.3.7. Both pure and Cu doped crystal shows a transmission of about 84% that reveals the high optical quality of the grown single crystals. In the case of a pure crystal there is no absorption band in the range of 200-800 nm whereas an onset of absorption started at about 200 nm which is similar to results reported by several researcher with a cut off at 165 nm.

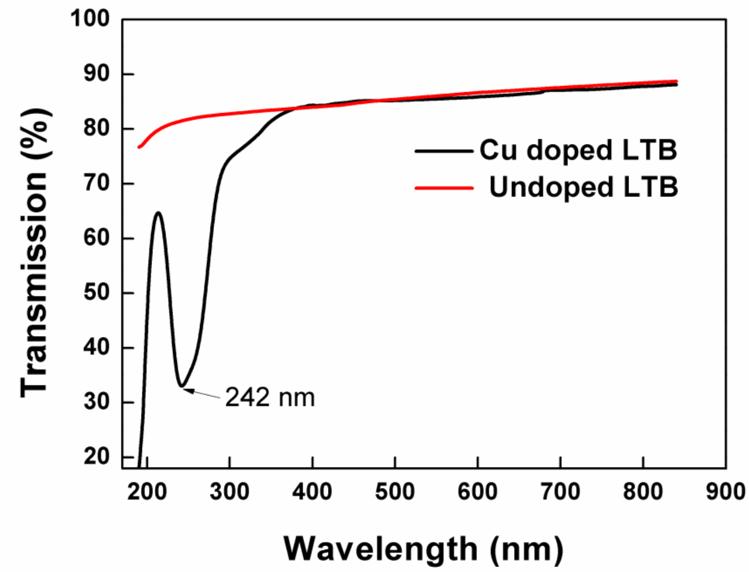

Figure 3.7: *Transmission spectra of pure/undoped and Cu-doped* $Li_2B_4O_7$ *crystals.*

The value of the direct optical band gap energy for an undoped LTB crystal obtained by extrapolation of the absorption coefficient to zero absorption is 7.4 eV considering the cut-off at 165 nm (not shown in figure), similar as reported by T. Adamiv et al. [135]. This is somewhat less than the reported band gap of 9.8 ± 0.5 eV (with a range from 8.9 ± 0.5 eV to 10.1 ± 0.5 eV) obtained from combined photoemission and inverse photoemission measurements [136]. For the LTB:Cu single crystals, there is an absorption bands at 242 nm (5 eV). This absorption corresponds to the $3d^{10} \rightarrow 3d^9 4s$ electronic transitions of Cu^+ ions [137]. Though these transitions, in free Cu^+, are generally considered symmetry or parity forbidden, they can take place due to symmetry breaking as a result of odd symmetry (transverse optical) vibrations of the crystal lattice. The absorption bands due to the Cu^+ ions in LTB exist in sites surrounded by deformed octahedral oxygen. Cu^+ ions are located at specific locations within the LTB crystal lattice, and not at random interstitial sites. With a substitution of Li^+ ion sites, the oxygen environment about the Cu^+ ions must be a deformed tetrahedron [138]. Though substitution take place but doping of Cu is difficult due to the large differences between the impurity ionic radii, i.e., r_{Cu+}=0.96 Å and the host lattice radii, r_{Li+}= 0.68 Å and r_{B3+} = 0.16 Å.

3.3 Photoluminescence Characterization

The emission and excitation spectra for the Cu-doped LTB crystals as presented in Fig.3.8, reveal strong excitation and emission band peaking at 260 nm and 370 nm respectively. This is in accordance with reported values by many research groups [71, 125 and 137]. The excitation spectrum consists of mainly two bands centered at 240 nm and 262 nm. The Cu^+ ion is the most probable candidate for the emitting center; accordingly its $3d^94s \rightarrow 3d^{10}$ transitions are considered to be responsible for the 370 nm emission band [139]. To assign the excitation bands of the emission at 370 nm one has to refer to the energy level scheme of the Cu^+ ion in the LTB crystals (Fig.3.9).

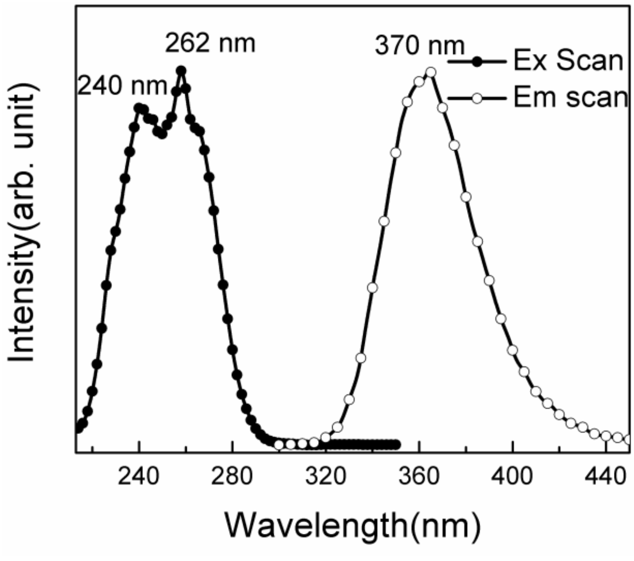

Figure 3.8: Excitation and emission spectra of a Cu doped $Li_2B_4O_7$ crystal.

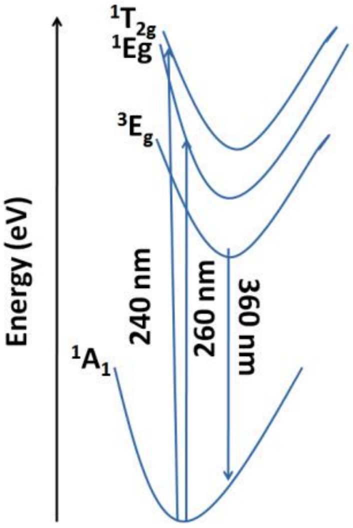

Figure 3.9: Energy level diagram for Cu^+ in $Li_2B_4O_7$ crystal.

The ground state of a free Cu^+ ion is of $3d^{10}$ configurations, while the lowest excited states are populated due to the $3d^{10}\rightarrow3d^94s$ and $3d^{10}\rightarrow3d^94p$ transitions, covering the energy ranges from 460 nm to 376 nm and 150 nm to 135 nm, respectively [140]. The 4s electron has a strong antibonding towards the ligands and the 4p electron is partly bonding, therefore, upon incorporation into the crystal, the $3d^94s$ levels are raised in energy and the $3d^94p$ levels are lowered by the same amount [141].

Tetragonal or octahedral crystal field splits the $3d^94s$ excited state into E_g- and T_{2g}-type components. Huy et al. have assigned energy level scheme for a Cu^+ ion in the LTB similar to that of a Cu^+ in octahedron halides crystals as the octahedron can be formed from a tetrahedron by temperature deformations in the growing process of the crystal [142]. These assignments have become definitive due to the experiments of McClure and co-workers, in which two photons spectroscopy was used to identify the ${}^1A_{1g}(3d^{10})\rightarrow{}^1E_g(3d^94s)$ and ${}^1A_{1g}(3d^{10})\rightarrow{}^1T_{2g}(3d^94s)$ transitions for several alkali halides doped with Cu [143]. Therefore, considering these facts and also comparing the results in the LTB:Cu with those published for Cu-doped alkali halide crystals (AHCs) [141, 144], the group of absorption and excitation bands near 250 nm may be ascribed to the $3d^{10}\rightarrow3d^94s$ transitions of the Cu^+ center. Now since the $3d^{10} \rightarrow 3d^94s$ transition is parity- and spin-forbidden, it may be partly allowed due to an off-center position of the Cu^+ ion, as it has been found for several AHCs [141, 144], or due to the original low symmetry of the crystal field at a site lacking inversion symmetry and even mirror symmetry. These effects result in the odd parity; multipole contribution in the potential and hence make the transitions allowed. The position (peaks at 240 nm and 262 nm) and splitting (~22nm) of the $3d^94s$ term are also close to the ones reported for those AHCs in which a Cu^+ ion occupies an off-center position at a cation site [144]. Accordingly, a substitution site of rather low symmetry is expected in the case of LTB:Cu. The splitting of $3d^94s$ level depends on the crystal field symmetry. While E_g level is higher in energy for an octahedral system, it is lower in the tetrahedral system.

As the oscillator strength and relative intensity of the two components provide a measure of an off-center displacement of the Cu^+ ground state, the temperature dependence of the excitation (240 nm and 262 nm) spectra was recorded with emission at 370 nm in the range from -196ºC to 25ºC and shown in Fig.3.10(a).

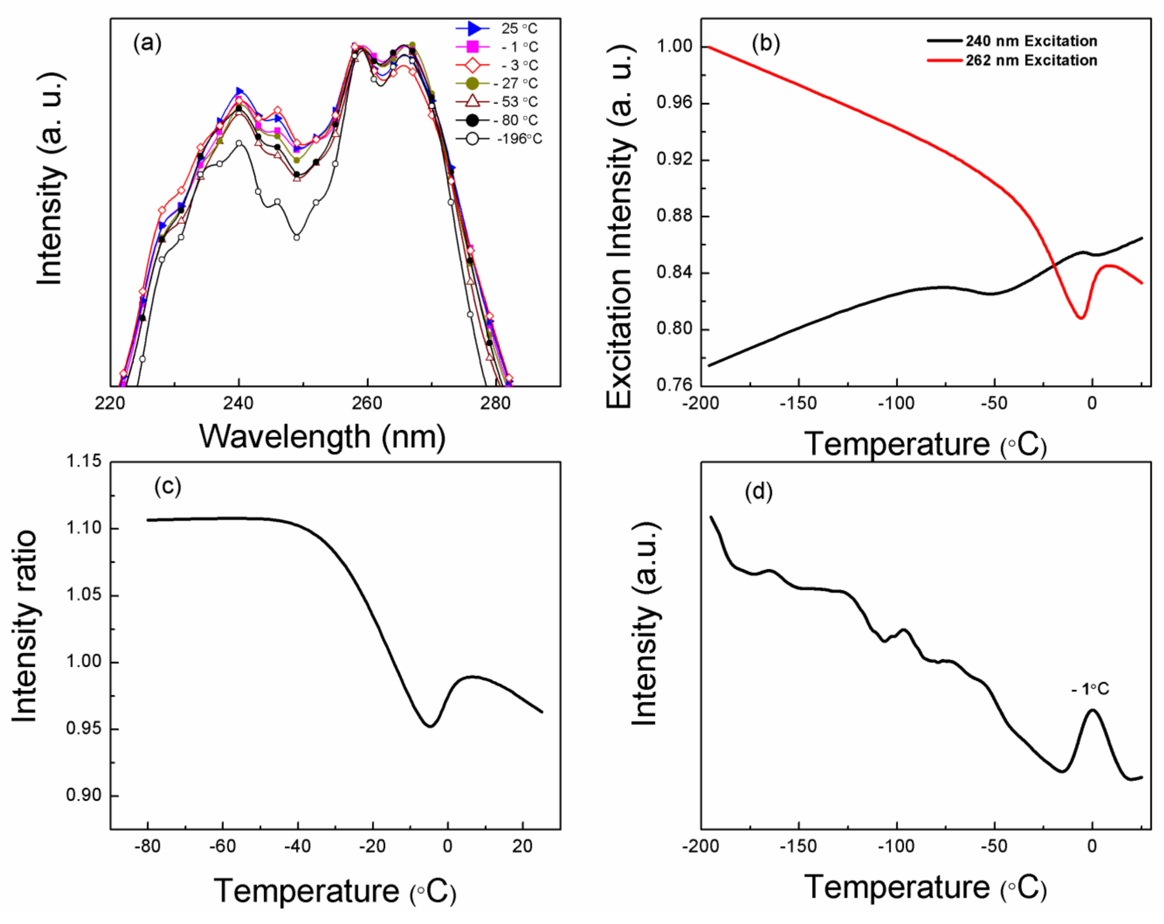

Figure 3.10: *Temperature dependence of (a) excitation spectra (b) peak excitation intensity value and (c) relative transition intensity of excitation (R_E/R_T) (d) 370 nm emission for 260 nm excitation of Cu doped $Li_2B_4O_7$ crystal.*

Each spectrum was fitted in two Gaussian peaks and maxima of both peaks were plotted with temperature and shown in Fig.3.10(b). From the figure it may be seen that with increasing temperature, the intensity of the peak at 262 nm reduces while that of the excitation peak at 240 nm increases. There is an intersection of intensities around -23ºC. The relative transition intensities of excitations from $^1A_{1g}\rightarrow{}^1E_g$ (262 nm) and $^1A_{1g}\rightarrow{}^1T_{2g}$ (240 nm) i.e. R_E/R_T can be calculated from the excitation spectrum [144]. As the change in potential due to off-center displacement or low symmetry encountered by the E_g orbital is steeper compared to that encountered by T_{2g} orbital, the relative transition strength increases with the off-center position. It has been reported that if Cu^+ is at the center, the R_E/R_T ratio is around 0.65 while for an off-center position this value should be higher than 0.65 [144]. From the fitted data, this ratio is plotted in Fig.3.10(c) with temperature which clearly shows that at each temperature the ratio is more than 0.65. Therefore it suggests a low-symmetry or off-center positions for the Cu^+ ion in the LTB lattice. It is also supported by the study of the excitation spectra for different temperature as it should increase with temperature in case of a centered Cu^+ ion [144]. However, the exact position of Cu^+ in its ground state cannot be verified with the methods used in the present investigation.

The temperature dependence of 370 nm emission intensity for the excitation at 260 nm is shown in Fig.3.10(d). As the temperature is increased, the emission intensity slightly decreases as non-radiative transition increase with temperature and an increase in the intensity at -1ºC is also observed. Though, this quenching with temperature is found much lesser in case of these crystals compared to those reported by Corradi et al [145]. This may be due to different defects present in the as-grown crystals with different growth parameters. A typical fluorescence decay spectrum of 370 nm at -196ºC is shown in Fig.3.11. A slight decrease in the decay time from 32 μS to 24 μS is also observed with increasing temperature from -196ºC to 27ºC.

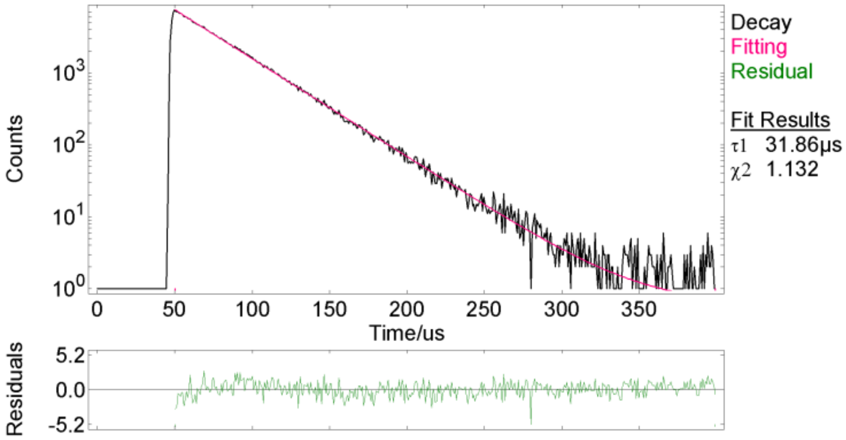

Figure 3.11: *Typical fluorescence decay spectrum of 370 nm emission at -196* °C.

3.4 TSL Characterization

A TSL glow curve recorded for a Cu doped LTB single crystal for a dose of 1 Gy is shown in Fig.3.12(a). It consists of two well defined and well separated glow peaks; first peak at 90°C which is unsuitable for the TLD application and a second peak at about 220°C for a heating rate of 1°C/s is similar to as reported by several research groups [146]. However, the dosimetric peak in LTB:Cu is reported in the range of 205 to 230°C [67]. The variation in the position of the peak may be attributed to the different synthesis routes followed that may introduce a slightly different defect structure in the host lattice with respect to each other [147]. It is also reported that TSL response of the LTB:Cu is approximately 900 times more sensitive than that of the undoped LTB [148]. The peak at 90°C fades completely within 24 h at room temperatures in dark whereas that at 220°C remains stable. However, the TSL peaks shifted to higher temperatures as the heating rate is increased from 0.5°C/s to 10°C/s as shown in Fig.3.12(b). The peak position does not shift in a dose range from 0.5 Gy to 10 Gy [Fig 3.13(a)]. The TSL emission spectrum of a Cu doped LTB crystal [Fig 3.13(b)] recorded at 150°C isotherm showed a band peaked around 360 nm, a characteristic emission from the Cu^+ center ($3d^{10} \rightarrow 3d^9 4s$) [68].

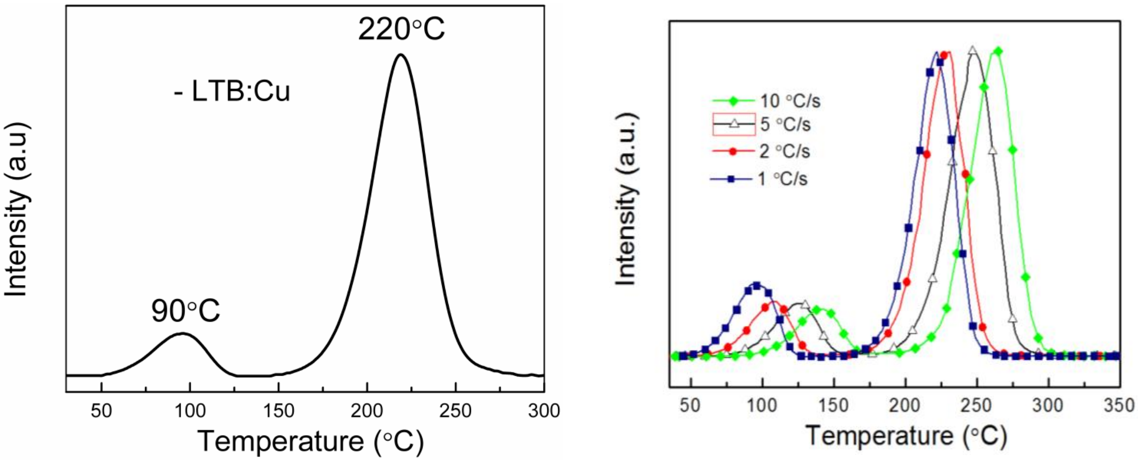

Figure 3.12: *(a) A typical TSL glow curve with heating rate of 1ºC/s (b) TSL glow curves of* $Li_2B_4O_7$*:Cu at different heating rates for an absorbed dose of 100 mGy.*

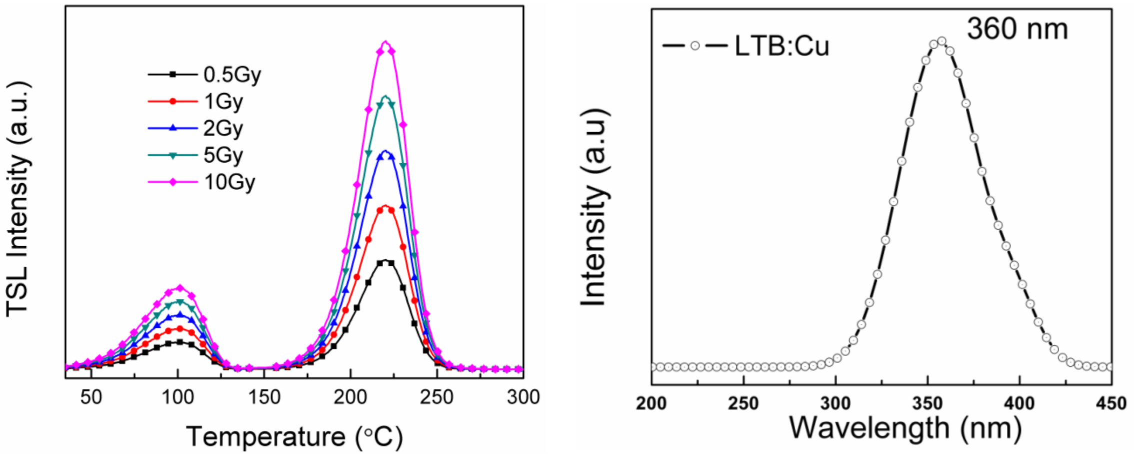

Figure 3.13: *(a) TSL glow curves for various absorbed dose obtained at 1ºC/s (b) TSL emission spectrum of* $Li_2B_4O_7$*:Cu recorded at 150 °C isotherm.*

The activation energy, frequency factor and order of kinetics were calculated employing the TLAnal software [149, 150] by taking general order approximation (GOK) (Table 3.1). The activation energy of the main peak at about 220°C is found 1.68 eV.

Table 3.1. Kinetic analysis of TSL peaks of $Li_2B_4O_7$*:Cu deconvoluted by GOK.*

Material	**Peak T (°C)**	**Trap depth E (eV)**	**Frequency Factor (s^{-1})**	**Kinetic Order (b)**	**Heating rate (ºC/s)**
LTB:Cu	220	1.6	2.1E+15	1.4	1

The LTB:Cu crystals showed a linear TSL dose response in the range from 1 mGy to 1 kGy as shown in Fig.3.14. The long range linearity of the material makes it suitable for dosimetry application.

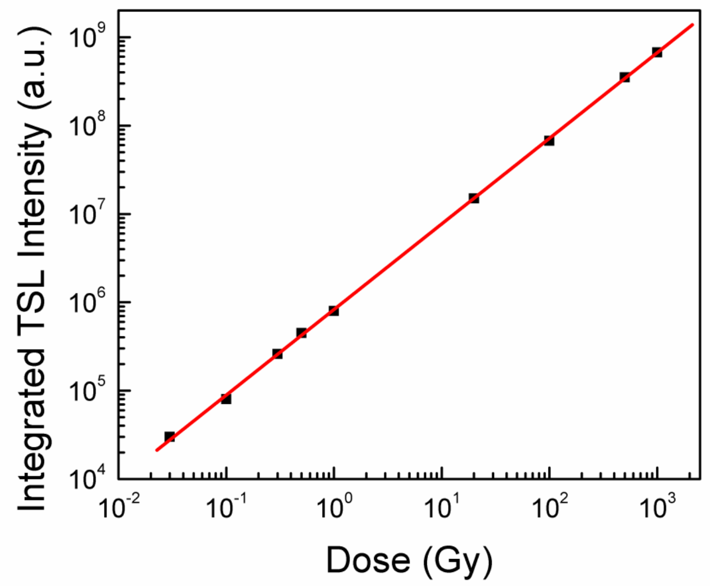

Figure 3.14: *Dose vs. TSL response of* $Li_2B_4O_7$*:Cu single crystals.*

Considering PL and TSL spectra of Cu doped LTB together, the following sequence of events that may be responsible for the TSL glow peak for LTB:Cu (similar to the scheme given for Ag^+ by A. T. Brant et al, [151]) may be proposed:

1) On exposure to an ionizing radiation at room temperature, electron and hole pairs are generated.
2) Electrons are combined with Cu^+ ions to form Cu^0 leaving a trapped hole.

$$Cu^+ + e^- \rightarrow Cu^0,\ Cu^+ + h^+ \rightarrow Cu^{2+}$$

3) As the crystal is heated above room temperature the trapped holes are released due to thermal agitation. The released holes then recombined at Cu^0 centers yielding an excited state of Cu^+ ($3d^94s$).

$$Cu^0 + Cu^{2+} \xrightarrow{\text{Heat}} (Cu^+)^*(\text{excited state } 3d^94s) + Cu^+$$

$(Cu^+)^*$ comes to ground state configuration ($3d^{10}$) by emitting a photon.

$$(Cu^+)^* \longrightarrow Cu^+ + h\nu \text{ (370 nm)}$$

3.4.1 Optical Fading Study in LTB:Cu Single Crystal

For potential use of LTB:Cu as TLD material, fading of TSL signal with time after the irradiation is investigated. It is desired the fading should be negligible during the storage period of the dosimeters. The fading study of the material was carried out for 30 days at room temperature. For this purpose, two sets of LTB:Cu samples (10 each) were exposed to 1 Gy dose. One set was kept under dark condition (wrapped in a carbon paper and kept in light-tight containers) while the second set was left in open to get exposed to day light. During this period the room temperature was monitored and found to be 30 ± 3ºC. TSL were recorded from each set at different interval and integrated TSL intensity were plotted with time as shown in Fig.3.15.

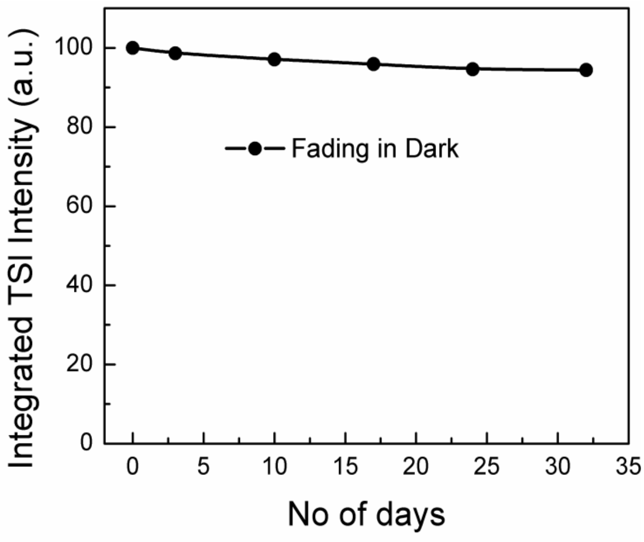

Figure 3.15: *The fading of TSL signal in $Li_2B_4O_7$:Cu at room temperature for a dose of 1 Gy.*

For the samples kept in day light, there is almost no TSL after 5 days of exposure (not shown in figure), indicating optical bleaching of the traps whereas the samples kept in dark show very negligible of fading with storing time. There is approximately 5% fading is observed after 30 days for the sampled stored in dark which is comparable to some commercially available TSL dosimeters [148].

3.5 OSL Characterization

Internal blue light emitting diodes (LEDs) (470 nm, 40 mW/cm^2) were used for optical stimulation, and the OSL signal was detected through Hoya U-340 filters. All the OSL measurements were performed in the continuous wave (CW-OSL) mode, and the power level was set at 90% of the maximum stimulation power for the blue LEDs controlling through the software and were performed at room temperature. The weight of the samples for the measurement was around 8-10 mg. The CW-OSL decay curves of LTB:Cu dosimetric crystal is shown in Fig.3.16 for a beta dose of 0.1 and 2 Gy.

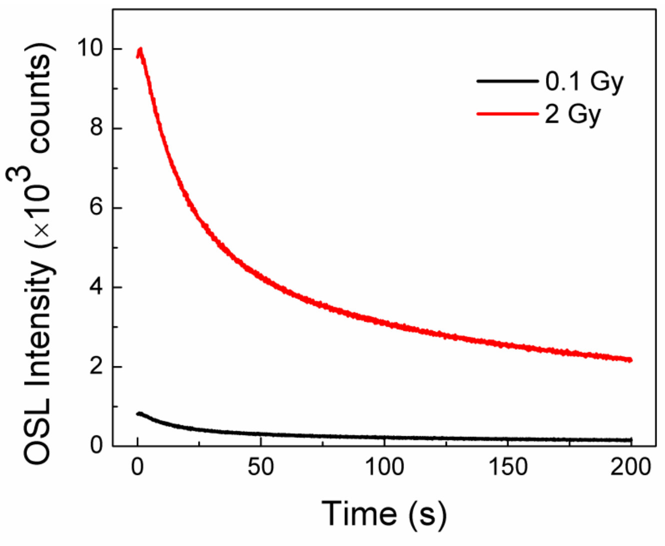

Figure 3.16: *CW-OSL decay curve for* $Li_2B_4O_7$*:Cu for a dose of 0.1 Gy and 2 Gy at room temperature.*

Considering no re-trapping, the CW-OSL decay curve is analyzed by fitting it to an exponential decay as per equation 2.22 (chapter 2), which gives the photo ionization cross section of different trap centers. The analysis of the OSL signal as given in Table 3.2

indicates that it is composed of two components: a fast component i.e. higher photo ionization cross section assigned to electrons that recombine directly with holes and a slow component i.e. lower photo ionization cross section due to the presence of shallow traps in the structure, in which electrons are re-trapped for several seconds before being recombined with holes. The results are similar as observed by T. Aydin et al [153].

Table 3.2. Calculated OSL parameters for $Li_2B_4O_7$*:Cu.*

Material	Optical absorption cross-section (cm^2)	Concentration of charge carriers	Photon fluence rate (photons/cm^2/s)
LTB:Cu	$\sigma_1 = {\sim}3.0x10^{-19}$, $\sigma_2 = {\sim}4.3x10^{-20}$	$n_1 = 8.88545 \times 10^5$ $n_2 = 4.16175 \times 10^6$	$\varphi = 9.24x10^{16}$

3.6 Conclusions

Highly transparent, crack free and clear single crystal of pure and Cu doped LTB has been grown by Czochralski method. High purity starting charge, slow rotation and pulling rates enabled the growth of highly transparent and core free single crystals of Cu doped LTB. XRD confirm the growth of $Li_2B_4O_7$ pure phase. UV–Vis transmission spectra indicate the good optical quality of grown pure and doped LTB crystals. The absorption bands at 240 nm indicate the presence of Cu^+ centers in the crystal. Further the presence of Cu^+ centers has been confirmed in PL studies which give the emission at 370 nm with an excitation band having a doublet structure at 240 nm and 262 nm that corresponds to $^1A_{1g}\rightarrow{}^1E_g$ and $^1A_{1g}\rightarrow{}^1T_{2g}$ crystal field components of the $3d^{10}\rightarrow 3d^9 4s$ transition of Cu^+. The transition probability of two excitation peaks for Cu^+ emission which are corresponding to $^1A_{1g}\rightarrow{}^1T_{2g}$ and $^1A_{1g}\rightarrow{}^1E_g$ transitions show opposite temperature dependences. The relative intensity of these components and their temperature dependence provide a measure of the off-center displacement of the Cu^+ ground state in the crystal lattice site. The ratio of these transition probabilities is greater than 0.67 for all the temperatures which suggests the off-center or lower symmetry position of Cu^+ ions in the lattice.

TSL response of the Cu-doped LTB crystal is found linear in the range from 1 mGy to 1 kGy and the TSL glow peak at about 220°C with a low TSL signal fading (in dark) of 5% in 30 days makes it suitable for dosimetry applications. Cu doped LTB is also shows efficient OSL signal which confirm its use in the OSL mode.

CHAPTER 4

SINGLE CRYSTALS GROWTH AND CHARACTERIZATION OF Cu+Ag DOPED $Li_2B_4O_7$

The Cu doped LTB, as described in chapter 3, was reported to be 20 times more sensitive for dosimetric application to that of LTB:Mn with an intense TSL emission at around 370 nm [40]. There have been many attempts to further increase the sensitivity of the material by various type of co-doping [79, 153]. There are several reports on co-doped LTB such as LTB:Cu,Ag,P, LTB:Cu,In, LTB:Cu,In,Ag [79, 125, 153, 154, 155, 156] in which the TSL sensitivity is found to be better to that of commonly used LiF:Mg,Ti (TLD-100). However, for effective energy transfer by co-doping, the emission of one ion should lie in the excitation range of the other. It has been observed that in the LTB crystals, Cu and Ag impurities are incorporated as Cu^+ and Ag^+ by substituting Li^+ wherein the emission of Ag^+ lies in the excitation region of Cu^+ states and it may increase the overall light yield through an energy transfer mechanism. It is further reported that co-doping with Ag makes it sensitive to optical stimulation of traps making it an efficient OSL material [83]. Though there are reports on the luminescence properties of Cu, Ag co-doped LTB, a detailed and satisfactory explanation about energy transfer mechanism and the role of Ag in TSL and OSL processes have not been elaborated earlier which may be helpful in developing it as an effective TSL or OSL material.

In this chapter, the single growth of LTB:Cu,Ag from melts using the Czochralski technique and a detailed dosimetric characterization study performed by using PL and TSL techniques have been described. The energy transfer mechanism in the Cu and Ag co-doped LTB single crystals are studied and explained. The PL and TSL studies suggest Cu and Ag co-doped LTB is more sensitive than the Cu doped LTB due to the sensitizer role of Ag. To realize its full potential for dosimetric application, a suitable readout for the co-doped LTB is also proposed.

4.1 Single Crystal Growth of Cu and Ag co-doped LTB

LTB single crystals co-doped with Cu and Ag were grown using the Czochralski technique in the air ambient. For Cu and Ag doping, commercial polycrystalline powder of CuO and Ag_2O having purity higher than 99.99% were mixed thoroughly to starting charge of commercially available high purity (99.998%) polycrystalline powders of LTB. Doping concentration of Cu and Ag in melt was 0.25 mole% for each. An optimized set of growth parameters, pull rate of 0.25 mm/h, a rotation rate of 10 rpm and a high longitudinal thermal gradient of about 70°C/cm was used for the growth of co-doped single crystals of LTB similar as achieved during the growth of LTB:Cu (discussed in chapter 3). The application of optimum growth parameters enabled the growth of clear, core-free, inclusion-free, bubble-free, colorless and transparent single crystals of 20 mm diameter and 10-20 mm in length. Few typical photographs of the grown crystals of LTB:Cu,Ag is shown in Fig.4.1.

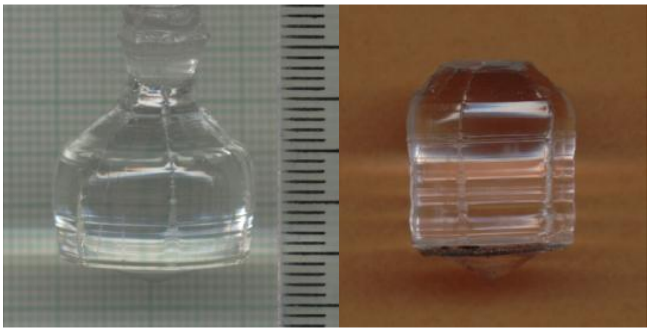

Figure 4.1: *Photograph of as grown single crystal ingot of* $Li_2B_4O_7$*:Cu,Ag.*

4.2 Optical Characterization

All the grown crystals showed over 80% transmission in the visible range, as shown in Fig.4.2 (For a 2 mm thick slices, cut perpendicular to the growth direction from the crystal ingots and polished) indicating a good optical quality of the grown crystals. The transmission spectrum shows two main absorption bands around 205 and 240 nm. The absorption at around 205 nm corresponding to the $4d^{10} \rightarrow 4d^{9}5s$ transition of Ag^+ centers [157] and absorption at 240 nm is due to the $3d^{10} \rightarrow 3d^{9}4s$ transition of Cu^+ centers as described in earlier chapter [142]. This suggests that both Cu^+ and Ag^+ ions are incorporated in the LTB lattice at the same site indicating a possibility of energy transfer between these two centers.

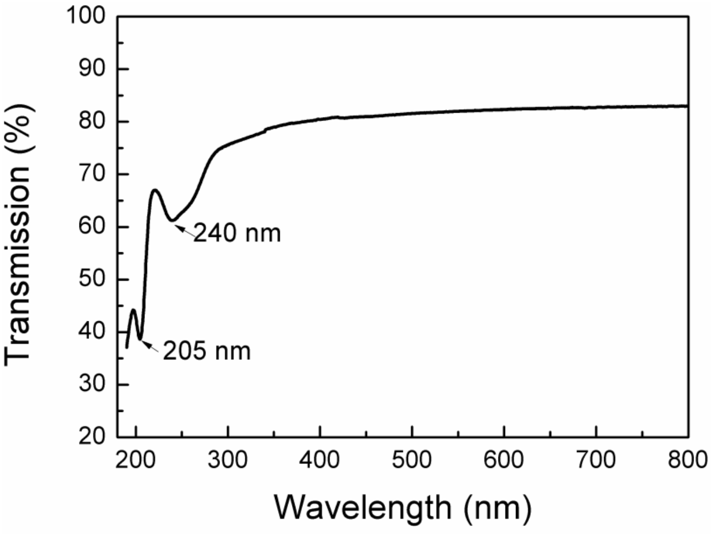

Figure 4.2: *Transmission spectrum of* $Li_2B_4O_7$*:Cu,Ag single crystal.*

The Cu impurity in the LTB lattice generally adopt the univalent Cu^+ ion state, independent of the valence of the initial chemical copper source used for Cu doping [135]. In case of Cu and Ag co-doping, it is also probably very important to take into account the large differences between the impurity ionic radii, *i.e.*, r_{Cu+}= 0.96 Å and r_{Ag+} = 1.13 Å, and the host site radii, r_{Li+} = 0.68 Å and r_{B3+} = 0.16 Å. The large difference in the ionic radii of

B^{3+} and that of Cu^+ and Ag^+ along with difference in their valence further insures that the Cu and Ag may occupy similar lattice position of Li in LTB matrix.

4.3 Photoluminescence Characterization

The PL studies of the LTB:Cu,Ag show two emissions band centered at 265 nm and 370 nm. The emission band at 370 nm belongs to Cu^+ centers with corresponding excitation bands centered at 242 nm and 260 nm as shown in Fig.4.3(a) [69, 139]. These transitions are ascribed to parity and spin-forbidden $3d^94s \rightarrow 3d^{10}$ transitions from the triplet state of Cu^+ with a large Stokes shift of ~10,000 cm^{-1}. The other emission band around 265 nm belongs to Ag^+ centers with corresponding excitation band around 205 nm as shown in Fig.4.3(b). The nature of the luminescence in this region is due to $4d^95s \rightarrow 4d^{10}$ transition of Ag^+ ion as reported in literature [158].

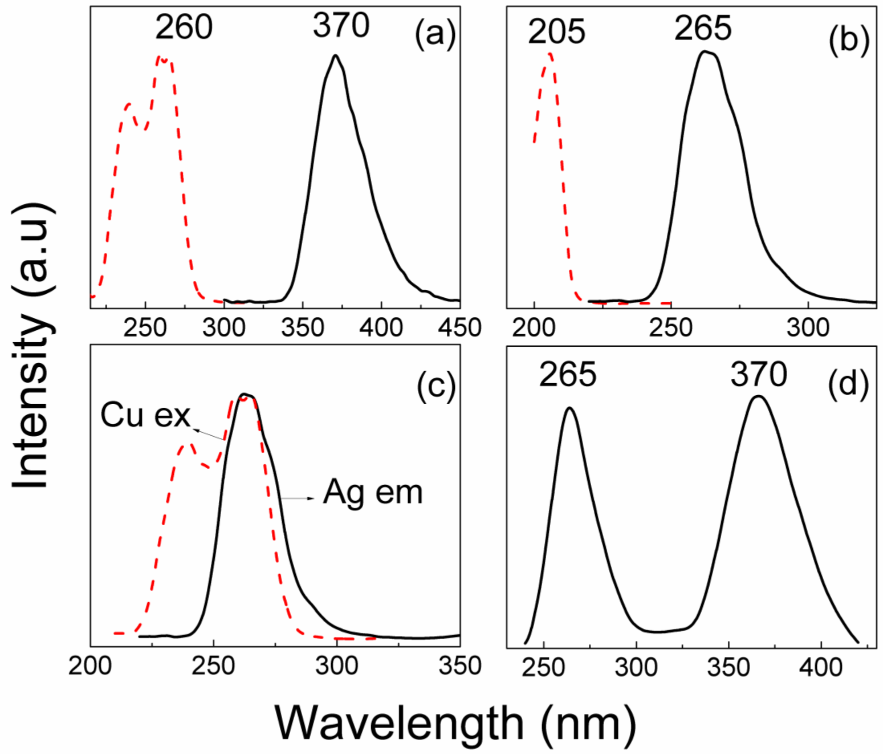

Figure 4.3.*(a) Photoluminescence excitation and emission spectra for Cu in $Li_2B_4O_7$:Cu, Ag. (b) Excitation and emission spectra for Ag in $Li_2B_4O_7$:Cu, Ag. (c) Overlapping of Ag emission and Cu excitation and (d) emission of $Li_2B_4O_7$:Cu,Ag for excitation at 205 nm (excitation- dashed red, emission- solid black).*

Fig.4.3(c) shows the emission band of Ag^+ overlapping with the excitation band of Cu^+ indicating a possibility of an energy transfer of these centers in the co-doped crystals. The spectra have been normalized in the figures for a better presentation of the observed overlapping. To check the feasibility of energy transfer mechanism, samples were excited with 205 nm (corresponds to Ag^+ excitation) and subsequent emission were recorded and shown in Fig.4.3(d). It shows two well resolved peaks at 265 nm and 370 nm corresponding to Ag^+ and Cu^+ emission centers. Thus it appears that Ag^+ centers have two routes for the radiative transition; one by its own emitting center (265 nm) and the other through an energy transfer to Cu^+ centers (370 nm). Hence, in case of co-doping of Ag^+ in LTB:Cu, the emission at 370 nm (due to Cu^+) is enhanced due to energy transfer from Ag^+ ion to Cu^+ ion. From emission spectra, it is clear that the emission of Ag^+ states sensitized the excitation of Cu^+ states and the overall light output improved. The overall process can be understood with a schematic of energy level diagram of Cu^+ and Ag^+ ion in LTB crystals as shown in Fig.4.4 [83].

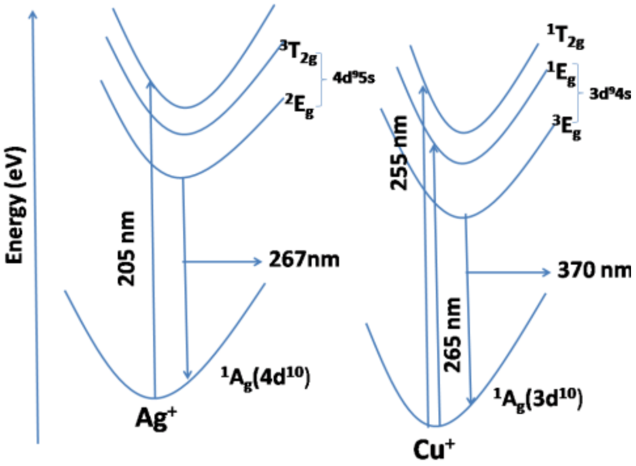

Figure 4.4: *Schematic of energy label representation of Cu^+ and Ag^+.*

Fig.4.5(a) shows the temperature dependence of 265 nm emission spectra of Ag for the excitation at 205 nm. Each spectrum was fitted with Gaussian peaks and maximum heights of the peak were calculated and plotted with temperature in Fig.4.5(b). It shows that the emission intensity getting higher with the temperature and it reached a maximum value at around -13ºC. Fig.4.5(b) also shows the temperature dependence of the 265 and 370 nm emission of Ag^+ and Cu^+ centers. In both emission spectra, a change in the emission intensity that reduces with the temperature is observed. This change in the intensity may be explained from the competition between non-radiative transition energy transfers from Ag^+ states to Cu^+ states in co-doped LTB crystals. However, a sudden increase in intensity of Cu^+ emission is observed at around -13ºC and needs further explanation.

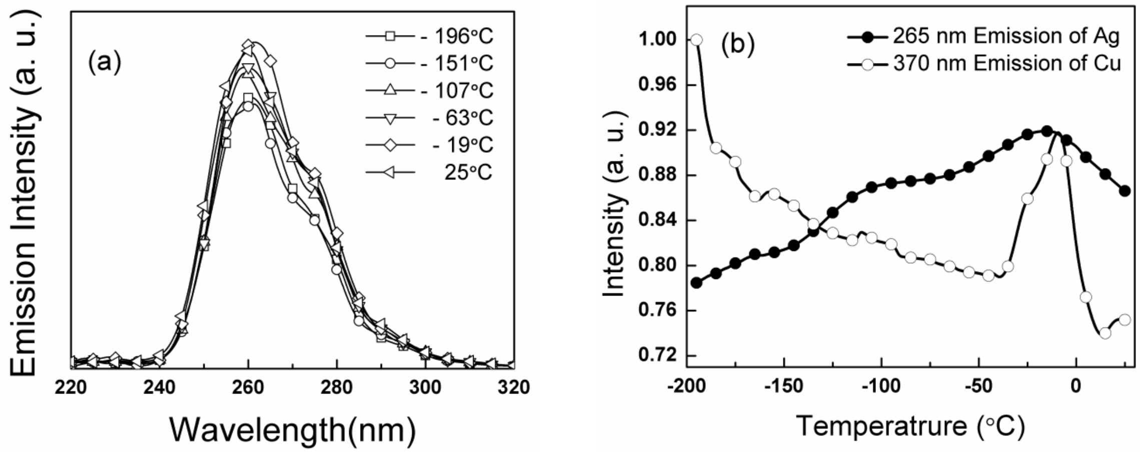

Figure 4.5: *Temperature dependence of (a) 265 nm emission spectra of Ag for 205 nm excitations and (b) Intensity of 265 and 370 nm emissions for Ag and Cu co-doped* $Li_2B_4O_7$ *crystal.*

It is reported that [159, 160] LTB lattice consists of $[B_4O_9]^{6-}$ complex comprising two planar trigonal (BO_3) and two tetrahedral (BO_4) units. The lithium atoms are located at two interstices, oxygen octahedrons and tetrahedrons. When metallic atoms like Cu are doped they enter into oxygenic octahedrons or tetrahedrons (replacing Li atom). Further, doping of activator like Ag affects the oxygen atoms of the octahedrons and tetrahedrons and thus the emission of Cu^+ ions. Adamiv et al. have reported that BO_3 triangles and BO_4 tetrahedral show opposite behavior with increase in the temperature from -263ºC to 17ºC in the LTB crystal [161]. The BO_3 triangle enlarges with increase in the <B–O> average distance where as BO_4 tetrahedral compresses on heating from -263ºC to 17ºC. The largest changes in the -263ºC to 17ºC temperature range were observed for structural parameters of the Li atom. The shift in the position of the Li atom can lead to change in the PL intensity of Cu with temperature. Further the ionic radii of Cu^+ and Li^+ are similar and therefore lattice distortion would be minimal on Cu doping. However, as the radius of Ag^+ is far larger than that of Li^+, the co-doping with Cu and Ag would distort the LTB crystal structure appreciably. In this case the thermal quenching of the PL intensity would be less and an increase in the PL intensity with increasing temperature will be observed. Therefore the peculiar temperature dependence around -13ºC in the ratio of transition probability of both crystal field components (R_E/R_T), as discussed for Cu doped LTB single crystals in the last chapter, leads to similar dependence of emission intensity and these can be explained based on thermal behavior of the crystal lattice.

4.4 TSL Characterization

For TSL studies, LTB crystal samples of 3x3x0.6 mm^3 were cut from the as grown crystal ingots. Prior to irradiation, the samples were given an annealing treatment at 300°C for 30 minutes to erase any irradiation history. It has been found that an annealing at 300°C for 30 minutes is adequate to erase the residual TSL signal of LTB and restore the original TSL sensitivity of the LTB dosimeters [162]. The TSL glow curve for co-doped LTB crystal, as shown in Fig.4.6(a), consists of two well resolved peaks at 160°C and 230°C (excluding the low temperature peak at 90°C). The peak at 160°C corresponds to Ag^+ centers as reported by several groups for Ag doped LTB [163]. The peaks at 230°C is similar to TSL peaks of LTB:Cu with a slight shift to higher temperature (220°C→230°C) and is therefore attributed to Cu^+ centers. This indicates the trap centers corresponding to Ag and Cu are independent and no new centers are formed with the interaction of Ag^+ and Cu^+ centers in the co-doped crystals. The glow peak at 160°C (from Ag^+ centers) is found to be intense equally to the peak at 230°C (from Cu^+ centers). Hence, both types of trap centers (Cu^+ and Ag^+) participate in the TSL process. The TSL emission spectrum of the co-doped crystal was recorded at a constant temperature of 120°C, as shown in Fig.4.6(b). It exhibited two well resolved peaks at 270 nm and 360 nm corresponding to Ag^+ and Cu^+ centers, respectively.

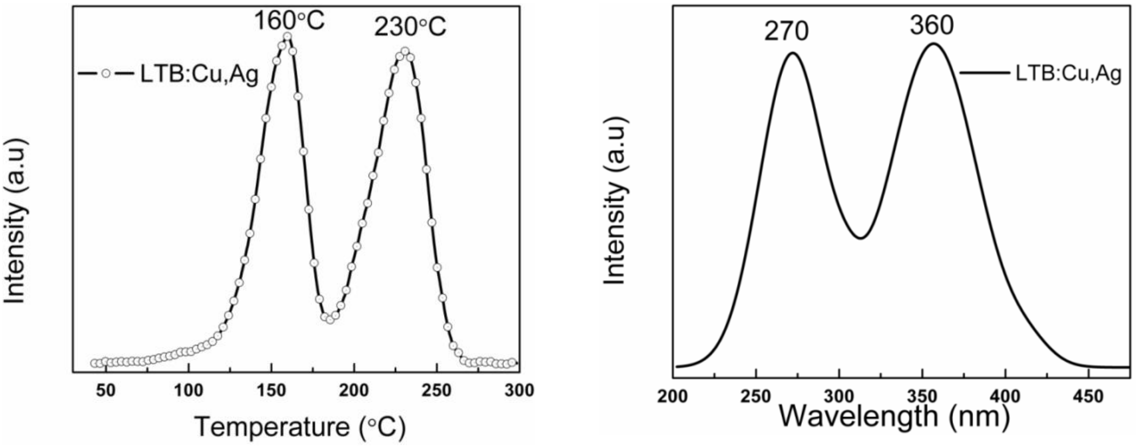

Figure 4.6: *Thermally stimulated luminescence (a) glow curve and (b) spectrum of* $Li_2B_4O_7$*:Cu,Ag.*

The activation energy, frequency factor and order of kinetics were calculated employing the TLAnal software [149, 150] by taking general order approximation (GOK) (Table 4.1). As both types of trap centers participate in the TSL process in the co-doped crystals and some changes like activation energy, frequency factor and order of kinetics related to peak of Cu takes place as compared with LTB:Cu.

Table 4.1. Kinetic analysis of TSL peaks of $Li_2B_4O_7$*:Cu,Ag deconvoluted by GOK (Heating rate was 1ºC/s in each experiment).*

Material	**Peak T (°C)**	**Trap depth E (eV)**	**Frequency factor (s^{-1})**	**Kinetic Order (b)**	**Heating rate** (ºC/s)
LTB:Cu,Ag	160	1.2	1.7E+13	1.0	1
LTB:Cu,Ag	230	1.3	1.6E+12	1.0	1

The spectral dependence of the glow curve was studied to understand the TSL process in co-doped crystals. The TSL glow curves corresponding to 270 nm and 360 nm wavelengths are shown in Fig.4.7. For the emission at 270 nm (radiative recombination at Ag^+ centers), the glow curve shows an intense peak at ~160°C which is analogous to the TSL glow peak of the Ag doped LTB crystal [163]. Thus it is clear that electron/holes released from the Cu^+ centers did not recombine at Ag^+ centers. Whereas, when the monochromator is fixed at 360 nm, the TSL glow curve shows two peaks at 160°C and 230°C corresponding to the Cu^+ and Ag^+ trap centers. Here, it is not electron or hole released from Ag^+ centers that travelled through and recombine at Cu^+ centers but an excited Ag^+ center (after recombination of electron and hole) transfers its energy to a Cu^+ center as in the PL process.

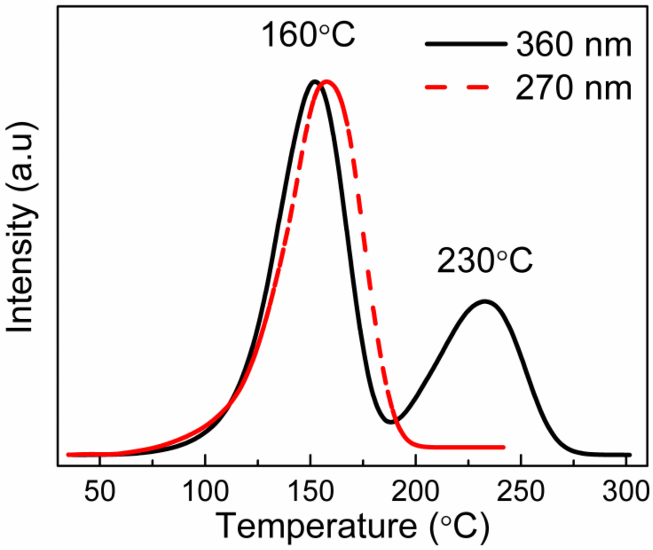

Figure 4.7: *Spectrally resolved TSL glow curve of* $Li_2B_4O_7$*: Cu,Ag.*

Thus it appears that Ag^+ centers have two routes for the radiative recombination during a TSL process. These observations clearly indicate that, though Ag^+ trap centers are transferring their energy to the Cu^+ centers during the recombining process, a considerable number of Ag^+ excited centers are radiatively recombining on its own.

Considering PL and TSL emission spectra of co-doped LTB together, the following sequence of events may be proposed for 270 nm (Ag^+) emission (similar to the scheme given for Cu^+ in the last chapter and Ag^+ by Brant et al. [151]) which are responsible for the TSL glow peak

1. On exposure to an ionizing radiation at room temperature, electron and hole pairs are generated.
2. Electrons are combined with A^+ ions to form A^0 leaving a trapped hole. (A= Ag)

$$A^+ + e^- \rightarrow A^0, A^+ + h^+ \rightarrow A^{2+}$$

3. As the crystal is heated above room temperature the trapped holes are released due to thermal agitation and recombined at A^0 centers yielding an excited state of A^+ ($4d^95s$).

$$A^0 + A^{2+} \xrightarrow{\text{Heat}} (A^+)^*(\text{excited state } 4d^95s) + A^+$$

4. $(A^+)^*$ comes to ground state configuration ($4d^{10}$) by emitting a photon.

$$(A^+)^* \longrightarrow A^+ + h\nu \text{ (emission of 270 nm photons)}$$

On the other hand, the emission at 360 nm (Cu^+) may be explained by considering two possible paths:

1) Trapping and detrapping of elctron and hole pairs in its own centers (Cu^+) as given below

$$Li_2B_4O_7{:}A^+ \rightarrow \text{Irradiated} \rightarrow Li_2B_4O_7{:}(A^0+h) \rightarrow \text{Heat} \rightarrow Li_2B_4O_7{:}(A^++STE) \rightarrow \text{Annihilation} \rightarrow Li_2B_4O_7{:}A^+ + h\gamma \quad (A^+ = Cu)$$

2) The other path may be through the energy transfer from Ag^+ to Cu^+ centers and the sequence may expressed as,

$$(Ag^+)^* + (Cu^+) \rightarrow Ag^+ + (Cu^+)^*$$

$$(Cu^+)^* \rightarrow Cu^+ + h\nu \text{ (emission of 360 nm photons)}$$

The TSL response of the LTB:Cu,Ag single crystals for different doses is shown in Fig.4.8. The dose response shows a linear behavior in 10 mGy to ~10 Gy range and a supra-linearity set in beyond 10 Gy.

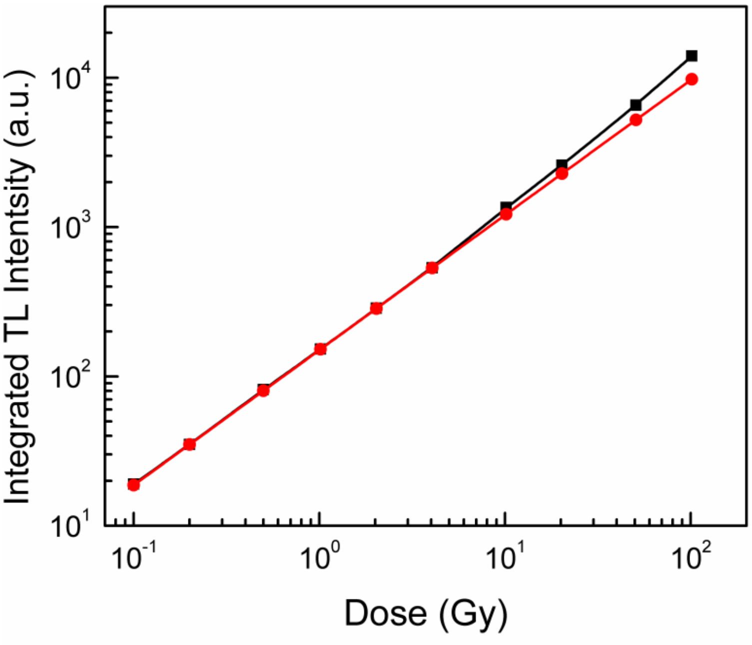

Figure 4.8: *TSL response of* $Li_2B_4O_7$*:Cu,Ag in 10 mGy to 100 Gy range.(Observed data-black, linearity plot- red)*

4.4.1 Minimum Detectable Dose (MDD)

The lowest level of detection, known as the minimum detectable dose, was calculated from the following relation [164].

$$D_o=2.26\cdot\sigma\cdot S$$

where σ is the standard deviation of the background reading value of un-irradiated samples in units of nanocoulomb (nC), and S represents the conversion factor in units of mGy/nC. The experimentally determined minimum detectable dose (MDD) is defined as three times the standard deviation of the zero dose readings of the annealed dosimeters after the conversion from machine output units to dose through an appropriate conversion factor (using the individual dosimeter calibration factors). For MDD measurements a group of samples (typically at least 10 number of samples with the same sensitivity) was used to get the zero dose value which provides mean and standard deviation and the MDD for LTB:Cu,Ag is found to be about 1 mGy which can be improved further by a suitable TSL reader system. The sensitivity of the material is found more than the LTB:Cu by two fold that indicates that sensitivity of the material is definitely higher than the well-known LiF:Mg,Ti (TLD-100) phosphor [72, 165].

4.5 Conclusions

High quality single crystals of LTB:Cu,Ag have been grown using the Czochralski technique. Transmission and PL studies confirm the incorporation of Cu^+ and Ag^+ in the LTB matrix. Luminescence studies revealed that Ag acting as sensitizer role in the LTB:Cu,Ag crystal as the emission of Ag^+ centers lies in the excitation region of Cu^+ centers. In TSL studies, glow peaks related to Cu^+ and Ag^+ trap centers are recorded. It is shown that the TSL spectrum of LTB:Cu,Ag consists of emission bands corresponding to Ag^+ (270 nm) and Cu^+ (360 nm) centers and a signature of energy transfer from Ag^+ centers to Cu^+ centers is also registered. This energy transfer process in LTB:Cu,Ag makes it a more efficient TSL phosphor than LTB:Cu. It is also found that, despite an energy transfer from Ag^+ to Cu^+ centers, emission from both the centers participate in the TSL process of LTB:Cu,Ag single crystals. A possible scheme for the TSL processes in the co-doped LTB crystal is proposed based on PL and TSL studies. The Ag^+ trap centers are shown to radiatively re-combine through two different roots giving rise to two TSL peaks at 270 and 360 nm. Therefore, to exploit the full potential of the co-doped LTB, a suitable TSL readout system consisting of a PMT having a peak response in the range of 200–600 nm that would cover the whole range of emitted light will be necessary.

CHAPTER 5

SINGLE CRYSTALS GROWTH AND CHARACTERIZATION OF Ag DOPED $Li_2B_4O_7$

The results of the previous studies performed on Cu and Ag co-doped LTB shows that Ag as co-dopant enhances the sensitivity of LTB:Cu by efficient energy transfer from Ag^+ to Cu^+ centers, however it also introduces a new glow peak in the 150–170ºC range that may be useful in dosimetry. Nevertheless, available literature on Ag doped LTB (without any co-dopant) material are scanty and has reported it as a less sensitive material compared to LTB:Cu [85]. This may be because the TSL emission wavelength of Ag in LTB, which is at 270 nm, is far from the response region of most of the PMTs (300–650 nm) used in conventional dosimeter readers [124]. Brant et al. had studied the TSL glow curve of Ag doped LTB, but their main focus was on the EPR study of Ag^+ related centers [151]. Though large size and high-quality single crystals of Ag doped LTB with controlled doping can readily be grown and their impurity-related radiative processes can be extremely efficient, [131, 135, 166, 167, 168, 169] to realize the full potential as TSL material it is necessary to develop a suitable read out system specific to the Ag doped LTB and to optimize the Ag concentration in the LTB matrix.

In this chapter, a description of the performance of the LTB:Ag as a TSL material showing unprecedented sensitivity using a readout set-up specific to LTB:Ag with a solar blind PMT have been presented. It also dwells briefly on single crystal growth of Ag doped LTB from melt and optimization of Ag concentration therein. The response of the material as a function of γ-exposure is also reported and a minimum detectable dose with the current setup has been estimated.

5.1 Growth of Single Crystal of Ag Doped LTB

Single crystals of $Li_2B_4O_7$ doped with Ag (0.1, 0.3, 0.5, 0.7, 1.0 and 1.1 wt.%) were grown under air ambient using the Czochralski technique employing an automatic diameter controlled crystal puller (Oxypuller, Cyberstar). Commercially available high purity polycrystalline powders of $Li_2B_4O_7$ (99.998% pure) and Ag_2O (99.99% pure) were taken as a starting charge for the growth. The solid state synthesize powder were also used for the growth of single crystals. Li and B were taken in their natural abundance without further enrichment. For the crystal growth, optimum growth parameter such as application of a pull rate of 0.2-0.25 mm/h, a rotation rate of 10 rpm and a high longitudinal thermal gradient of about 70ºC/cm were applied as achieved during the growth of LTB:Cu and LTB:Cu,Ag. Clear, transparent, crack-free, core free, colorless, inclusion and bubbles free single crystals (approximately 20 mm diameter, 15 mm length) have been grown in all the experiments using both commercial and synthesized powder. Some of the photographs of as grown single crystals with different concentration of Ag are shown in Fig.5.1.

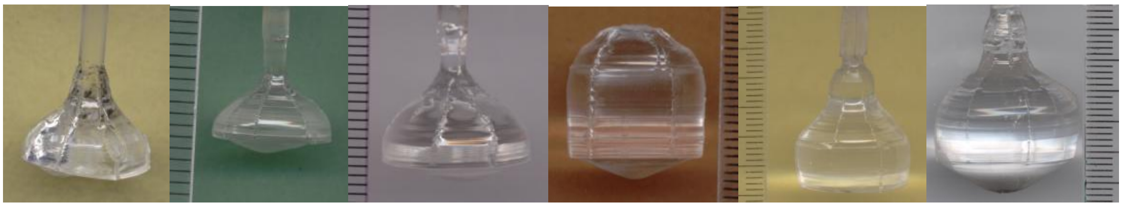

Figure 5.1: *Photograph of as grown single crystal ingot of 0.1, 0.3, 0.5, 0.7, 1.0 and 1.1 wt% silver doped* $Li_2B_4O_7$.

5.2 Optical and Structural Characterization

All the crystals showed over 85% transmission in the visible range, indicating a good optical quality of the grown crystals. All the crystals showed an absorption band at around 205 nm corresponding to the $4d^{10} \rightarrow 4d^9 5s$ transition of Ag^+ centers [171]. This confirmed that the Ag is incorporated as Ag^+ ions in the LTB lattice. Though the actual concentration of Ag in the LTB crystal was not measured, the absorbance at 205 nm increased monotonically for increasing concentration of Ag in the melt [Fig.5.2(a)] and started to saturate beyond 0.5 wt% Ag and saturated for 1.0 wt% of Ag in the melt [Fig.5.2(b)]. A further increase beyond 1.0 wt% Ag degraded the optical quality of grown crystals (opaque and containing inclusions). The saturation in the absorbance of Ag doped LTB indicates that there is an upper limit on the amount of Ag that can be incorporated in the LTB single crystal. Though inductively coupled plasma mass spectrometry (ICP-MS) studies carried out on the samples did not provide very accurate results, an upper limit of nearly 500 ppm of Ag in the LTB crystal has been estimated. This indicates a fairly low (approximately 0.1) segregation coefficient for Ag in solid state LTB presumably because of a large mismatch in the ionic radii of Li^+ (76 pm) and Ag^+ (127 pm) [170].

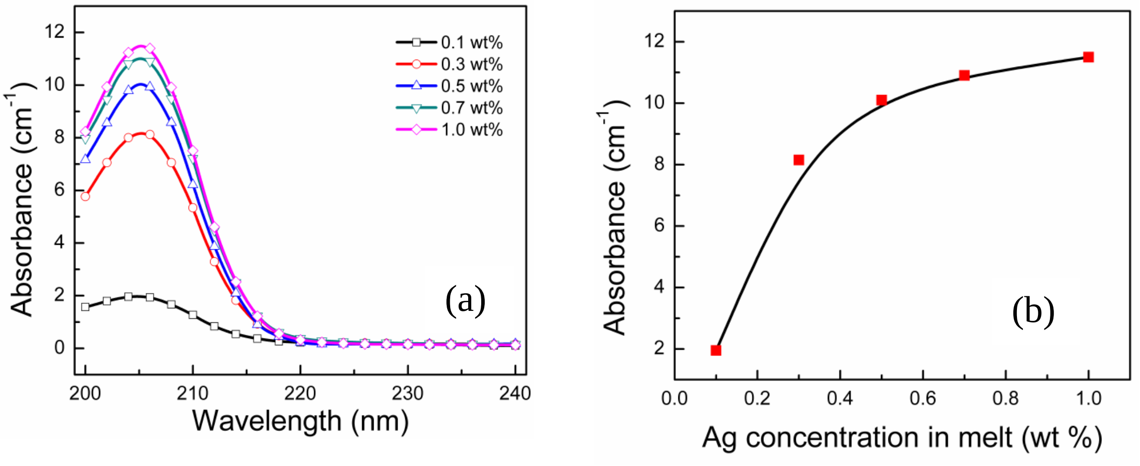

Figure 5.2:*(a) Comparison of absorption spectra with varying concentrations of Ag in $Li_2B_4O_7$.*

(b) A plot of Absorbance vs. Ag concentration in melt of $Li_2B_4O_7$.

Phase purity of the grown crystals was checked by recording X-ray powder diffraction (XRD) pattern. The XRD pattern of the grown crystals, as shown in Fig.5.3, matches with the reported JCPDS-84-2191 data of LTB crystal. However, due to incorporation of Ag^+ ions in the lattice, all the peaks were slightly shifted towards lower 2θ values as seen in the inset of the Fig.5.3, indicating a marginal expansion in the lattice volume. The larger ionic radii of Ag^+ substituting the Li^+ ions in the lattice results in an increase in the lattice parameters and therefore shifting of peaks to lower 2θ values. This further supported the view that a large mismatch in ionic radii of Li^+ and Ag^+ may be one of the reasons responsible for low Ag content in the LTB crystal.

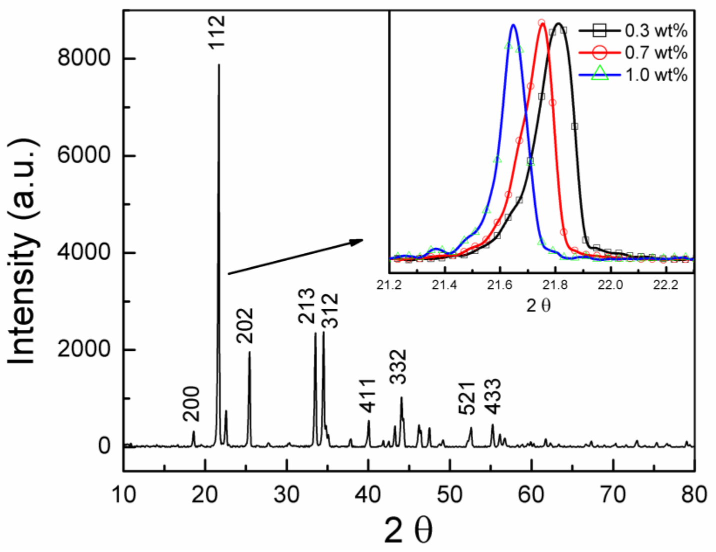

Figure 5.3: *Powder X-ray diffraction pattern recorded for pulverized $Li_2B_4O_7$ single crystal. The inset shows the effect of Ag concentration on the position of the peak corresponding to (112).*

5.3 Luminescence Characterization and Analysis

All Ag doped LTB crystals show a strong emission band peaking around 270 nm on excitation at 205 nm as shown in emission and excitation spectra in Fig.5.4(a). This emission corresponds to the transition of Ag^+ ($4d^95s \rightarrow 4d^{10}$), similar as reported earlier by several research groups [157, 172]. The emission spectra (for excitation at 205 nm) of LTB containing varying concentration of Ag are shown in Fig.5.4(b). For better presentation, area under the curve of 270 nm emissions for different concentration of Ag was plotted against the doping as shown in inset of Fig.5.4(b). The results show that with increasing Ag in LTB, the emission peak at 270 nm (corresponding to Ag^+ ions) first increases till 0.5 wt% of Ag in the melt and thereafter it decreases with further increase in the Ag content. This suggests a concentration quenching of luminescence in the LTB:Ag containing Ag above 400 ppm considering an upper limit of 500 ppm of Ag in LTB. Further, a small emission peak at 370 nm is also observed for excitation at 265 nm (observed in undoped LTB too). This emission corresponds to Cu^+ ions that may get incorporated unintentionally during the growth or could have already presented in raw materials.

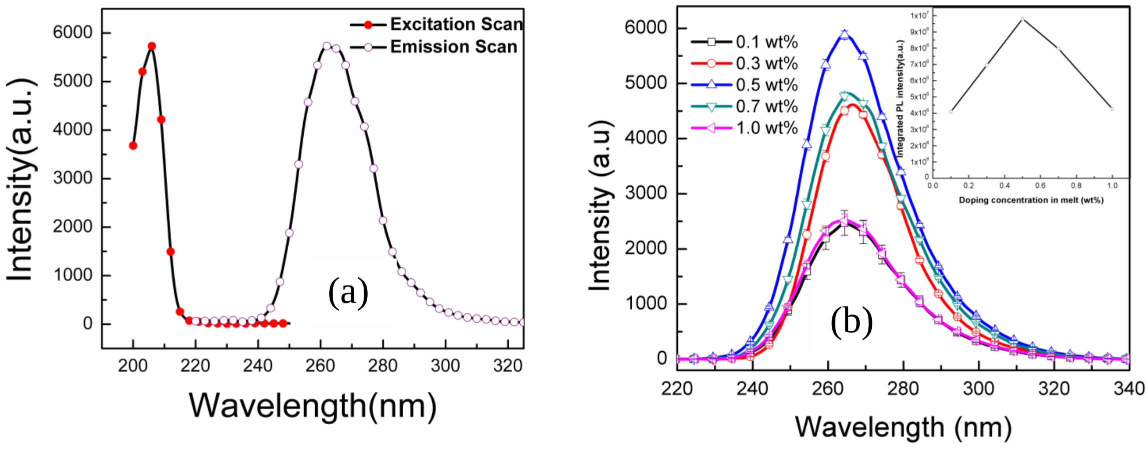

Figure 5.4:*(a) Emission and excitation spectra of Ag doped $Li_2B_4O_7$ crystal.*

(b) Effect of Ag concentration (in melt) on the emission spectra of $Li_2B_4O_7$:Ag crystals.

The time resolved fluorescence spectrum of the 270 nm emission as shown in Fig.5.5 revealed a single exponential decay with a decay time of 12 μs.

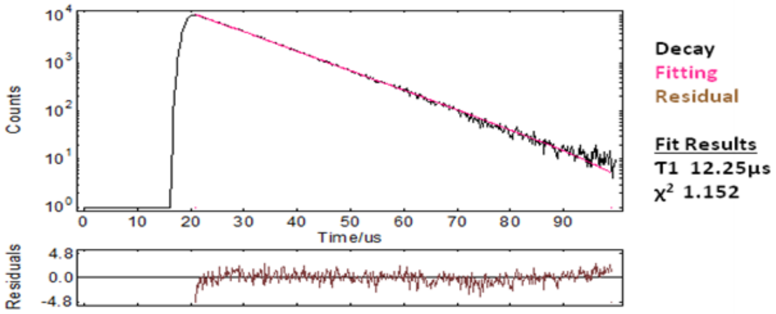

Figure 5.5: *Luminescence decay curve and difference between the fitted and measured data of a Ag doped $Li_2B_4O_7$ crystal.*

The X-ray excited luminescence (XEL) or radio-luminescence (RL) was measured by exciting the LTB:Ag samples of 6 mm cube using an X-ray source with Cu target operated at a tube voltage of 40 kV and current of 30 mA. The emission spectrum in the range of 200-1100 nm was recorded with the help of an optical fiber based spectrometer (Avantes make, Model-3648). All measurements were carried out at room temperature. The RL shows a single emission peak at 270 nm as shown in Fig.5.6. This emission corresponds to the $4d^9 5s \rightarrow 4d^{10}$ transition of Ag^+ centers. Upon X-ray excitation the X-ray energy was transferred to excite the Ag^+ centers and corresponding emission takes place.

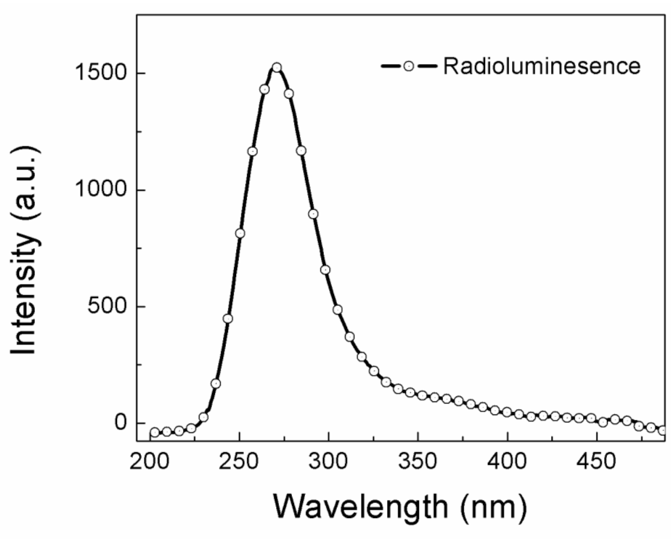

Figure 5.6: *Radio-luminescence of LTB:Ag single crystal.*

The RL emission at 270 nm is well matched with recorded PL emission. A small hump at about 370 nm in the RL spectrum is also observed, which is characteristic emission of Cu^+ centers, also support the incorporation of the Cu impurity in LTB:Ag crystal.

5.4 TSL Characterization

5.4.1 Modification in TSL reader

In the recent past, researchers found that silver is not a good activator of LTB for dosimetry application due to its low sensitivity to radiation dose. Even, some of the research group claimed that it shows inferior quality than the LTB:Mn. These reports were based on the TSL measurements carried out by employing blue sensitive photomultiplier tubes (PMTs) with photosensitivity range from 300 to 650 nm [174]. To check whether these PMTs having such range of sensitivity are suitable to cover the Ag emission, TSL emission spectrum was recorded for LTB:Ag at a 120°C isotherm. The thermal glow curve emission of the LTB:Ag is centered at 270 nm as shown in Fig.5.7(a), which is far from the operational range of the such PMTs. This may be the main reason as to why the potential of LTB:Ag as dosimetry material could not be fully realized so far, as the PMTs are not suitable for the LTB:Ag material and resulted in poor performance compared to conventionally used LTB:Cu (10 μGy of MDD [88]). This study suggests that one can find a suitable PMT having sensitivity in the UV range which can match the emission of LTB:Ag at 270 nm. With the study of TSL glow curve of LTB:Ag and photosensitivity curve of several photo-cathodes, it was found that the response curve of Cs-Te photocathode used in solar blind PMTs [Fig.5.7(a)] matches well with the peak emission of 270 nm from LTB:Ag as observed in the TSL glow spectrum. Therefore, a new TSL read-out setup using a solar blind PMT (ET 9422B) having Cs-Te photocathode with a spectral response in the range of 110 to 360 nm and an MgF_2 window was fabricated. Rest of the system was similar to the previous setup. The schematic of the modified TSL reader is shown in the Fig.5.7(b).

This modified TSL set-up will provide the maximum sensitivity for the LTB:Ag or other TLD phosphors whose emission lies in the UV region whereas for the other normal TLD phosphors, this system will shows a lower sensitivity compared to commercial TLD reader as sensitivity of solar blind PMT in the visible region is low and may not be suitable for application.

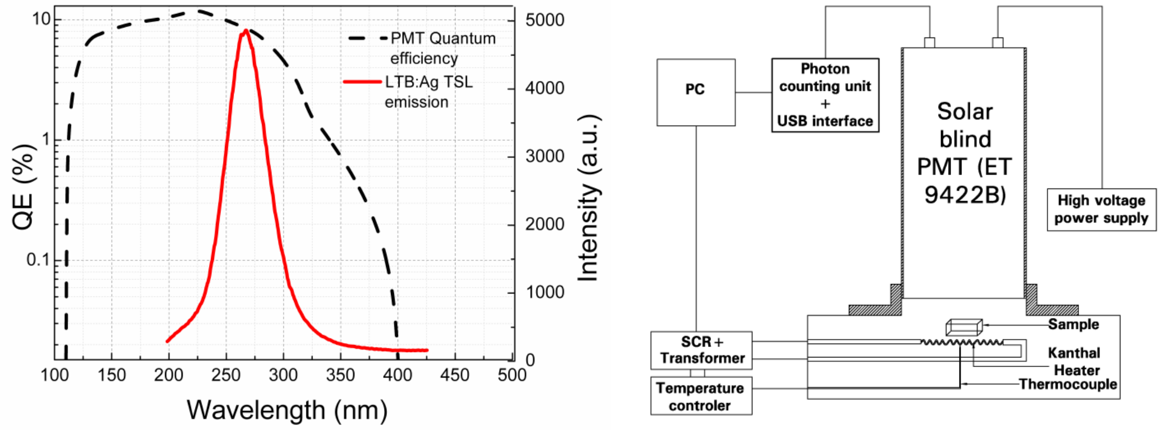

Figure 5.7: *(a) The thermally stimulated luminescence spectrum of Ag doped* $Li_2B_4O_7$ *along with the photo sensitivity curve of Cs–Te photo cathode.*

(b) Schematic diagram of the modified TSL reader set-up consist of solar blind photomultiplier tube.

This modification in the TSL read out system has significantly improved the TSL performance of LTB:Ag by enhancing the signal because of better matching between the emission from Ag^+ ions and PMT response. Due to a lower quantum efficiency (~10%) of the solar blind PMT at 270 nm the signal is reduced a little bit but there are other advantages of using this type of PMT including significantly reduced background noise (more than one order) of the set-up which is contributed predominantly due to visible light leakage as it is insensitive to the visible light. Thus the signal-to-noise ratio of the set up enhanced significantly and makes it’s more sensitive. This set up also immune to thermal emission (mainly in the IR region) generated from the heating element so that the PMT can be directly used without any heat or IR filter between sample and PMT. These advantages of solar blind PMT make the set-up an ultra low noise system that can detect very low doses with good accuracy and repeatability.

5.4.2 TSL Glow Curve

The glow curve of LTB with varying Ag concentrations for a fixed dose was recorded and is shown in Fig.5.8. The glow curve consists of a single intense peak around 160°C and is in accordance with the reported values in the literature [151, 173]. As the Ag concentration in LTB increases the TSL output is increased as well. This is contrary to the concentration quenching observed in the photoluminescence. This may be because the TSL process involves trap centers as well as luminescence centers while photoluminescence involves only luminescence centers. Therefore the effect of concentration quenching due to high Ag concentration is overcompensated in the TSL process by an increase in number of the trap centers. With this study it was found that a single crystal of LTB grown from melts containing 1.0 wt% Ag exhibits an optimum performance as a dosimetry material. The TSL process involved in the LTB:Ag can be explained with a sequence of events analogous to LTB:Cu as discussed in chapter 3.

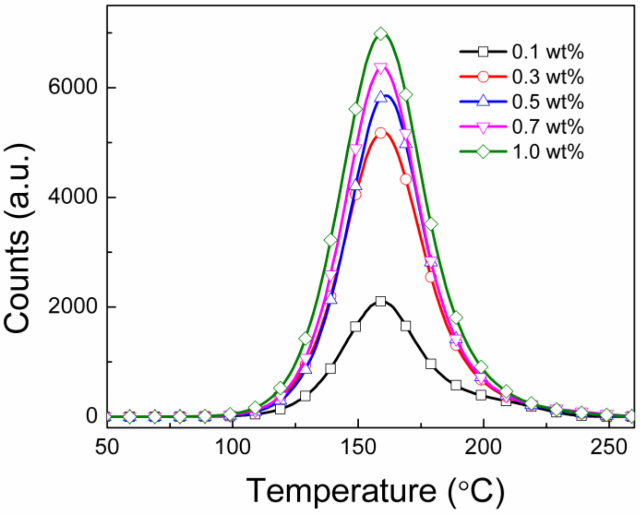

Figure 5.8: *Thermally stimulated luminescence glow curves for different Ag concentrations in $Li_2B_4O_7$ crystals for a dose of 100 mGy.*

The TSL glow curves as a function of dose in the range from 200 mGy to 3 Gy were recorded and shown in Fig.5.9 for LTB:Ag (1.0 wt% in melt). The peak temperature does not shift in this dose range which is similar to LTB:Cu [175]. However, the position of the peak shifted towards higher temperatures with increasing heating rate.

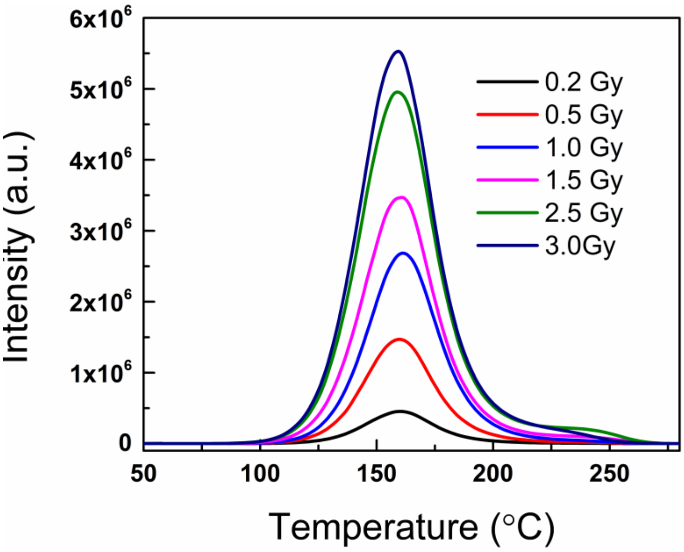

Figure 5.9: *TSL glow curve for various doses from 200 mGy to 3 Gy of 1.0 wt% (in melt) Ag doped* $Li_2B_4O_7$ *crystal.*

The kinetic parameters for the material were calculated for employing the TLAnal software by taking general order approximation (GOK) and are given in Table 5.1. The trap depth is found to be 1.35 eV while the frequency factor is 5.8x10^{15} and order of kinetic is 1.6.

Table 5.1. *Kinetic analysis of TSL peak of* $Li_2B_4O_7$*:Ag. (Heating rate: 1ºC/s)*

Dose (Gy)	**Peak T (°C)**	**Trap depth E (eV)**	**Frequency factor (s^{-1})**	**Kinetic Order (b)**
1	160	1.35	5.8E+15	1.6

5.4.3 Dose Linearity

The dose vs. TSL response of the LTB:Ag single crystals for a dose range from 3×10^{-6} Gy to 100 Gy is plotted in Fig.5.10. The LTB:Ag dose response is found to be linear up to 10 Gy and a slight nonlinear behavior sets in beyond this dose.

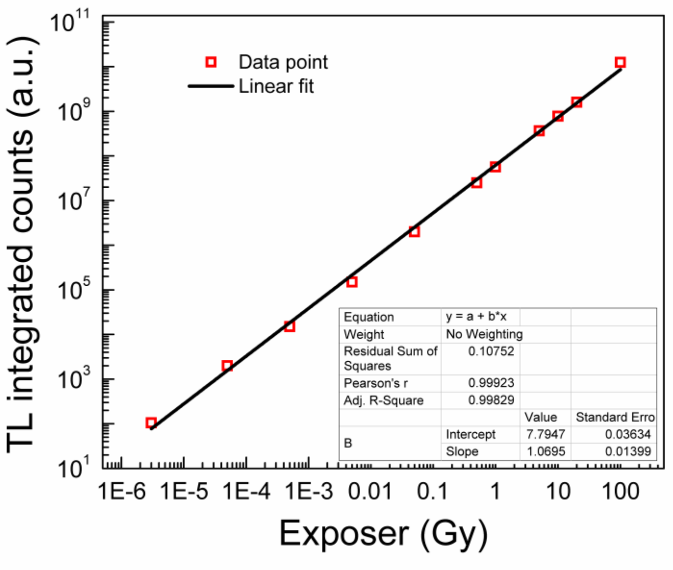

Figure 5.10: *Dose linearity plot for 1.0 wt% (in melt) Ag doped $Li_2B_4O_7$ crystal for a dose range from $3x10^{-6}$ to 100 Gy (sample size: $9x9x0.5\ mm^3$, weight: 100 mg and heating rate: 1ºC /s).*

5.4.4 Minimum Detectable Dose (MDD)

The zero dose measurement data of the experimental set-up (as described) are shown in Fig.5.11(a). The standard deviation (σ) of the zero dose background was calculated as discussed in the previous chapters (section 4.4.1) and the value is approximately 15 counts per second (cps). A low dose of 3 μGy could be measured with an LTB:Ag sample of size $9x9x0.5\ mm^3$ using the set-up and shown in Fig.5.11(b) The zero dose background data are given in the same plot to show the signal-to-noise ratio for the low dose of 3 μGy. The sensitivity of the material was further increased by 1.2 times when one of the surfaces was coated with aluminum, which increased the light collection. There are reports in literature of minimum dose detection limit of 25 μGy using conventional material and TSL set-up considering the 3σ of the zero dose measurement method [176]. While for the present system the 3σ is 45 cps and from calculations the limit to detect minimum dose would be about 500 nGy.

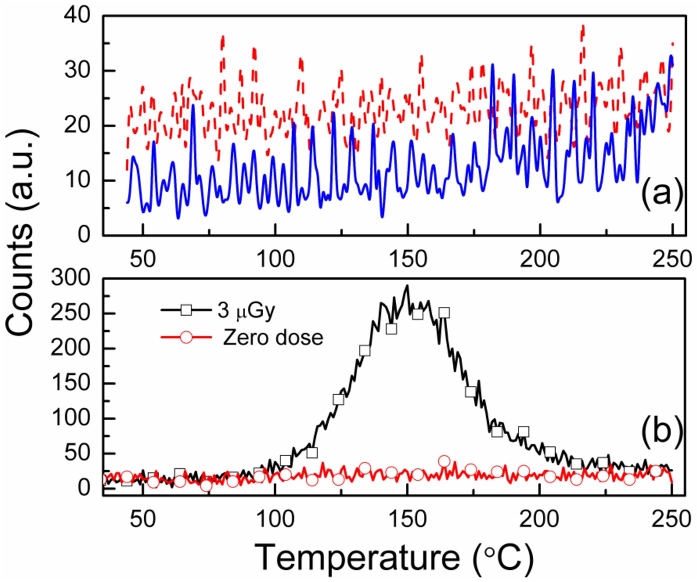

Figure 5.11: *(a) Two extreme zero dose signals (TSL signal from the Ag doped* $Li_2B_4O_7$ *with zero dose) in five measurements in identical settings (heating rate: 1°C/s). (b) 3 μGy dose measured with the present setup and optimally Ag doped* $Li_2B_4O_7$ *sample (size: 9x9x0.5* mm^3*, 100 mg and heating rate: 1°C/s). A zero dose signal is also plotted for comparison. (Both are experimentally recorded data).*

5.4.5 Fading of TSL Signal

The fading study of the material was carried out under two conditions, namely i) samples stored under dark conditions and ii) samples kept under day light after irradiation. For this study, two set of 10 samples were exposed to a fixed dose of 1 Gy. After the irradiation, one set of samples wrapped with aluminum foil and kept in light tight room (referred as dark condition) where as other set of samples were kept in such a way that normal day light falls on the samples in room temperature. The fading study of the material was carried for a time span of 30 days. During this period, the room temperature

(RT) was monitored and found that temperature varies in the range of 30 ± 3ºC. The fading of the material is shown in Fig.5.12 for the two different conditions. A faster rate of fading is observed for samples stored in day light compared to those kept in dark cover indicating the material's sensitivity to light. This indicates the optical bleaching of the traps. For the samples kept in dark, there is approximately 15% fading after 30 days that is comparable to some commercially available TL dosimeters [152, 177]. Thus the material to be used as dosimeter needs a proper light tight encapsulation.

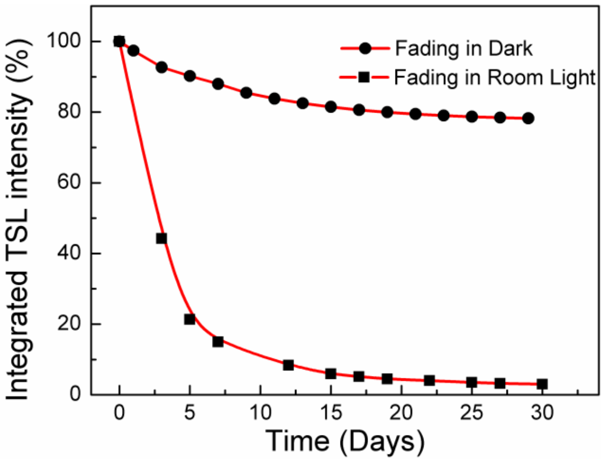

Figure 5.12: *Fading of the TSL signal as a function of time for set of samples kept in dark and room light of* $Li_2B_4O_7$*:Ag single crystal.*

5.4.6 Low Dose Calibration and Environment Dose Monitoring using LTB:Ag

As the LTB:Ag is able to measure very low doses (less than 5 µGy), the material was tested for environmental dose measurement. For this purpose, to generate a calibration curve in the low dose range a set of LTB:Ag samples was irradiated using a calibrated source of ^{60}Co with a dose rate of 330 µGy/min (at a distance of 70 cm from the source) in the dose range from 20 µGy to 60 mGy. Therefore, the TSL integrated intensity was plotted as a function of dose. Fig.5.13 shows the TSL integrated intensity vs. dose (linearity plot) in the dose range from 20 µGy to 60 mGy.

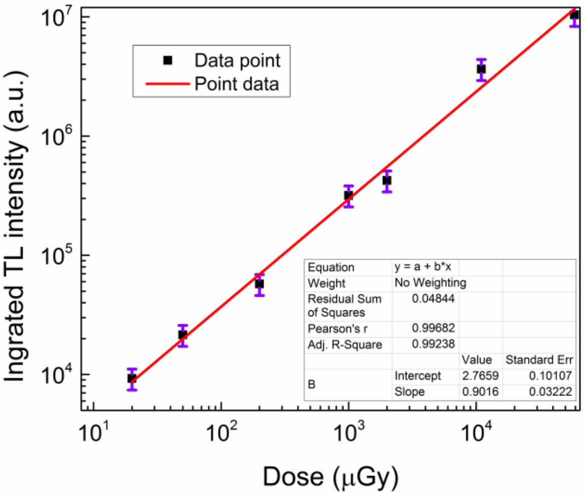

Figure 5.13: *Dose linearity plot of* $Li_2B_4O_7$*:Ag.*

A few LTB:Ag samples of size 6×6×0.6 mm^3 were used to measure the environmental doses for a period of 60 days. For this purpose samples were first annealed at 300°C for half an hour and subsequently wrapped individually in aluminum foil so that no visible light falls on the samples and kept at outside of the Crystal Technology Laboratory, BARC/Mumbai for different durations. Thereafter the TSL were recorded for the samples after 7, 15, 30, 45 and 60 days environment exposure. Fig.5.14(a) shows the TSL output for 7, 15, 30, 45 and 60 days environmental exposure with reference to zero dose.

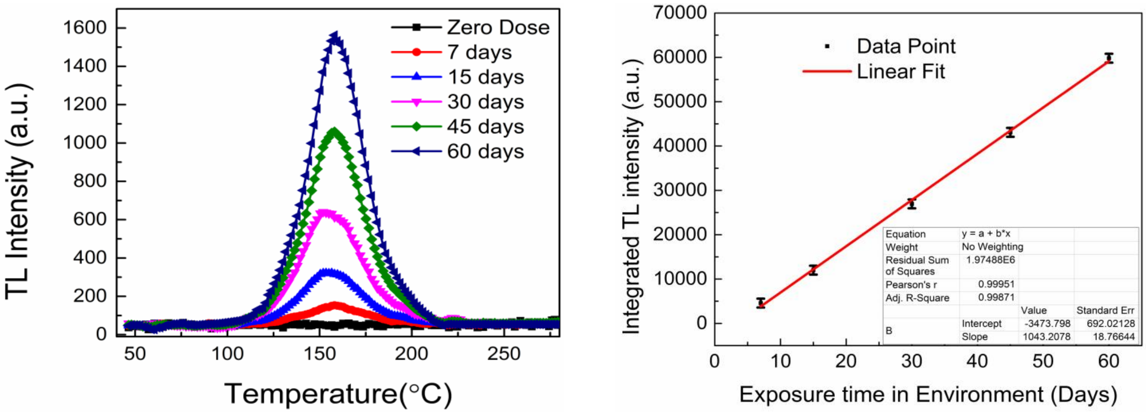

Figure 5.14: *(a) TSL response for environmental dose for 7, 15, 30, 45 and 60 days (b) Dose linearity plot of* $Li_2B_4O_7$*:Ag with time of environmental exposure.*

The height of the peak is increased with increasing time of exposure suggesting accumulation of environmental dose in the samples. Fig.5.14(b) shows that integrated intensity for different environmental doses. The integrated intensity is found to be linear in this environmental dose range. From calibration curve the estimated dose for 7 days is found to be approximately 12 µGy and for 60 days environmental dose it is around 100 µGy. As per the radiation data reported by IERMON/BARC [178], the environmental dose for a period of one week is around 10 - 14 µGy from background (such as cosmic rays, terrestrial rays, earth surface, food etc) in the experimental place (Mumbai, India). These measurements suggest the potential use of LTB:Ag in environment dose monitoring applications.

5.4.7 Optical Bleaching Study of LTB:Ag

For optical bleaching studies in 1.0% Ag doped LTB samples, at first the samples were irradiated to a fixed dose of 2 Gy. Thereafter, the samples were optically bleached using a laser of 5 mW output power having emission in the 450-600 nm range for different time. Then TSL glow curves were recorded for each samples and integrated intensity was plotted with time of laser exposure as shown in Fig.5.15. It is found that integrated intensity decreases with time of laser exposure. The results suggested that the material is sensitive to optical stimulation and there is a possibility of generating OSL signals from the material.

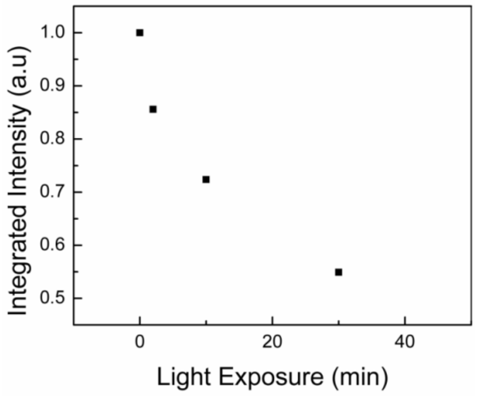

Figure 5.15: *Integrated TSL intensity versus different time of light exposure of* $Li_2B_4O_7$*:Ag.*

5.4.8 *Medical Dosimetry*

Any dosimeters to be used in medical dosimetry applications should have more than 95% confidence level i.e. variation in sensitivity from dosimeter to dosimeter should be less than 5 %. To check the uniformity of the LTB:Ag, 60 samples of LTB:Ag (3x3x0.5 mm^3) were exposed to 2 Gy dose using Linac (6 MeV) at Hinduja hospital, Mumbai and subsequently TSL were recorded. The TSL glow peak of each sample was integrated over temperature and integrated area versus samples were plotted and shown in Fig.5.16. From the figure we can see that there is a maximum 20% variation of light output from sample to sample. For medical dosimetry, 16 samples out of 60 were chosen for which the variation of light output varies within 3% and were exposed to dose equivalent to dose received by a malignant tumour during radiotherapy [179]. After that, corresponding TSL were taken and from calibration curve the unknown dose were calculated and compared with actual machine value and is given in Table 5.2. As shown in table, the calculated values of the different samples differ from the actual value is not more than 4%. This suggests that the LTB:Ag has a potential to be used as a medical dosimeter.

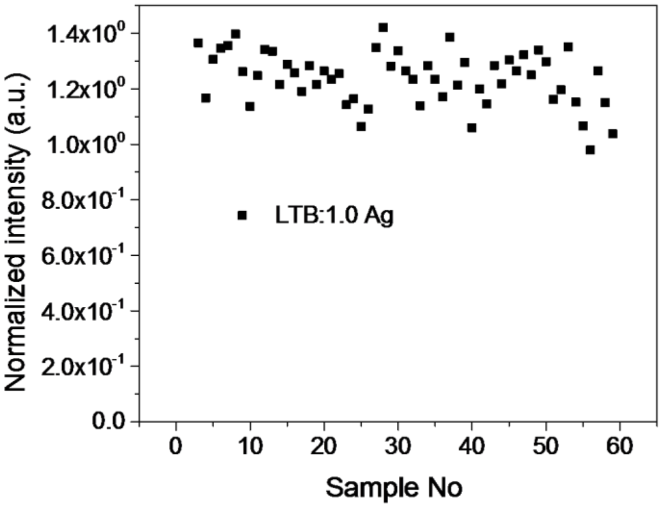

Figure 5.16: *TSL light output for different samples of* $Li_2B_4O_7$*:Ag for a given dose of 2 Gy.*

Table 5.2. Estimated and actual dose for different $Li_2B_4O_7$:Ag samples.

Sample no	Estimated Dose (variation) [Gy]	Given dose (Actual) [Gy]
G7	1.95 (-1.5%)	1.98
G8	1.94 (-2%)	1.98
G9	1.97 (0.5%)	1.96
G10	1.93 (-1.5%)	1.96
H7	1.91 (-4%)	1.99
H8	2.04 (2.5%)	1.99
H9	2.06 (3.5%)	1.99
H10	1.95 (-2%)	1.99
I7	2.06 (3%)	2
I8	2.06 (3%)	2
I9	1.97 (-2%)	2.01
I10	1.96 (-3%)	2.02
J7	2.03 (1.5%)	2
J8	1.96 (-2%)	2
J9	2.08 (3%)	2.02
J10	1.95 (-4%)	2.03

5.5 Conclusions

High quality single crystals of Ag doped LTB of 20 mm diameter and 20 mm length with varying Ag concentration have been grown by CZ technique using commercial and solid state synthesis polycrystalline powder. It was found that beyond the 1.0 wt% doping in melt the quality of the crystal was not good and the absorbance at 205 nm get saturated at this level. From the transmission, PL and RL studies it is confirmed that Ag^+ is incorporated in LTB matrix and gives it characteristic emission. In PL, a concentration quenching of 270 nm emission peak of Ag^+ is observed beyond 0.5 wt% doping. The optimum concentration of Ag for the best TSL performance was determined through the TSL studies. The optimum Ag concentration in the LTB was found to be about 500 ppm (1.0 wt% in melt) for the best TSL properties. It was found that TSL emission of LTB:Ag belongs to Ag^+ (270 nm) luminescence centers that matches with the photo-response of Cs-Te photo-cathode. A material specific TSL readout system was built using a solar blind photo-multiplier tube. This system resulted in improved detection efficiency and lower noise that could measure a dose as low as 3 μGy experimentally while the calculated minimum detectable dose was estimated at 500 nGy. The TSL set-up and LTB crystal with optimum Ag concentration have been proposed as promising system in low level personal and environmental dosimetry applications. This material was demonstrated for environment dose monitoring applications with a dose estimation of 100 µGy for 60 days of environmental dose. There was approximately 15% fading after 30 days for samples stored under dark conditions. The fading studies also revealed the optical bleaching of the traps. LTB:Ag was also successfully tested in medical dosimetry application with a confidence level of 97%. All these studies indicate that the LTB:Ag single crystal phosphor has potential for its use in various radiation dosimetric applications, particularly in medical dosimetry due to its tissue equivalence.

Single crystals TLDs have advantages compared to powder TLDs. However as the production of single crystals is not simple, so the cost of single crystal TLD may be higher than the powder/pelletized TLDs. To minimize the cost one can grow large size single crystals as the crystal growth process for some materials are well established and in the recent times one can grow big size crystals of 4 inch diameter and 6 inch length. Such big crystal can give around 1200 number of 8 mm diameter and 0.6 mm thick dosimeters in a single shot. Out of this 500 dosimeters may be suitable for application in personal dosimetry and the production cost may be comparable to powder TLDs.

CHAPTER 6

OSL CHARACTERIZATION OF Ag DOPED $Li_2B_4O_7$ AND THERMAL NEUTRON DETECTION

The optically stimulated luminescence (OSL) is a relatively new technique than TSL that works on the same basic concepts but for the stimulation energy, which is supplied by photons instead of heat in the former case. The OSL technique has few notable advantages over the TSL [180]. The most important of these advantages is that only the trapping levels most sensitive to light are sampled and stimulation can be performed at room temperature thus avoiding the thermal quenching of the emission [181]. Also all-optical readout system offers greater versatility and faster dose-assessment that can be used in applications like in-situ dose monitoring in radiation medicine and spatial dose mapping in image plates etc.

So far, TSL properties of the LTB material have been widely studied but OSL properties have not been investigated in details. In the recent past, there are few reports on OSL studies of Cu doped LTB and (Ag, Cu) co-doped LTB have been reported [81, 83]. However, to my best knowledge the OSL properties of Ag doped LTB crystal have not been studied and there are no published results on the OSL properties of LTB crystal exclusively doped with Ag in literature. In the previous chapter of this thesis, TSL properties of LTB:Ag crystal were investigated and found quite sensitive even up to micro Gy level exposure. In this chapter, the study on the LTB:Ag single crystal as a potential OSL material has been presented in details along with its potential use in thermal neutron detection.

6.1 OSL Characterization of LTB

The crystal ingots were cut into samples with size of 3 mm × 3 mm × 0.5 mm for the OSL measurement. A continuous-wave OSL (CW-OSL) response of a LTB:Ag crystal samples were measured in 0.1 Gy to 1 kGy dose range using a β-source ($^{90}Sr/^{90}Y$, 1.95 GBq). The optical stimulation was provided by blue light emitting diodes (λ_p = 458 nm and $\Delta\lambda$= 10 nm) and the emission was detected by a PMT (ET make, Model-ET9235-QB). A 5 mm thick glass filter (Hoya U-340) was used to prevent the stimulating radiation reaching the PMT. The light intensity at the sample position was measured to be 40 mW/cm^2. The recorded OSL curves for different doses (0.1, 1.0, 10, 50, 100 and 500 Gy) are shown in Fig.6.1.a. The measurements were carried out immediately after β-irradiation. For a comparison of LTB:Ag with LTB:Cu, the OSL curve corresponding to LTB:Cu for 0.1 and 2 Gy doses are shown in Fig.6.1.b.

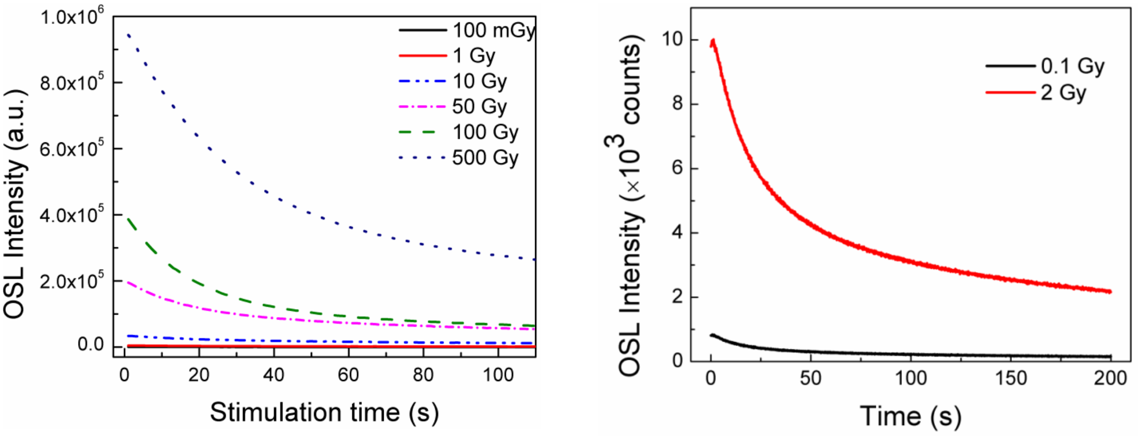

Figure 6.1: *The OSL curves recorded for (a) $Li_2B_4O_7$:Ag sample immediately after the β-irradiation for doses of 0.1, 1.0, 10, 50, 100 and 500 Gy. (b) $Li_2B_4O_7$:Cu sample with dose 0.1 Gy and 2 Gy.*

The decay of the OSL signal as a function of time is modulated by the intensity of the stimulation light. A simple OSL model with multi trap centers but with no re-trapping given by equation (6.1) was considered for the preliminary analysis of the CW-OSL signal from the LTB:Ag:

$$I_{osl} = \sum_{i=1}^{n} n_i p_i \exp(-tp_i), \quad p_i = \sigma_i \varphi \tag{6.1}$$

Where, n_i is the initial concentration of charge carriers trapped in i^{th} type trap after irradiation, σ_i is the photoionization cross-section of the trapping center, and φ is the photon fluence rate of stimulation light (photons/cm^2/s). The OSL curve of LTB:Ag and LTB:Cu were fitted (not shown in figure) with the above equation and different parameters were calculated as given in Table 6.1. The OSL curve of the LTB:Ag was found to be a three component exponential decay whereas LTB:Cu (0.5 wt%) crystal has two component exponential decay. From Table 6.1 it is cleared that two photo-ionization cross-sections (out of three) of LTB:Ag are quite similar to two photo-ionization cross-sections of LTB:Cu. These photo-ionization cross-sections are assigned to trap centers related to Cu (unintentionally doped) in the LTB:Ag crystal. The remaining third photo-ionization cross-section of the LTB:Ag is assigned to trap centers related to Ag$^+$ ions. The photo-ionization cross-section of Ag related trap centers is one order higher than that of the Cu related trap centers suggesting superior OSL properties of the LTB:Ag.

Table 6.1. Calculated OSL parameters for LTB:Cu and LTB:Ag

Material	Optical absorption cross-section (cm^2)	Concentration of charge carriers	Photon fluence rate (photons/cm^2/s)
LTB:Cu	$\sigma_1 = \sim 3.0x10^{-19}$, $\sigma_2 = \sim 4.3x10^{-20}$	$n_1 = 8.88545 \times 10^5$ $n_2 = 4.16175 \times 10^6$	$\varphi = 9.24x10^{16}$
LTB:Ag	$\sigma_1 = \sim 4.3x10^{-19}$, $\sigma_2 = \sim 8.6x10^{-20}$, $\sigma_3 = \sim 3.0x10^{-18}$	$n_1 = 1.85870 \times 10^5$ $n_2 = 1.57319 \times 10^6$ $n_3 = 1.91834 \times 10^6$	$\varphi = 9.24x10^{16}$

The emission of LTB:Ag is at 270 nm which is far from the wavelength of stimulation (~ 458 nm). This large difference between the wavelength of the stimulation source and emission from the LTB:Ag may be exploited to develop a simple OSL set-up using suitable filters and a solar blind PMT to enhance the signal-to-noise ratio enabling the measurement of low doses.

It may be mentioned here that currently Al_2O_3:C crystal is used for applications in OSL dosimetry [182]. This OSL phosphor is grown (at ~ 2100°C) by the Czochralski method in a highly reducing atmosphere and in the presence of graphite [183]. Here the necessary F and F^+ centers are created due to oxygen vacancies. Therefore, TSL and OSL properties of Al_2O_3:C exhibit significant variations even with a slight change in the growth conditions. It is very difficult to control the ambient and any change in it can affect the concentration of F and F^+ centers and their relative ratio [184]. However, in the case of LTB:Ag the luminescence properties and trap-centers depend on the amount of Ag in the crystal which can be controlled very precisely by controlling the Ag concentration in the melt that is easier than controlling the ambient. Also variations in ambient would not affect the TSL and OSL properties of the material (as it is not related to oxygen vacancies) ensuring consistency in the batch-to-batch performance. Thus present study indicates that the LTB:Ag can be a good candidate for OSL based dosimetry applications.

6.1.1 Dose Linearity

The dose response of LTB:Ag for different doses, in the range from 0.1 Gy to 1 kGy is plotted in the Fig.6.2. The dose response was calculated by time integration of the OSL signal during the stimulation. As shown in Fig.6.2, the sample showed a linear behavior in the dose range of 0.1 Gy to 500 Gy beyond that it started to show non-linearity or supra-linearity behavior.

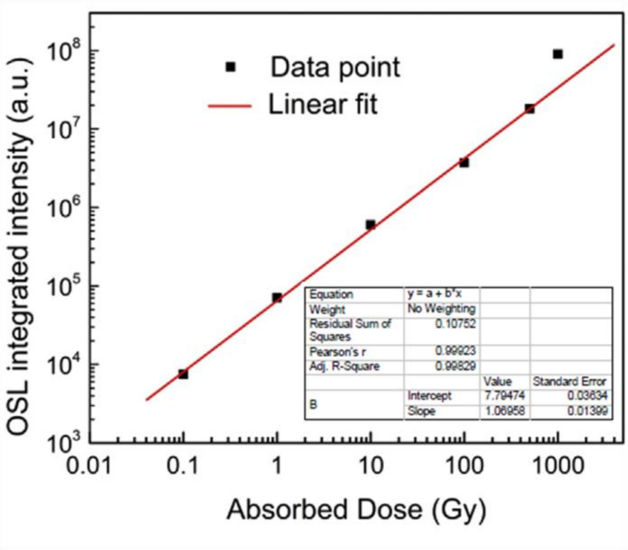

Equation	y = a + b*x		
Weight	No Weighting		
Residual Sum of Squares	0.10752		
Pearson's r	0.99923		
Adj. R-Square	0.99829		
		Value	Standard Error
B	Intercept	7.79474	0.03634
	Slope	1.06958	0.01399

Figure 6.2: *The time integrated OSL intensity at fixed time intervals for different doses in the range from 0.1 Gy to 1 kGy.*

6.1.2 Minimum detectable dose (MDD) in OSL

For MDD measurements, 10 number of LTB:Ag samples were annealed at 300ºC for 1 h which brings the dosimeters back to a typical zero dose "background" level similar as discussed in section 4.4.1. Reading of these background dosimeters gives a mean and standard deviation. The value of three times of standard deviations was taken to calculate the MDD after the conversion from machine output units to dose through the appropriate conversion factor (using the individual dosimeter calibration factors). The minimum detectable dose of LTB:Ag through OSL was calculated as 1 mGy.

6.1.3 Stability of OSL Signal

Fading of OSL signal was also investigated similar to fading of TSL signal. Few samples were irradiated for 200 mGy dose at room temperature and kept in dark. The OSL response of the irradiated samples (integrated intensity) was measured as a function of time after 1 h of irradiation as shown in Fig.6.3. Each data point in Fig.6.3 is an average of the response of two individual samples. Fading of about 36% is observed over a period of 48 h. Higher fading of OSL signal compared to TSL signal is assigned to the influence of all the shallow traps centers which contribute to the OSL signal [13]. However, detailed fading study for longer time is needed to find out the stabilization time of the OSL signal.

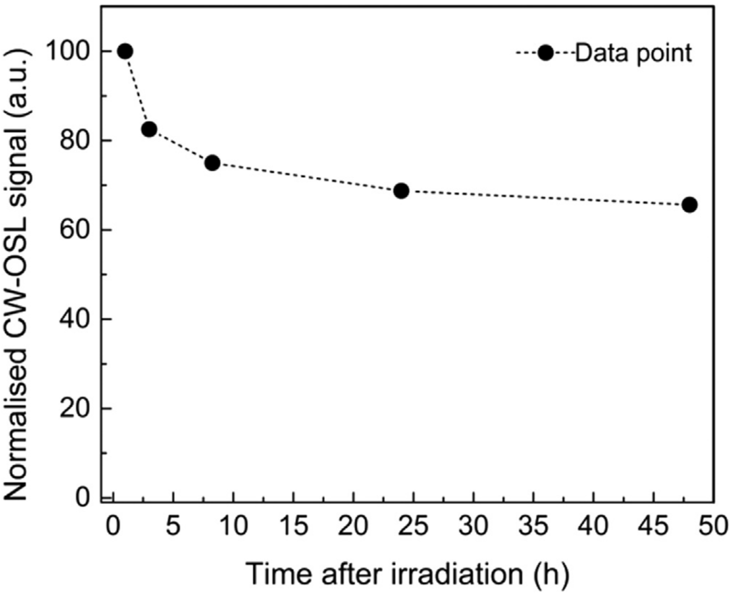

Figure 6.3: *Fading of the OSL signal of* $Li_2B_4O_7$*:Ag as a function of time.*

6.1.4 Comparison of OSL properties of LTB:Ag and Al_2O_3:C

For a comparison of OSL properties of LTB:Ag with some other dosimeters, Bhabha Atomic Research Centre (BARC) developed α-Al_2O_3:C polycrystalline powder were taken as a reference materials [185, 186]. As the reference material is in powder form, single crystal of LTB:Ag were crushed and sieved to 50 micron particle size that makes it similar to the BARC developed α-Al_2O_3:C polycrystalline powder. For this study, equal weights of these samples were taken. The TSL and OSL response of the BARC developed α-Al_2O_3:C polycrystalline powder and the LTB:Ag sample are shown in Fig.6.4(a) and Fig.6.4(b) . It may be noted that the area under the curve of the dosimetry peak in TSL of LTB:Ag is approximately 30% of the BARC developed α-Al_2O_3:C.

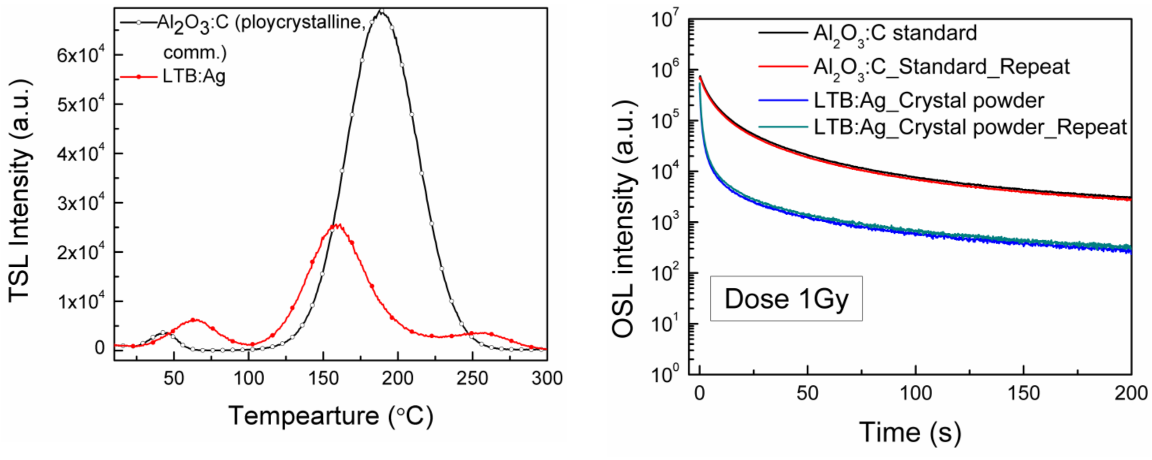

Figure 6.4: *(a) TSL glow curves of BARC developed α-Al_2O_3:C and $Li_2B_4O_7$:Ag phosphors for 300 mGy absorbed dose.*

(b) *CW-OSL response of the BARC developed α-Al_2O_3:C and $Li_2B_4O_7$:Ag samples irradiated to 1 Gy using $^{90}Sr/^{90}Y$ beta source.*

6.2 Thermal Neutron Detection Employing TSL and OSL Properties of Ag Doped LTB

Neutron detectors are essential tools in variety of fields like nuclear power, nuclear medicine, particle physics, magnetism, etc. Currently, thermal neutron detection relies on gas filled tube based detectors at high pressure containing either Helium-3 (^{3}He) or Boron Trifluoride (BF_3) gases [187]. These gas filled detectors require high bias voltages and use either toxic BF_3 or rare ^{3}He gases. Though ^{3}He is ideal for high pressure gas based neutron sensors owing to its high capture cross-section for thermal neutrons, yet this state-of-the-art detector is bulky, and difficult to configure. Further, ^{3}He isotope has extremely low natural abundance and mostly produced as a byproduct of nuclear device manufacturing. The production of nuclear weapons has been drastically reduced over the past two decades causing a shortage in ^{3}He supply [188]. Therefore the demand for alternate thermal neutron detectors is continuously increasing due to above challenges.

A neutron is an electrically neutral particle that interacts only with a nucleus, so the material for its detection must contains an element with high neutron capture cross-section.

In order to be detected, this interaction must produce charged particles. There are few isotopes that meet these criteria: ^{6}Li (n,α) (σ = 938b), ^{10}B (n,α) (σ = 3845 b), and ^{nat}Gd (n,β) (σ = 49153 b), where n is neutron, α is alpha particle and σ is the neutron capture cross-section. Elements with lower atomic numbers are preferable in order to reduce gamma ray absorption. The solid state detectors are more advantageous due to their higher atomic density (compact size and much higher efficiency compared to gas-filled detectors) and stability for prolonged useful life. An intensive search for a ^{3}He detector replacement yielded new technologies like organic liquid scintillators containing Li, B, or Gd, thin film neutron absorber coatings for semiconductor devices and gas discharge counting tubes. Research on a few materials like ^{6}Li-glass:Ce, ^{6}LiF/ZnS:Ag, $LiBaF_3$:Ce,K, $LiBaF_3$:Ce,Rb, ^{6}LiI:Eu, Cs^6LiYCl_6:Ce, $^6Li^{dep}Gd(^{11}BO_3)_3$:Ce, $^6Li^{dep}Gd(^{11}BO_3)_3$:Ce, etc. is currently at the fore front to develop alternative materials that could replace ^{3}He [189, 190].

6.2.1 Interaction of Thermal Neutrons with LTB

One of the advantages related to the materials in the Li_2O-B_2O_3 system is the presence of Li and B with naturally occurring isotopes (^{6}Li and ^{10}B) that have large capture cross-sections (with a possibility to further improve the performance using enriched materials) for thermal neutrons, useful in neutron and mixed-filed dosimetry application [72]. LTB is one of the members in the Li_2O-B_2O_3 system that has been studied as a dosimeter material. For neutron detection, LTB in the form of single crystals has advantages compared to other forms as it has high density, broad transmission range, better mechanical hardness, better energy proportionality and higher resolution. Thermal neutrons interact with ^{6}Li and ^{10}B in the LTB matrix to produce energetic charged particles (alpha particles) and other particles (^3_1H and ^7_3Li). The energy released (Q value) in the process are shared between these particles.

The details of the reaction are given below.

Upon absorbing a thermal neutron, ^{6}Li undergoes the following reaction,

$$^{6}_{3}Li + ^{1}_{0}n \rightarrow ^{3}_{1}H + ^{4}_{2}\alpha + 4.78MeV$$

^{10}B undergoes a similar nuclear reaction,

$$^{10}_{5}B + ^{1}_{0}n \rightarrow ^{7}_{3}Li + ^{4}_{2}\alpha + 2.8MeV \text{ -94\% yield}$$

$$^{10}_{5}B + ^{1}_{0}n \rightarrow ^{7}_{3}Li^{*} + ^{4}_{2}\alpha + 2.3MeV \text{-6\% yield}$$

Subsequently these charged particles deposit their energies resulting in the generation of electron and holes that are trapped in trap centers present in the material. The absorbed dose information may be retrieved by heating the samples in a thermally stimulated luminescence (TSL) set-up. Thus, the neutron flux could be measured both in passive mode (neutron dosimetry [191, 192]) by ex-situ heating of the sample after the neutron exposure and in real-time by collecting the signal with a continuous heating of the sample during the neutron exposure. The natural isotopic abundant of ^{6}Li is 7.5% and ^{10}B is 19.9% abundant in nature and widely available in separated form [193]. The microscopic cross-sections of thermal neutrons (0.025 eV) for absorption for ^{10}B are 3845.24 barns and 955.47 barns for ^{6}Li, and are among the largest known [194].

6.2.2 Neutron Dosimetry using Ag doped LTB

For application in neutron dosimetry, first LTB:Ag crystals were irradiated with thermal neutrons and immediately after irradiation TSL glow curve of irradiated samples were recorded using the TSL set-up described in chapter-5. For neutrons exposure, few samples of size 6 mm × 6 mm × 0.6 mm were irradiated with thermal neutrons (λ: 5Å) of about 10^{6} n/s/cm^{2} flux through a 2 mm slit (neutron beam line at the Dhruva reactor, BARC, India). Exposure for different time period was given to get variation in neutron fluence on the sample. Thereafter, TSL glow curves were recorded at a constant heating rate of 1°C/s. The TSL curve for all the neutron irradiated samples show a peak at about 160°C, similar to TSL peak for gamma irradiation [151]. Fig.6.5. shows the response of the material from a very low neutrons fluence to high fluence (1.0×10^6 n/cm^2). The response of the material is found to be linear in this fluence range. To predict the low fluence detection limit the data range has been extrapolated. The extrapolated curve shows that a neutron fluence of less than 100 n/cm^2 can be easily detected using the present set-up.

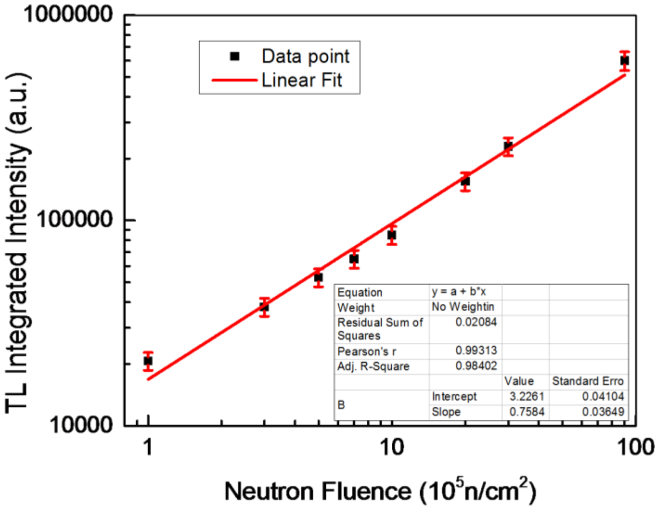

Equation	y = a + b*x		
Weight	No Weightin		
Residual Sum of Squares	0.02084		
Pearson's r	0.99313		
Adj. R-Square	0.98402		
		Value	Standard Erro
B	Intercept	3.2261	0.04104
	Slope	0.7584	0.03649

Figure 6.5: *Response of $Li_2B_4O_7$:Ag crystal to different thermal neutrons exposures.*

To demonstrate the ability to distinguish different low neutron fluxes, the single crystal pieces were exposed for an hour to two different neutron fluxes of 150 and 250 n/s/cm^2 (at RPAD, BARC). During these experiments, contribution from gamma background has been taken into account. The gamma backgrounds are same for both the two neutron fluxes. To cut gamma contribution, a lead (Pb) block of thickness 50 mm was used in front of the single crystal pieces for both fluxes. The TSL curves for neutron with lead block and without lead block (having gamma and neutrons both) are shown in Fig.6.6(a) for a neutron flux of 250 n/s/cm^2. These results show that TSL intensity increased with gamma background and similar results are obtained for a neutron flux of 150 n/s/cm^2 (not shown in figure).

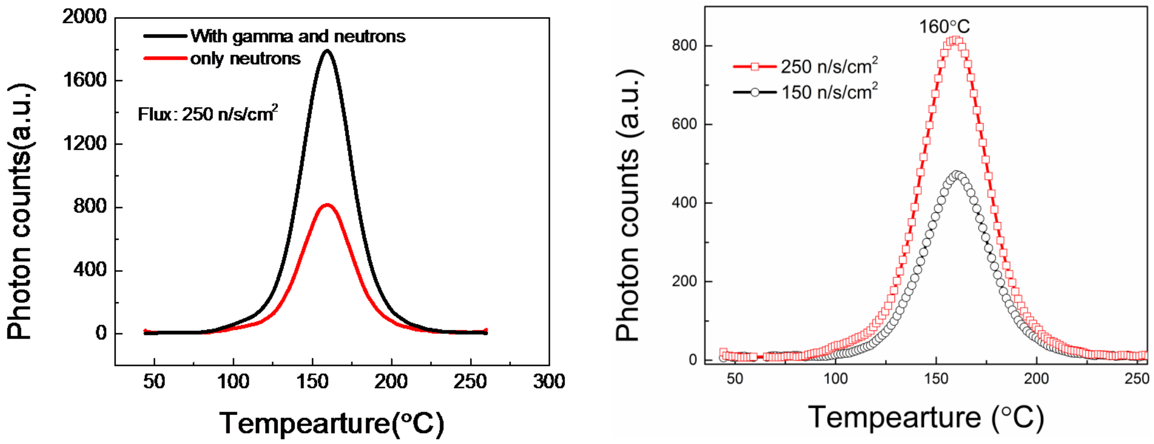

Figure 6.6:*(a) TSL glow curve for neutron and neutron+Gamma of* $Li_2B_4O_7$*:Ag*

(b) TSL glow curve of $Li_2B_4O_7$*:Ag for two different neutron fluxes.*

As the gamma background are same in the both the fluxes, the TSL intensity only for neutron exposure for two different fluxes are shown in the Fig.6.6(b). The peak height for two different fluxes is different and the ratio of the integrated area of the two peaks is measured as 1.6 which is very close to the theoretical ratio of 1.67. Here the theoretical ratio means the ratio of two different neutron fluxes of 250 and 150 n/s/cm^2 i.e. 250/150=1.67. Thus the crystal in the TSL mode can easily distinguish between two low level neutron fluxes.

6.2.3 In-Situ Real Time Thermal Neutron Detection

For online monitoring of thermal neutrons, a detector system was developed by fixing two Pt-100 thermal sensors (working both as heater and temperature sensor) on a small LTB:Ag (6x6x0.6 mm^3) crystal plate. To protect the PMT from direct exposure to the neutron beam, the LTB plate was placed in a 45° reflecting geometry, as shown in Fig.6.7.

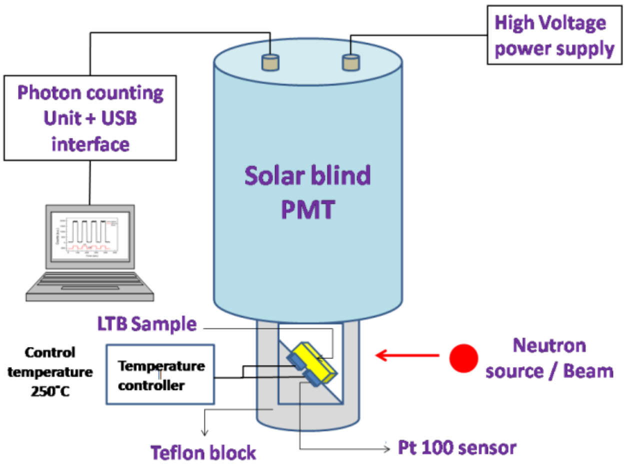

Figure 6.7: *Schematic diagram of the set-up to detect thermal neutrons in real-time.*

This set-up was tested on a thermal neutron beamline at the Dhruva reactor, BARC. A neutron (λ: 5Å) flux of about 10^6 n/s/cm^2 was passed through a 2.0 mm slit on the LTB:Ag crystal. To reduce gamma background a 50 mm thick lead shield was used in front of the detector. Temperature of the LTB:Ag plate was kept constant at about 250°C by adjusting the current passing through Pt-100 as the TSL glow-peak for LTB:Ag lies in the 150-200°C range. This heating ensured the de-trapping of electrons from the Ag$^+$ trap centers immediately after being populated by charge carriers. These charge carriers are produced due to generated alpha particles by (n,α) reactions at ^{6}Li and ^{10}B nuclei in LTB crystals. During the experiment a borated rubber sheet was used as shutter to fully stop the thermal neutron flux. The current from the PMT was recorded in DC mode as a function of time. Fig.6.8 shows the response of the PMT when the LTB:Ag crystal is exposed to thermal neutrons. The use of borated rubber sheet in front of the set up allows only gamma from neutron source or the gamma contribution from the Pb (n,γ) reaction fall on the set up. But in this condition there was no count in the detection set up i.e. the gamma contribution is merged with the system noise. The signal (counts) comes down to nearly zero instantaneously after the neutron beam was stopped and again comes back to the original value when the shutter is removed. Using this set-up, a neutron flux of less than 1000 n/s/cm^2 can be measured.

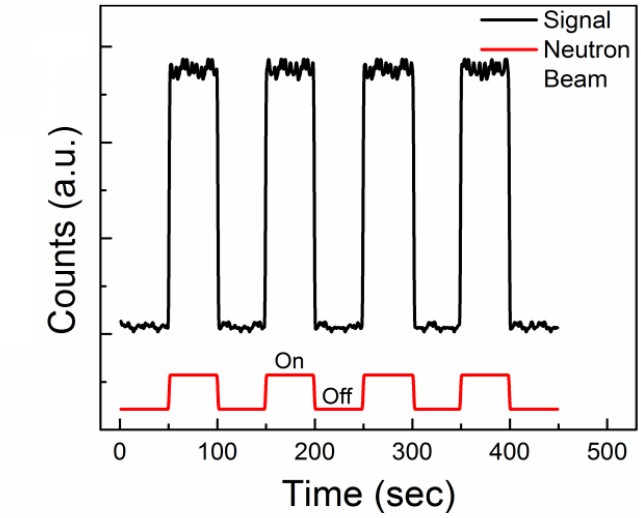

Figure 6.8: *Real-time detection of thermal neutrons using a* $Li_2B_4O_7$*:Ag crystal mounted on Pt-100 heaters. The PMT current is plotted as a function of time as the thermal neutron beam was switched ON/OFF using a borated rubber shutter.*

6.2.4 OSL Response Of Neutron Irradiated LTB:Ag Single Crystal

To record the OSL response of the material to thermal neutrons, few samples (size: 6 x 6 x 0.6 mm^3) were irradiated by thermal neutrons on a neutron beam line (flux: about 10^6 n/cm^2/s) of the Dhruva research reactor, Bhabha Atomic Research Center, India. The samples were exposed to neutron fluences in the range from 10^8 to10^9 neutrons/cm^2. In order to determine the contribution from gamma background, one sample was wrapped in a borated rubber sheet that absorbs neutrons (experimentally verified using a BF_3 neutron detector) but allows most of the gamma-rays to pass (due to its low density and low effective Z).

The OSL was measured for the LTB:Ag after exposures to different neutron fluences and shown in Fig.6.9(a). The recorded gamma background is also shown in the same figure. The OSL response of the LTB:Ag to different neutron fluences (from 3x10^8 to 3x10^9 n/cm^2) is found linear and is shown in the of Fig.6.9(b). This range of fluence is corresponding to equivalent doses from 3 mSv to 30 mSv [195]. Considering only thermal neutrons and using quality factor $Q_f = 2$, this range corresponds to absorbed doses from 1.5 mGy to 15 mGy. The results show that thermal neutrons can be efficiently detected by LTB:Ag along with a suitable OSL set-up.

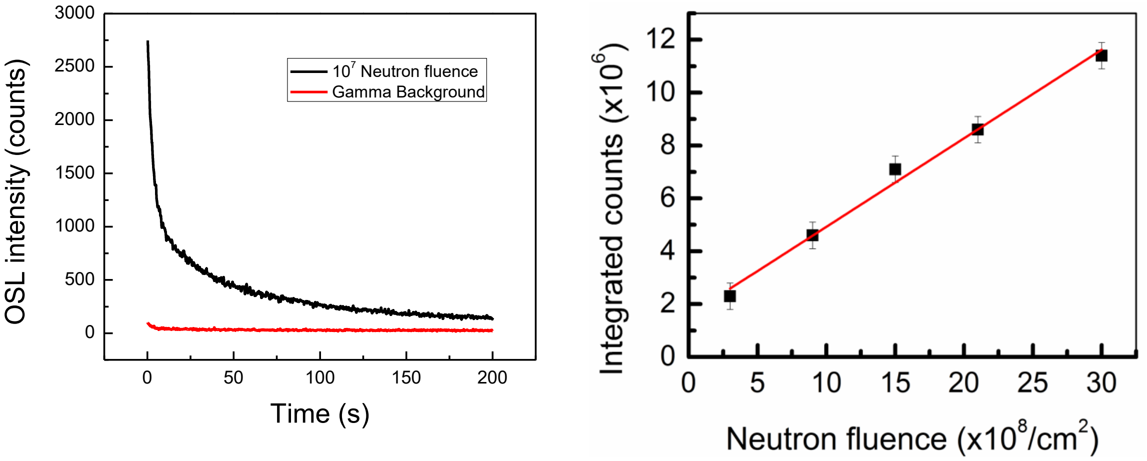

Figure 6.9: *(a) The OSL curve for a LTB:Ag sample immediately after the exposure to a fluence of 3x10^8 neutrons (black line) along with the gamma background (red line).*

(b) The time integrated OSL intensity calculated from the curves for fixed time intervals for different neutrons fluences (not shown in the figure).

This property of the LTB:Ag can also be used to develop imaging screens for neutron radiography with a suitable OSL readout. Though presently a few Al_2O_3:C based OSL devices are being studied for neutron dosimetry, they are based on neutron sensitive coatings on Al_2O_3 or mixing of materials like ^{6}LiF, Gd_2O_3, etc. with Al_2O_3:C [196, 197]. While in the present work the neutron sensitivity is intrinsic to the LTB:Ag that makes it a more suitable phosphor for applications in OSL based neutron dosimetry.

6.3 Conclusions

The OSL properties of the LTB:Ag single crystal were investigated in the present study that revealed the efficacy of the LTB:Ag as an OSL sensitive material with a linear response in the measured range of doses (0.1 to 500 Gy). The fading of OSL signal is found to be about 36% after 48 h. This material was also used as a neutron sensing material. The material exhibited high sensitivity to thermal neutrons with a linear dose response. The samples were tested with various thermal neutrons sources and small variation in the neutron flux was easily distinguished in the TSL glow curve. The detection of thermal neutrons in real-time was also demonstrated using the LTB:Ag crystal kept at about 250°C with a heater. The studies indicate that LTB:Ag may be useful to develop devices based on OSL for mixed-field dosimetry and imaging applications in neutron-radiography. The sensitivity of this material can be further enhanced by growing LTB crystal from compounds enriched in ^{6}Li and ^{10}B.

CHAPTER 7

CONCLUSIONS AND FUTURE SCOPE OF WORK

During the course of this thesis, single crystals of lithium tetraborate (LTB) have been grown and studied for a variety of dosimetric applications. The material has a distinct advantage of tissue equivalence and neutron sensitivity. Further, various dopants and co-dopants were employed to tailor the luminescent properties of lithium tetraborate to make it an efficient dosimeter material. Lithium tetraborate doped with copper, silver and co-doped with copper and silver have been particularly considered for detailed investigations and presented in the thesis because of their superior dosimetric properties such as high TSL and OSL sensitivity, long range dose linearity, neutron dosimetry, etc. For each doping, various characterizations like transmission, PL studies, TSL dosimetric studies, estimation of kinetic parameters and mechanism of TSL and OSL have been carried out. In the course of work, the problems related to single crystal growth of LTB by the Czochralski method were addressed and different growth parameters were optimised to obtain highly transparent, crack-free and clear single crystal of pure and variously doped LTB. High purity starting charge, slow rotation and optimum pulling rates enabled the growth of highly transparent core-free LTB single crystals. Findings of studies on various doped LTB can be summarized as follows

Cu Doped $Li_2B_4O_7$:

From the transmission and PL studies, it is established that Cu is incorporated in the host LTB lattice as Cu^+. The PL emission at 370 nm was characteristic of Cu^+ in LTB. It shows an excitation band having a doublet structure at 240 nm and 262 nm that corresponds to

$^1A_{1g}\rightarrow{}^1E_g$ and $^1A_{1g}\rightarrow{}^1T_{2g}$ crystal field components of the $3d^{10}\rightarrow3d^94s$ transition of Cu^+. The temperature dependence of the emission at 370 nm suggests the off-center or lower symmetry position of Cu^+ ions in the lattice. The TSL response of the crystal is found linear in the dose range from 1 mGy to 1 kGy and the TSL glow peak at about 220°C with a low TSL signal fading (in dark) of about 5% in 30 days. The relatively lower fading rate makes it a suitable material for dosimetry applications. The kinetic parameter of the phosphor was determined with a trap depth of around 1.6 eV. The frequency factor was of the order of 2.1×10^{15} s^{-1} and the order of kinetics is 1.4. The material has also shown a significant OSL signal which suggests its use for dosimeters in the OSL mode.

Cu+Ag Doped $Li_2B_4O_7$:

PL studies revealed that Ag may act as a sensitizer in the co-doped LTB as the emission of Ag^+ centers at 270 nm lies in the excitation region of Cu^+ centers at 260 nm. In TSL studies, an energy transfer from Ag^+ to Cu^+ centers was observed that confirms the sensitizer role of Ag. The energy transfer process in LTB:Cu,Ag makes it a more efficient TSL phosphor than LTB:Cu. However, it is shown that the TSL spectrum of the LTB:Cu,Ag consists of emission bands corresponding to both Ag^+ (270 nm) as well as Cu^+ (370 nm) centers. A possible scheme for the TSL processes was proposed based on PL and TSL studies. The Ag^+ trap centers were shown to radiatively re-combine through two different routes giving two separate TSL peaks at 270 nm and 370 nm. Therefore to exploit the full potential of the co-doped LTB, a suitable TSL readout system with sensitivity in the range 200-600 nm has been proposed and developed.

Ag Doped $Li_2B_4O_7$:

The concentration of Ag in LTB was optimized and 1.0 wt% doping in the melt was found optimum for the growth of good quality single crystals suitable for dosimetric applications. The UV-Vis transmission, PL and RL studies confirmed that Ag^+ is incorporated in the LTB matrix with its characteristic emission at 270 nm. In the PL emission of 270 nm peak of Ag^+, a concentration quenching was observed beyond 0.5 wt% doping. In TSL studies, the glow curve showed an intense peak at 160ºC with emission at 270 nm and 1.0 wt% concentration in melt (about 500 ppm in the crystal) was found optimum for the best TSL properties. A special TSL readout system was built for this material using a solar blind photo-multiplier tube which improved the detection efficiency and lowered the noise level. A dose of 3 μGy was measured experimentally employing the optimized system. The TSL set-up and LTB crystal with optimum Ag concentration have been proposed as a promising system in low level personal and environmental dosimetry applications. Further, there was approximately 15% fading after 30 days for samples stored under dark conditions. The fading studies also revealed the optical bleaching of the traps. The LTB:Ag was also successfully tested in medical dosimetry applications with a confidence level of 97%.

The OSL properties of the material were further investigated and found to be an excellent candidate for OSL dosimetry. The OSL response of LTB:Ag was measured in a doses range from 0.1 Gy to 500 Gy and found quite sensitive and linear. The fading of OSL signal was found to be about 36% after 48 hours.

Further the sensitivity of the material to thermal neutrons was established. The material exhibited high sensitivity to thermal neutrons with a linear dose response (Fluence range: 10^8 to 10^9 neutrons/cm^2) in TSL and OSL modes. The detection of thermal neutrons was also demonstrated in real-time employing a specific setup based on LTB:Ag crystal.

Challenges and Scope of Future Studies

This research work highlighted the properties of LTB material for dosimetric applications and the effect of copper and silver doping on the luminescent properties of LTB single crystals. Though in the course of this work dosimetric properties of this material are studied in details, still there are several aspects that can be listed as a future scope of the study. The different aspects of the materials which can be further characterized or examined are given below.

- **Minimization of optical fading:** Although the sensitivity of LTB:Ag is very high but the problem associated with this material is its optical fading due to its low temperature peak. To overcome this, efforts may be put on co-doping (In, P or Si etc) to make the glow curve more stable.
- **Mixed field dosimetry:** This material is eligible for neutron dosimetry along with gamma ray dosimetry making it suitable for the mixed field dosimetry. The only concern is in finding the way to distinguish between the dose component from neutrons and gamma ray. This limitation can be addressed by taking a combination of LTB:Ag and other phosphor which is only sensitive to gamma rays (LTB grown using materials fully depleted in ^{6}Li and ^{10}B). By a proper and elaborate calibration it may be possible to figure out the dose from different types of radiation. Further, to enhance the sensitivity of LTB as neutron dosimeter, the effect of enriched ^{6}Li and ^{10}B can be studied.
- **Energy response of the phosphors for clinical application**: A flat energy response over a broad energy range is one of the important requirements for a dosimeter to be

used in clinical or personnel dosimeter. This can be studied in details along with the effect of co-doping on the energy response of LTB. Further, in order to demonstrate the use of the phosphors as personnel and clinical dosimeters, field tests may be carried out under different conditions along with the presently used standard dosimeters.

REFERENCES

1. G.F. Knoll, *Radiation Detection and Measurements,* **2000**, John Wiley & Sons, Inc.
2. D.M. Christensen, C.J. Iddins, S.L. Sugarman, *Emerg. Med. Clin. North. Am,* **2014**, *32 (1),* 245-265.
3. *International Commission on Radiation Units and Measurements (ICRU),* Report 24, **1976**, Bethesda, Maryland.
4. E.H. Donnelly, J.B. Nemhauser, J.M. Smith, *South. Med. J.,* **2010**, *103(6),* 541-544.
5. M. Durante, FA. Cucinotta, *Rev. Mod. Phys.,* **2011**, *83,*1245-1281.
6. E.B. Podgorsak, *"Radiation Oncology Physics: A Handbook for Teachers and Students"* **2005**, International Atomic Energy Agency, STI/PUB/1196.
7. *Medical Physics,* **1998**, *25(11),* 2093-2115.
8. A.B. Rosenfeld, *"Concepts and trends in medical radiation dosimetry",* **2011**, 48-74.
9. Clemens Woda, Céline Bassinet, François Trompier, Emanuela Bortolin, Sara Della Monaca and Paola Fattibene, *ANN IST SUPER SANITA,* **2009**, *45 (3),* 297-306.
10. Y.S. Horowitz, (ed.), *"Thermoluminescence and Thermoluminescent Dosimetry",* **1983**, CRC Press, Boca Raton.
11. T. Kron, L. DeWerd, Mobit, *Phys. Med. Biol.,* **1999**, *44,* L15-L17.
12. T. Kron, *Australas Phys. Eng. Sci. Med.,* **1995,** *18(1),* 1-25.
13. E.G. Yukihara, S.W.S. Mckeever, *"Optically Stimulated Luminescence-fundamentals and applications',* ISBN: 978-0-470-69725-2.
14. V. Kortov, *Radiat. Meas.,* **2007**, *42 (4–5),* 576–581.
15. S.W.S. McKeever, *"Thermoluminescence of solids"*, **1985**, Cambridge Univ. Press, 376 p.

16. K. Becker, CRC Press, Inc., **1973**, Cranwood Parkway, Cleveleand, Ohio 44128, U.S.A.
17. E.Wiedemann, Zurmechanik des Leuchtens, *Ann. Phys-Berlin.*, **1889**, *37,* 177-248.
18. E. Wiedemann and G.C. Schmidt, Über luminescenz. *Ann. Physik*., **1895**, *54*, 604-625.
19. F. Daniels and D.F. Saunders, *Science*, **1950**, *111*, 461-469.
20. J.T. Randall and M.H.F. Wilkins, *Proceedings of the Royal Society of London*, **1945**, *184*, 366-389
21. G.Fj. Garlick and A.F. Gibson, *Proceedings of the Physical Society*, **1948**, *60*, 574-590.
22. J. R. Cameron, F. Daniels, N. Johnson, G. Kenney, *Science*, **1961**, *134*, 333-334.
23. United States Patent, **1963**, US 3320180 A.
24. J. McKeever, F.D. Walker and S.W.S. McKeever, *Nucl. Tracks Radiat. Meas.,* **1991**, *21,* 179-183.
25. L.E. Moore, *J. Phys. Chem*, **1957**, *61*, 636-639.
26. R.J. Ginther and R.D. Kirk, *Electrochem. Soc.,***1957**, *104*, 365-369.
27. W. Binder, S. Disterhoft and J.R. Cameron, *Proc. 2nd Int. Conf. On Luminescence Dosimetry*, Gatlinburg, 1968, CONF 680920 (NTIS, Springfield, VA), 43.
28. A.C. Lucas and B.M. Kasper, Proc. 5th Int. Conf. On Luminescence Dosimetry, **1977**, Sao Paulo, 131.
29. K. Jitendra, Srivastava, J. Supe Sudhakar, *Nucl. Instrum. Methods*, **1978**, *155(1–2)*, 233-235.
30. M.S. Akselrod, V.S. Kortov, *Radiat. Prot. Dosim.,* **1990**, *33*, 123–126
31. R.G. Fairchild, P.L. Mattern and K. Lengweiler, *J. Appl. Phys*., **1978**, *49*, 4523-4533.

32. T. Nakajima, Y. Murayama, T. Matsuzawa and A. Koyano, *Nucl. Instrum. Methods*, **1978**, *157*, 155-162.

33. G. Massillon-JL, I. Gamboa-deBuen, A.E. Buenfil, M.A. Monroy-Rodríguez, M.E. Brandan, *Nucl. Instrum. Methods Phys. Res.*, **2008**, *Sect. B, 266(5)*, 772–780.

34. S.G. Gorbics, F.H. Attix and K. Kerris, *Health Phys.*, **1973**, *25*, 499-506.

35. T. Yamashita, N. Nada, H. Onishi and S. Kitamura, *Health Phys.*, **1971,** *21*, 295-300.

36. U. Madhusoodanan, M.T. Jose, A. Tomita, W. Hoffmann and A.R. Lakshmanan, J. *Lumin.*, **1999,** *82*, 221-232.

37. E. Tochilin, N. Goldstein, and W.G. Miller, *Health Phys.*, **1969**, *16*, 1-91.

38. K.W. Crase, and R.B. Gammage, *Health Phys.*, **1975**, *29*, 189.

39. J.H. Schulman, R.D. Kirk and E.J. West, *USAEC Symposium series 650637, Luminescence dosimetry*, **1967**, 113-117.

40. Mutsuo Takenaga, Osamu Yamamoto and Tadaoki Yamashita, *Nucl. Instrum. Methods*, **1980**, *175(1)*, 77-78.

41. M.S. Akselrod, V.S. Kortov and E.A. Gorelova, *Rad. Prot. Dosim.*, **1990**, *33*, 119-122.

42. T. Nakajima, *Health Phys.*, **1972**, *23*, 133-136.

43. M. Prokic, *Nucl. Instrum. Methods*, **1980**, *175*, 83-86.

44. P. Braunlich, D. Schafer, A. Scharmann, *Stanford: Proc International Conf on Lum. Dosim.*, USAEC, **1967**, 57–73.

45. EN. Sanborn, EL. Beard, *Stanford: Proc International Conf on Lum. Dosim.*, USAEC; **1967**, 183–191.

46. CR. Rhyner, WG. Miller, *Health Phys.*, **1970**, *18*, 681–684.

47. B.L. Justus, C.D. Merritt, K.J. Pawlovich, A.L. Hustus, S. Rychvovsky, *Radiat. Prot. Dosim.,* **1999**, *84 (1-4)*, 189-192.

48. A.J J. Bos, M. Prokic and J C. Brouwer, *Radiat. Prot. Dosim.*, 2006, *119 (1-4)*, 130-133.

49. E. De la Rosa , R.A. Rodríguez, L.A. Díaz-Torres, P. Salas, R. Meléndrez, M. Barboza-Flores, *Optical Materials*, **2005**, *27(7)*, 1245–1249.

50. R.A. Barve, R.R. Patil, S.V. Moharil, B.C Bhatt, M.S. Kulkarni, *J. Lumin.*, **2016**, 171, 72–78.

51. M. Salis, *J. Lumin.*, **2003**, *104 (1–2)*, 17–25.

52. M.S. Akselrod, and S.W.S. McKeever, *Radiat. Prot. Dosim.*, **1999**, *81*, 167–176.

53. S.W.S. McKeever, and M.S. Akselrod, *Radiat. Prot. Dosim.*, **1999**, 84, 317–320.

54. M. Sommer, and J. Henniger, *Radiat. Prot. Dosim.*, **2006**, *119*, 394–397.

55. A.J.J. Bos, M. Proki´c, and J.C. Brouwer, *Radiat. Prot. Dosim.*, **2006,** *119*, 130–133.

56. J.A. Rowlands, *Phys. Med. Biol.*, **2002,** *47*, R123-R166.

57. P.M. Denby, L. Bøtter-Jensen, A.S. Murray et al, *Radiat. Meas.*, **2006,** *41*, 774–779.

58. R.J. Clark, and I.K. Bailiff, *Radiat. Meas.*, **1998**, *29*, 553–560.

59. L.Dusseau, D. Plattard, J.-R. Vaill´e, *et al.* *IEEE Trans. Nucl. Sci*, **2000**, *47*, 2412–2416.

60. D. Lapraz, H. Prevost, K. Idri *et al., Phys. Status Solidi A*, **2006**, *203*, 3793–3800.

61. F. Ravotti, D.Benoit, P. Lefebvre, *et al.*, *J. Appl. Phys.*, **2007**, *102*, 123102.

62. H. Nanto, K. Murayama, T. Usuda, *et al., Radiat. Prot. Dosim.*, **1993**, *47*, 281–284.

63. Y. Douguchi, H. Nanto, T. Sato, *et al., Radiat. Prot. Dosim.*, **1999**, *84*, 143–148.

64. C.A. Jayachandran, *Phys. Med. Biol.*, **1971**, 16 (4), 617-623.

65. B. Padlyak, W.R. Romanowski, R. Lisiecki, B. Pieprzyk, A. Drzewiecki, V. Adamiv, Y. Burak, I. Teslyuk, *Optica Applicata*, **2012**, Vol. XLII, No. 2,

66. J.H. Schulman, R.D. Kirk, E.J. West, *Proceedings of the international conference on luminescence dosimetry,* **1965**, Conf: 650637.25, 113–117.

67. M. Takenaga, O. Yamamoto, T. Yamashita, *Health Phys.*, **1983**, *44 (4),* 387-393.

68. D.I. Shahare, B.T. Deshmukh, S.V. Moharil, S.M. Dhopte, P.L. Muthal, V.K. Kondawar, *Phys. Status Solidi A*, **1994**, *141(2),* 329-334.

69. J.K. Srivastava, S.J. Supe, *J. Phys. D*, **1989**, *22*, 1537–1543

70. M. Prokic, *Proceedings of the IRPA Reg. Congress on Radiation Protection in Central Europe*, **1999**. Budapest, Hungary, 231–239.

71. M. Ignatovych, V. Holovey, A. Watterich, T. Vidoczy, P. Baranyai, A. Kelemen, C. Chuiko, *Radiat. Meas.,* **2004,** *38*, 567–570.

72. A.C. Fernandes, M. Osvay, J.P. Santos, V. Holovey, M. Ignatovych, *Radiat. Meas.*, **2008,** *43*, 476 – 479.

73. Mehmet Kayhan, Aysen Yilmaz, *J. Alloys and Compd.*, **201**1, *509(30)*, 7819–7825.

74. M. Ishii, Y. Kuwano, S. Asaba, T. Asai, M. Kawamura, N. Senguttuvan, T. Hayashi, M. Koboyashi, M. Nikl, S. Hosoya, K. Sakai , T. Adachi ,T. Oku, H.M. Shimizu, *Radiat. Meas.*, **2004**, *38*, 571 – 574.

75. M. Ignatovych, V. Holovey, A. Watterich, T. Vidóczy, P. Baranyai, A. Kelemen, V. Ogenko, O. Chuiko, *Radiat. Phys. Chem.,* **2003**, *67(3–4)*, 587–591.

76. B. Rzyski, KSV. Nambi, *In: Proc. 5th Int. Conf. on luminescence dosimetry,* **1977**, Sao Paulo, Brazil.

77. B.M. Rzyski, S.P. Morato, *Nucl. Instrum. Methods*, **1980**, *175(1)*, 62-64.

78. B.T. Huy, V.X. Quang, H.T.B. Chau, *J. Lumin.*, **2008,** *128,* 1601–1605.

79. Zhengye Xiong, Qiang Tang, Xiaomin Xiong, Daling Luo, Ping Ding, *Radiat. Meas.*, **2011**, 46(3), 323–328.
80. N. Senguttuvan, M. Ishii, M. Shimoyama, M. Kobayashi, N. Tsutsui, M. Nikl, M. Dusek, H.M. Shimizu, T. Oku, T. Adachi, K. Sakai, J. Suzuki, *Nucl. Instrum. Methods Phys. Res. A*, **2002**, *486*, 264–267.
81. Talat Aydın, Hayrünnisa Demirtas, Samet Aydın, *Radiat. Meas.*, **2013,** *58,* 24-32.
82. M. Danilkin, I. Jaea, M. Kerikmäa, A. Lusa, H. Mändaa, L. Pung, A. Ratas, V. Seeman, S. Klimonsky, V. Kuznetsov, *Radiat. Meas.*, **2010**, *45(3–6)*, 562–565.
83. N.S. Rawat, M.S. Kulkarni, M. Tyagi, P. Ratna, D.R. Mishra, S.G. Singh, B. Tiwari, A. Soni, S.C. Gadkari, S.K. Gupta, *J. Lumin.*, **2012**, *132*, 1969–1975.
84. L. Boetter-Jensen, P. Christensen, *Acta Radiol. Suppl.*, **1972**, *313*, 247-252.
85. J.J. Thompson, P.L. Ziemer, *Health Phys.*, **1973**, *25 (4)*, 435-441.
86. M. Takenaga, O. Yamamoto, T. Yamashita, *5th Int. Conf. on Luminescence dosimetry*, **1977**, page 148.
87. S.W.S. McKeever, "*Thermoluminesce of Solids*", Cambridge University Press, **1985**, pp. 225.
88. M. Martini, F. Meinardi, L. Kovács, K. Polgar, *Radiat. Prot. Dosim.*, **1996**, *65(1-4)*, 343-346.
89. Z. Xiong, Ye, Q. Tang, C. Zhang, *Sci. China-Phys. Mech. Astron.*, **2007**, *50(3)*, 311-320.
90. B.M. Hunda, P.P. Puga, A.M. Solomon, H.M. Holovey, *Semiconductor Physics, Quantum Electronics and Optoelectronics*, **2000**, *3(2)*, 227-232.
91. Eduardo G. Yukihara and S.W.S. McKeever, *Optically Stimulated Luminescence: Fundamentals and Applications*, **2011**, A John Wiley and Sons, Ltd., Publication.

92. A. Kumaresh, R. Arun Kumar, N. Ravikumar, U. Madhusoodanan, B.S. Panigrahi, K. Marimuthu, and M. Anuradha, *Chin. Phys. B.* **2016**, *25(5)*, 058105.

93. A. Ratas, M. Danilkin, M. Kerikmäe, A. Lust, H. Mändar,V. Seeman, and G. Slavin, *Proceedings of the Estonian Academy of Sciences,* **2012**, *61(4),* 279–295.

94. D.J. Wooten. "Electronic structure of lithium tetraborate." *PhD dissertation, Air Force Institute of Technology,* **2010**.

95. S. Toschev, *"Crystal Growth: An Introduction",* ed. P. Hartman, North Holland, Amsterdam, **1973**.

96. Willard. Gibbs, *Transactions of the Connecticut Academy,* **1876**, *3*, 108-248.

97. Willard. Gibbs, *Transactions of the Connecticut Academy*, **1878**, *16*, 343-524.

98. Hans J. Scheel, *J. Cryst. Growth*, **2000**, *211*, 1-517.

99. Eugenii Khamskii, *"Crystallization from Solutions and Melts",* Springer Publishing. **1969**,

100. S.A. Arrhenius, *Z. Phys. Chem.*, **1889**, *4*, 96–116.

101. J.C. Brice, *"Crystal Growth Processes"*, John Wiley and Sons, New York, **1986.**

102. K. Nassau, *J. Cryst. Growth*, **1969,** *5*, 338-344.

103. K. Nassau, J. Nassau, J. Lapidary, *J. Cryst. Growth*, **1971**, *24*, 1284.

104. J. Czochralski, *Z. Phys. Chem.*, **1918, *92***, 219-221.

105. F.R. Charvet, *"Growth of Crystals",* **1984**, *12,* ed. A.A. Chernov, 210.

106. V.L. Indenbom, I.S. Zhitomirskii, T.S. Chebanova, *"Growth of Crystals"*, **1969**, Ed. N.N. Sheftel, Consultant Bureau, New York, 249.

107. Sangeeta, Babita Tiwari, S.C. Sabharwal, *J. Cryst. Growth*, **2004**, *273*, 167–171.

108. Claudio Furetta, "*Handbook of Thermoluminescence'*, **2003**, World Scientific.

109. C.E. May, and J.A. Partridge, *J. Chem. Phys.*, **1964**, *40*, 1401-1409.

110. M.S. Rasheedy, *J. Phys.: Condens. Matter*, **1993**, *5*, 633-636.

111. J.L. Lawless, R. Chen, V. Pagonis, *Radiat. Meas.*, **2009**, *44*, 606–610.

112. L. Bøtter-Jensen, E. Bulur, G.A.T. Duller, A.S. Murray, *Radiat. Meas.*, **2000**, *32*, 523–528.

113. E.G. Yukihara and S W S. McKeever, *Phys. Med. Biol.* **2008**, *53*, R351–R379.

114. J.J.D. Winefordner, S.G. Schulman, T.C. O'haver, *"Luminescence Spectrometry in Analytical Chemistry"*, **1972**, Wiley-Interscience, New York.

115. http://www.edinst.com/fl920p.htm.

116. https://www.edinst.com/wp-content/uploads/2015/08/TN2-What-is-TCSPC-Red.pdf.

117. J. Michael Hollas, "*Modern Spectroscopy*" 4th Ed., John Wiley & Sons, Inc., **2003**.

118. W.H. Bragg, *Nature*, **1908**, *77*, 270-271.

119. H.P. Clug, L.E. Alexander, *"X-ray Diffraction Procedures for Polycrystalline and Amorphous Materials"*, **1954**, John-Willey, London.

120. M.I. Pope, E.D. Judd, "*Differential thermal analysis: A guide to the technique and its applications*", **1977**.

121. C. Marín, E. Diéguez, *"Orientation of Single Crystals by Back-Reflection Laue Pattern Simulation"*, World Scientific Publishing Co. Pte. Ltd., **1999**.

122. Babita Tiwari, N.S. Rawat , D.G. Desai, S.G. Singh, M. Tyagi, P. Ratna, S.C. Gadkari, M.S. Kulkarni, *J. Lumin.*, **2010**, *130*, 2076–2083.

123. https://na.industrial.panasonic.com/sites/default/pidsa/files/downloads/files/radiationmeasurementsystems_tld_catalog.pdf

124. G. Kitis, C. Furetta, M. Prokic and V. Prokic, *J. Phys. D: Appl. Phys.*, **2000,** *33*, 1252–1262.

125. M. Prokic, *Radiat. Protect. Dosim.,* **2002**, *100(1-4),* 265-268.

126. Patent US20030062486 A1.

127. M. Ishii, Y. Kuwano, T. Asai, N. Senguttuvan, T. Hayashi, M. Kobayashi, T. Oku, K. Sakai, T. Adachi, H.M. Shimizu, J. Suzuki, *J. Cryst. Growth,* **2003**, *257(1–2),* 169–176.

128. I.N. Ogorodnikov, V.A. Pustovarov, A.V. Kruzhalov, L. Isaenko, M. Kirm, G. Zimmerer, *Phys. Sol. Stat.,* **2000**, *42,* 464-472.

129. B.S.R. Sastry, F.A. Hummel, *J. Am. Ceram. Soc.,* **1959**, *42,* 216-218.

130. J.D. Garrett, M. Natarajan-Iyer and J. E. Greedan, *J. Cryst. Growth,* **1977**, *41*, 225-227.

131. Jiayue Xu, Shiji Fan, Baoliang Lu, *J. Cryst. Growth,* **2004**, *264*, 260–265.

132. D.S. Robertson, I.M. Young, *J. Mater. Sci.,* **1982**, *17,* 1729-1738.

133. Tamotsu Sugawara, Ryuichi Komatsu, Satoshi Uda, *J. Cryst. Growth,* **1998**, *193(3),* 364–369.

134. A.R.M. Fayed, PhD thesis, *"Growth of lithium borate crystals for use in thermoluminescence dosimetry",* **1982**, Ref. No. 18042501

135. V.T. Adamiv, Y.V. Burak, D. J. Wooten, J. McClory, J. Petrosky, I. Ketsman, J. Xiao, Y. B. Losovyj and P. A. Dowben, *Materials,* **2010**, *3*, 4550-4579.

136. D. Wooten, I. Ketsman, J. Xiao, Ya. B. Losovyj, J. Petrosky, J. McClory, Ya. V. Burak, V. T. Adamiv, J. M. Brown and P. A. Dowben , *Eur. Phys. J. Appl. Phys.,* **2010**, *52*, 31601.

137. V. Nagirnyi, A. Kotlov, G. Corradi, A. Watterich, M. Kirm, *Phys. Stat. Sol. (c),* **2007**, *4,* 885-888.

138. O.T. Antonyak, V.T. Adamiv, Ya.V. Burak, I.M. Teslyuk, *Adv. Func. Mater.*, **2002**, *9*, 452-455.

139. O.T. Antonyak, Y.V. Burak, I.T. Lyseiko, N.S. Pidzyrailo, Z.A. Khapko, *Opt. Spect.*, **1986**, *61*, 550-553.

140. C.E. Moore, *Atomic Energy Levels, Natl. Bur. Std. (U.S.) Circ. 2*, **1952**, 467.

141. D.S. McClure, S.C. Weaver, *J. Phys. Chem. Solids*, **1991**, *52*, 81-100.

142. B.T. Huy, V.X. Quang, M. Ishii, *J. Lumin.*, **2010**, *130*, 2142-2145.

143. A.B. Goldberg, D.S. McClure, C.Pedrini, *Chem. Phys. Lett.*, **1982**, *87(5)*, 508-511.

144. S.A. Payne, *Phys. Rev. B*, **1987**, *36*, 6125-6131.

145. G. Corradi, V. Nagirnyi, A. Kotlov, A Watterich, M Kirm, K Polgar, A Hofstaetter, M Meyer, *J. Phys.: Condens. Matter*, **2008**, *20*, 025216-1-9.

146. Ya.V. Burak, V.T. Adamiv, O.T. Antonyak, S.Z. Malynych, M.S. Pidzyrailo, I.M. Teslyuk, *Ukr. J. Phys.*, **2005**, *50(10)*, 1153-1158.

147. *"Techniques and Management of Personnel Thermoluminescence Dosimetry Services"* **1993**, Springer Netherlands, ISBN:978-0-7923-2436-2.

148. Talat Aydın, Hayrünnisa Demirtaş, Samet Aydın, *Radiat. Meas.*, **2013**, *58*, 24–32

149. K.S. Chung, H.S. Choe, J.I. Lee, J.L. Kim and S.Y. Chang, *Radiat. Prot. Dosim***.,** **2005**, *115(1-4)*, 345-349.

150. K.S. Chung, , H.S. Choe, J.I. Lee, J.L. Kim, *Radiat. Meas.*, **2007**, *42(4-5)*, 731-734.

151. A.T. Brant, B.E. Kananan, M.K. Murari, J.W. McClory, J.C. Petrosky, V.T. Adamiv, Ya.V. Burak, P.A. Dowben, and L.E. Halliburton, *J. Appl. Phys.*, 2011, *110*, 093719-6.

152. C. Furetta, P. Weng, *"Operational Thermoluminescence Dosimetry"*, World Scientific Publishing Co., Singapore, **1998**.

153. O. Annalakshmi, M.T. Jose, U. Madhusoodanan, B. Venkatraman, G. Amarendra, *J. Lumin., 141*, **2013**, 60–66.

154. N. Can, T. Karali, P.D. Townsend and F. Yıldız*, J. Phys. D: Appl. Phys.,* **2006***, 39,* 2038–2043.

155. M. Prokic, *Radiat. Meas., 33,* **2001**, 393–396.

156. A.N. Singh, S.N. Singh, L.L. Singh, *Indian J Phys,* **2015**, *89(1),* 41.

157. M. Ignatovych, V. Holovey, T. Vidocazy, P. Baranyai, A. Kelemen, V. Laguta, O. Chuiko*, Func. Mater.,* **2005**, *12(2),* 313-317.

158. Magdalyna Ignatovych, Mauro Fasoli, András Kelemen, *Radiat. Phys. Chem.,* **2012**, *81(9),* 1528–1532

159. Mazharul M. Islam, Thomas Bredow, Christian Minot, *J. Phys. Chem. B*, **2006**, *110* (35), 17518–17523

160. T. D. Kelly, L. Kong, D. A. Buchanan, A. T. Brant, J. C. Petrosky, J. W. McClory, V. T. Adamiv, Y. V. Burak, P. A. Dowben, *Phys. Status Solidi B,* **2013,** *250(7),* 1376–1383.

161. V.T. Adamiv, Y.V. Burak, I.M. Teslyuk, *J. Alloys Compd.,* **2009**, *475(1-2),* 869-873.

162. C. B. Palan, *Global Journal of Science, Engineering and Technology,* **2013**, *14,* 1-17.

163. D.A. Buchanan, M.S. Holston, A.T. Brant, J.W. McClory, V.T. Adamiv, Ya.V. Burak, L.E. Halliburton, *J. Phys. Chem. Solids,* **2014**, *75(12),* 1347–1353.

164. S.W.S. McKeever, M. Moscovitch, P.D. Townsend, "*Thermoluminescence Dosimetry Materials: Properties and Uses",* **1995**, Nuclear Technology Publishers, Ashford

165. A. Kelemen, D. Mesterházy, M. Ignatovych, V. Holovey, *Radiat. Phys. Chem.*, **2012**, *81(9)*, 1533–1535.

166. N. Tsutsui, Y. Ino, K. Imai, N. Senguttuvan, and M. Ishii, *J. Cryst. Growth,* **2001**, *229,* 283-288.

167. B.E. Kananen, A.T. Brant, D.A. Buchanan, M.K. Murari, J.W. McClory, *IEEE Nuclear Science Symposium Conference Record,* **2012**, *6154532,* 427-430.

168. D.A. Buchanan, M.S. Holston, A.T. Brant, J.W. McClory, V.T. Adamiv, Ya.V. Burak, L.E. Halliburton, *J. Phys. Chem. Solids,* **2014**, *75(12),* 1347–1353.

169. M. Ignatovych, V. Holovey, T. Vidóczy, P. Baranyai, A. Kelemen, *Radiat. Phys. Chem.,* **2007**, *76(8–9),* 1527–1530.

170. Donald S. McClure, Christian Pedrini, *J. Lumin.,* **1984**, *31–32(1),* 197–200.

171. R.D. Shannon, *Acta Cryst.,* **1976**, *A32* , 751-767.

172. K.P. Popovych, P.P. Puga, V.T. Maslyuk, V.M. Krasylynec, V.M. Holovey and G.D. Puga, *Acta Physica Polonica A*, **2010**, *117(1)*, 174-176.

173. C.R. Ronda, *"Proceedings of the Sixth International Conference on Luminescent Materials',* **1998**, Published by Electrochemical Society, ISBN 10: 156677182X ISBN 13: 9781566771825.

174. B. F. Wall, C. M. H. Driscoll, J. C. Strong, and E. S. Fisher, *Phys. Med. Biol.,* **1982,** *27,* 1023-1034.

175. Ngo Quang Thanh, Vu Xuan Quang, Nguyen The Khoi, Nguyen Dac Dien, *VNU Journal of Science, Mathematics – Physics*, **2008**, *24*, 97-100.

176. John A. Harvey, PhD thesis *"Performance of Thermoluminescent Dosimeters Under As-Deployed Conditions*" **201**1, Nuclear Engineering and Radiological Sciences, the University of Michigan.

177. B. Burgkhardt, R. Herrera,E. Piesch, *Nucl. Instrum. Methods*, **I976**, *I37*, 41-47.

178. http://www.aerb.gov.in/AERBPortal/pages/English/t/prsrel/IERMON18032011AF.pdf

179. David Thwaites, *7th International Conference on 3D Radiation Dosimetry (IC3DDose), Journal of Physics: Conference Series*, **2013**, *444*, 012006.

180. Lars Bétter-Jensen, *Radiat. Meas.*, **1997**, *27(5/6)*, 749-768.

181. L.Botter-Jensen, A.G. Wintle, S.W.S. Mckeever, "*Optically Stimulated Luminescence Dosimetry*" **2003**, Elsevier, Amsterdam.

182. V. Schembri_ and B. J. M. Heijmen, *Med. Phys.*, **2007**, *34(6)*, 2113-2118.

183. M.S. Akselrod, V.S. Kortov, D.J. Kravetsky, V.I. Gotlib, *Radiat. Prot. Dosim.*, **1990**, *32*, 15-20.

184. O.A. Plaksin, V.A. Stepanov, P.A. Stepanov, V.M. Chemov, V.A, Skuratov, *J. Nucl. Mater.*, **1996**, *233*, 1355-1360.

185. M.S. Kulkarni, D.R. Mishra, K.P. Muthe, Ajay Singh, M. Roy, S.K. Gupta, S. Kannan, *Radiat. Meas.*, **2005**, *39*, 277-282.

186. D.R. Mishra, M.S. Kulkarni, K.P. Muthe, C. Thinaharan, M. Roy, S.K. Kulashreshtha, S. Kannan, B.C. Bhatt, S.K. Gupta, D.N. Sharma, *Radiat. Meas.*, **2007**, *42*, 170-176.

187. R.T. Kouzes, J. R. Ely, A. T. Lintereur, and D. L. Stephens, *PNNL-18903," PNNL Report*, **2009**.

188. R.T. Kouzes, *Report PNNL-18388*, **2009**, Dept. of Energy.

189. C.W.E. van Eijk, *Nucl. Instrum. Metheds A*, **2001**, 460, 1-14.

190. C.W.E. van Eijk, A. Bessiere, P. Dorenbos, *Nucl. Instrum. Methods A*, **2004**, *529*, 260-267.

191. H. Ing, *Radiat. Meas.*, **2001**, *33*, 275-286.

192. Francesco D'Errico, Ravinder Nath, Giovanni Silvano, Luigi Tana, *International Journal of Radiation Oncology.Biology.Physics*, **1998**, *41(5*), 1185-1192.

193. J.R. Parrington, *15th Ed. "Nuclides and Isotopes"*, **1996**, San Jose: General Electric Co. and KAPL, Inc.

194. Bruker Corporation. *EPR/ENDOR Frequency Table.* Table, Billerica, MA: Bruker Daltonics Inc.

195. Neutron and Gamma Ray Fluence to Dose Factors, *American Nuclear Society*, **1977**, ANSI standard ANSI/ANS-6.1.1-1977.

196. J.C.R. Mittani, A.A.R. Da Silva, F, Vanhavere, M.S. Akselrod, E.G. Yukihara, *Nucl. Instrum. Methods Phys. Res., Sect. B,* **2007**, *260*, 663-671.

197. E.G. Yukihara, J.C, Mittani, F. Vanhavere, M.S. Akselrod, *Radiat. Meas.*, **2008**, *43(2-6),* 309-314.